BIODEGRADABLE NANOPARTICLES FOR INTRAVASCULAR DRUG DELIVERY

PROEFSCHRIFT

ter verkrijging van
de graad van doctor aan de Universiteit Twente,
op gezag van de rector magnificus,
prof. dr. F.A. van Vught,
volgens besluit van het College voor Promoties
in het openbaar te verdedigen
op vrijdag 31 januari 2003 te 13.15 uur

door

Miechel Lambertus Theodorus Zweers

geboren op 25 februari 1974
te Zevenaar

Dit proefschrift is goedgekeurd door:

Promotor: prof. dr. J. Feijen
Assistent-promotor: dr. ir. G.H.M. Engbers
Referent: dr. D.W. Grijpma

Biodegradable nanoparticles for intravascular drug delivery / Miechel Zweers
Thesis University of Twente, Enschede, The Netherlands
With summaries in English and Dutch

Explanation of the cover:
A microporous balloon catheter is schematically shown. This balloon catheter is used for the intravascular administration of drug-loaded nanoparticles (see Chapter 7). Three figures are included to explain the title:
(Left) "*Biodegradable nanoparticles*": Scanning electron microscopy image of poly(DL-lactic-co-glycolic acid) nanoparticles (see Chapter 3).
(Right) "*intravascular*": Fluorescence microscopy image of a cross-section of an artery to which fluorescent labeled particles of 120 nm were administered (see Chapter 7).
(Middle) "*drug delivery*": Plot of the release of rapamycin from nanoparticles as a function of time (see Chapter 8).

Voor u ligt het eindresultaat van ruim 4 jaar onderzoek. Velen hebben mij de afgelopen 4 jaar op verschillende wijzen gesteund en zijn van grote betekenis geweest voor het wetenschappelijke werk dat in dit proefschrift beschreven staat. Hen wil ik op deze plaats daarvoor bedanken.

Allereerst wil ik mijn promotor, prof. Feijen, bedanken voor de mogelijkheid, die hij mij heeft geboden om na het afstuderen zelfstandig onderzoek uit te voeren. Ik waardeer de tijd die hij heeft gestoken in het kritisch lezen van de hoofdstukken. Daarnaast ben ik veel dank verschuldigd aan mijn assistent-promotor, Gerard Engbers. Gerard, jouw enthousiasme voor onderzoek en jouw grote kennis op een breed vakgebied maakten het zeer plezierig met jou samen te werken. Tevens wil ik mijn referent, Dirk Grijpma, graag bedanken voor zijn raadgevingen en ideeën, die soms nieuwe wegen openden. I thank Cordis for financing this research, and in particular George Papandreou for the interest in my work and the valuable discussions we had on the phone or by e-mail. Verder weet ik de moeite die Bob Geelkerken gedaan heeft om aan menselijke bloedvaten te komen en de tijd, die hij aan het lezen en corrigeren van hoofdstuk 7 heeft besteed, zeer te waarderen.

Daarnaast werden de bloedvaten vakkundig ingebed en in dunne coupes gesneden door Marijke van den Berg van het streeklab "Oost Nederland" in Enschede en werd ik geholpen bij de microscopische bestudering en interpretatie door Anne Hampsink, Joop van Baarlen en Richard Rieksen. Allen hartelijk bedankt!

De experimenten met de bloedvaten waren niet mogelijk geweest zonder slachthuis Haaksbergen en enige keurmeesters. Ik dank hen dan ook hartelijk voor de moeite die zij hebben genomen om mij in mijn onderzoek te steunen.

In de afgelopen 4 jaar heb ik 3 afstudeerders en 1 stagiair begeleid. Delen van hun werk zijn terug te vinden in hoofdstuk 3 (Anoek Nollen en Ugur Ülker), hoofdstuk 4 (Karin Probst) en hoofdstuk 8 (Marloes Theusink). Ik heb altijd veel plezier beleefd jullie te begeleiden en waardeer jullie inzet om uren deeltjes te staan maken en te karakteriseren enorm.

Tevens wil ik graag mijn twee paranimfen op deze plek bedanken. Lé, je was een leuke huisgenoot en collega. Ik zal nooit de feestjes met cocktails, de hakmuziek, de gezellige etentjes en snookerpartijtjes vergeten. Ook wil ik je bedanken voor de snelle correcties en de steun van de afgelopen en komende tijd. I would like to thank Audrey for the great time we had as roommates for more than 4 years. Whereas others sometimes had some problems with your stubbornness, we always could get along fine. I also think that you are the best roommate one can have.

Natuurlijk wil ik de collega's van PBM, RBT, STEP en MTP bedanken voor de gezellige koffiepauzes, de barbecues en borrels en in het bijzonder de bierproefavonden met Louis,

Miechel

Table of contents

CHAPTER 1

General introduction

Atherosclerosis is a disease characterized by a progressive narrowing and hardening of arteries [1]. It is a process that may already occur in childhood [1] and might become more pronounced at increasing age [1,2]. The heart attacks and strokes that result from this disease exceed cancer as a cause of death in the western society and are becoming more prevalent in developing countries as well. Risk factors for the development of atherosclerosis are high blood levels of LDL cholesterol [1], high blood pressure [3], smoking [4] and diabetes [3].

Percutaneous transluminal angioplasty (PTA) [5] and stenting [6] are techniques used for the treatment of atherosclerotic blood vessels. Although initially the blood flow is restored, reocclusion of arteries, restenosis, is the most important drawback of these techniques. An important step in the process that leads to restenosis is the activation of the migration and proliferation of smooth muscle cells [7]. Therefore, the delivery of drugs that prevent migration and proliferation of smooth muscle cells seems a promising approach to reduce the incidence of restenosis. As smooth muscle cell migration and proliferation take place in the first four weeks after treatment [8-11], sustained drug delivery for at least one month is desirable.

Because systemic administration of drugs appeared to be inefficient and hampered by toxic side effects [12], several local drug delivery approaches have been studied. The most promising approaches seem to be the use of drug-eluting stents and local delivery of biodegradable drug-loaded nanoparticles. While drug-eluting stents are non-biodegradable and permanently present in the artery, which could lead to long-term adverse tissue reactions, the use of biodegradable drug-loaded nanoparticles may avoid the risk of adverse tissue reactions in the long-term.

AIM OF THIS STUDY

The aim of this study was to design biodegradable nanoparticles that can be used as carriers for an effective release of anti-proliferative drugs in atherosclerotic vascular walls.

STRUCTURE OF THIS THESIS

A literature overview of the causes of restenosis, and approaches towards its prevention is given in **Chapter 2**. A description of atherosclerosis, the current treatments and the development of restenosis are given. The processes that are involved in the development of restenosis and the approaches, which have the potential to reduce the incidence of restenosis, are reviewed. The possible use of biodegradable nanoparticles for the administration of drugs in a diseased vascular wall is discussed.

The preparation of nanoparticles based on poly(DL-lactic acid) (PDLLA) and poly(DL-lactic-co-glycolic acid) (PLGA) using the salting-out method is described in **Chapter 3**. Since the particle size is an important parameter in the effectiveness of penetration of particles in the arterial wall, the influence of several process variables on the final nanoparticle size was determined.

A stabilizer is needed in the preparation of PLGA nanoparticles. This has as disadvantage that the stabilizer might affect biological interactions and targeting of the nanoparticles. The subject of **Chapter 4** is therefore the preparation of nanoparticles from poly(ethylene oxide)-PLGA (PEO-PLGA) without additional stabilizer. The ratio of PEO-PLGA to PLGA in the nanoparticle preparation was varied to determine the minimal required PEO content to obtain stable particle dispersions.

In **Chapter 5** the *in vitro* degradation of PDLLA, PLGA and PEO-PLGA nanoparticles is described. The influence of the copolymer composition on the degradation characteristics is highlighted.

The introduction of functional groups on the surface of PEO-PLGA nanoparticles is subject of **Chapter 6**. Nanoparticles based on PEO-PLGA block copolymers containing functional groups at the PEO-chain end were prepared. The potential to modify the surface of these particles for targeting purposes was studied by coupling a model amine group-containing compound.

The location of nanoparticles after intravascular administration using an *in vitro* model is described in **Chapter 7**. Polystyrene model nanoparticles of different surface charge and particle size and biodegradable PEO-PLGA nanoparticles were administered to carotid porcine arteries using a microporous balloon catheter.

Finally, the preparation of drug-loaded PEO-PLGA nanoparticles and their release behavior in PBS at 37 °C is described in **Chapter 8**. The release of two anti-restenosis drugs, rapamycin and dexamethasone, was studied. The effect of treatment of the drug-loaded nanoparticles with aqueous gelatin or albumin solutions on the release rate of the drug was evaluated.

REFERENCES

1. McGill, H.C.; McMahan, C.A.; Malcom, G.T.; Oalmann, M.C. and Strong, J.P., *Arterioscler. Thromb. Vasc. Biol.,* **1997**, *17*, 95-106.

2. Pathobiological Determinants of Atherosclerosis in Youth (PDAY) Research Group, *Arterioscler. Thromb.,* **1993**, *13*, 1291-1298.

3. Schettler, F.G. and Boyd, G.S. *Atherosclerosis - Pathology, physiology, aetiology, diagnosis and clinical management*; Elsevier: Amsterdam, **1969**.

4. Botti, T.P.; Amin, H.; Hiltscher, L.; Wissler, R.W.; Robertson, A.L.; Strong, J.P.; Cornhill, J.F.; McGill, H.C.; McMahan, C.A.; Oalmann, M.C. *et al.*, *Atherosclerosis,* **1996**, *124*, 191-202.

5. Lincoff, A.M.; Topol, E.J. and Ellis, S.G., *Circulation,* **1994**, *90*, 2070-2084.

6. Gershlick, A.H., *Atherosclerosis,* **2002**, *160*, 259-271.

7. Nagae, T.; Louie, A.Y.; Aizawa, K.; Ishimaru, S. and Wilson, S.E., *J. Cardiovasc. Surg.,* **1998**, *39*, 709-715.

8. Murakami, S.; Toda, Y.; Seki, T.; Munetomo, E.; Kondo, Y.; Sakurai, T.; Furukawa, Y.; Matsuyama, M.; Nagate, T.; Hosokawa, N. *et al.*, *Atherosclerosis,* **2001**, *157*, 361-368.

9. Johnson, L.L.; Schofield, L.M.; Verdesca, S.A.; Sharaf, B.L.; Jones, R.M.; Virmani, R. and Khaw, B.A., *J. Nucl. Med.,* **2000**, *41*, 1535-1540.

10. Fingerle, J.; Müller, R.M.K.; Kuhn, H.; Pech, M. and Baumgartner, H.R., *Arterioscler. Thromb. Vasc. Biol.,* **1995**, *15*, 1945-1950.

11. Zeymer, U.; Fishbein, M.C.; Forrester, J. and Cercek, B., *Am. J. Pathol.,* **1992**, *141*, 685-690.

12. Chorny, M.; Fishbein, I. and Golomb, G., *Crit. Rev. Ther. Drug Carrier Syst.,* **2000**, *17*, 249-284.

CHAPTER 2

Local drug delivery to decrease the incidence of restenosis - A literature survey

INTRODUCTION

Atherosclerosis is a disease that is characterized by the formation of a plaque and hardening of arteries (the formation of a lesion) [1]. In the western world, heart attacks and strokes that result from this disease exceed cancer as a cause of death. In The Netherlands for instance, 36% of all deaths are caused by atherosclerotic heart disease as compared to 27% by cancer [2]. This is comparable to the situation in the UK, in which one third of all deaths are caused by atherosclerotic heart disease. In the US, heart disease is also the major cause of death. In fact, twice as many women die from heart disease each year as from all types of cancer combined, including breast cancer [3]. In 1998, more than 6 billion dollars were spent in the US for the treatment of heart attacks [3]. Besides aging [1,4], high blood levels of LDL cholesterol [1], high blood pressure [5], smoking [6] and diabetes [5] increase the change for the development of atherosclerosis.

Before a description of the development of an atherosclerotic lesion is given, the structure of a healthy artery is described. A healthy arterial wall consists of three layers (schematically shown in Figure 2.1). The inner layer, the intima, consists of endothelial cells that are supported by a thin layer of fibrocollagenous tissue and by the internal elastic lamina. The middle layer, the media, is mainly composed of smooth muscle cells incorporated in a matrix of organized layers of elastic tissue. The outer layer, the adventitia, is predominantly composed of collagen, fibroblasts, nerve fibers and a network of small blood vessels, the vasa vasorum [7].
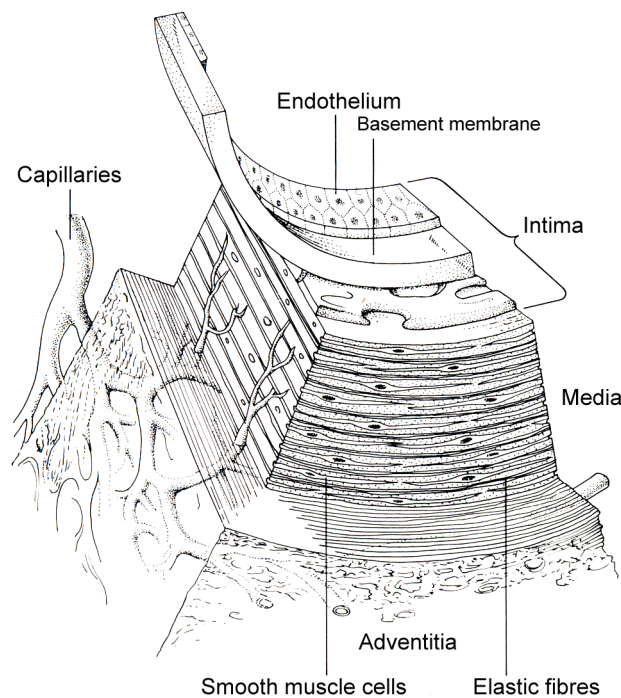
Figure 2.1 *Schematic three-dimensional drawing of a cross-section of an arterial wall showing three identifiable layers: the inner layer (intima), the middle layer (media) and the outer layer (adventitia) (reprinted with permission from [8]).*

The formation of atherosclerotic lesions affects the structure of the artery and can be distinguished in three phases [9].

The earliest recognizable lesion is the *fatty streak*. It is an accumulation of lipid-rich macrophages and T-lymphocytes within the intima at places where the endothelial cells are injured. This process may already occur in childhood [1].

Fibrotic streak formation starts when platelets adhere at sites where the endothelium is injured and release platelet-derived growth factor. This growth factor stimulates migration of smooth muscle cells from the media to the intima. Proliferation of smooth muscle cells is also promoted by this factor. It leads to the formation of a fibrotic plaque, which is mainly composed of foam cells (macrophages and to a lesser extent smooth muscle cells) and extracellular matrix [10-12]. Frequently, these plaques show regions of calcification, necrosis and microvascular ingrowth of "plaque vasa" [11].

Advanced lesion formation is initiated by the fracture of the fibrotic plaque. Following plaque fracture, thrombi are formed and the coagulation cascade is initiated.

An excellent detailed description of the pathology, physiology and aetiology of atherosclerosis is described in the book by Schettler and Boyd [5] and in a recent article in the Scientific American [13].

The formation of an advanced lesion results in (partial) occlusion of the artery. The tissue behind the occlusion will therefore not be supplied with (sufficient) oxygen or nutrients. This leads to severe complications, such as a heart attack or a stroke, and necrosis of tissue.

There are several methods to restore the blood flow at the site of an atherosclerotic lesion. One of the methods is the bypass technique. In this technique, the blood flow is diverted using healthy veins to bypass one or more occluded arteries. The healthy vein originates from the patient himself, usually from the leg. Instead of autologous blood vessels, artificial blood vessels can be used as well. Disadvantages of this technique are the need for surgery, which is a burden for the patient and costly. Consequently, bypass surgery is only performed on lesions with severe stenosis. [14]. A technique, which minimizes the disadvantages of bypass grafting is percutaneous transluminal angioplasty (PTA) and is nowadays most often used. Except for lesions with severe stenosis, PTA has a higher success rate than bypass grafting [14].

PTA

PTA is a minimal invasive procedure and is performed under X-ray guidance. The patient is given a mild sedative to help him relax but remains awake during the procedure to allow him to answer questions regarding his comfort level, any chest pain or shortness of breath. A guide wire is inserted through an artery in the groin or arm. Contrast fluid is injected into the artery and angiography is performed to determine the location and percentage of the stenosis. X-ray is used to guide the wire up into the atherosclerotic artery. The guide wire is flexible, which enables it to reach places that are difficult to access. Subsequently, a catheter with a deflated balloon on the tip is inserted by moving it over the guide wire until the place of stenosis is reached. The balloon is then inflated with contrast fluid and deflated. The contrast fluid is used to monitor the procedure under radioscopy. The inflation and deflation procedure is repeated until the plaque is deformed to such an extent that the diameter equals the original diameter of the artery.

By dilating the lesion, the atherosclerotic plaque will fracture and dissect. The internal elastic lamina and underlying media are often fractured as well [11]. Dilation of the lesion results in vascular remodeling after retraction of the balloon catheter [15]. The formation of tears and dissections upon dilation will trigger a healing process, leading to abnormal multiplication of cells in the intima (termed intimal hyperplasia), which may lead to reocclusion of the artery. This process of reocclusion is called restenosis and takes place in 30 to 50% of the patients with successfully treated coronary lesions within three to six months after the treatment [16].

RESTENOSIS

Although the mechanism of restenosis is not fully understood, it is recognized that intimal hyperplasia and vascular remodeling play an important role in this process [15,17]. Intimal hyperplasia is the response to balloon angioplasty, initiated by the release of platelet-derived growth factor by injured endothelium and by an angiogenic factor released as a result from adventitial irritation. This leads to platelet activation and the infiltration of monocytes/macrophages in the region of the arterial injury [18]. These leukocytes release

several growth factors, such as basic fibroblast growth factor and transforming growth factor-β [19]. As a result, smooth muscle cells in the media change their phenotype from contractile to synthetic [20]. The synthetic smooth muscle cells migrate from the media to the intima and proliferate [20,21]. These synthetic smooth muscle cells synthesize and secrete extracellular matrix including collagen, resulting in intimal thickening [20]. Vascular remodeling is the elastic response of the artery after dilation and the extensive collagen production in the adventitia to compensate for intimal thickening [22]. Migration of the smooth muscle cells occurs within 2-5 days after PTA [20]. The proliferation of smooth muscle cells peaks at day 7 and returns to normal level both in media and intima between 14-28 days [15,23,24].

The restenotic lesion can be treated with the same techniques as described before for the treatment of atherosclerotic lesions. However, reducing the incidence of restenosis after PTA is preferred. This can be achieved by stenting, by medication or a combination of both.

REDUCING THE INCIDENCE OF RESTENOSIS

Stenting

A successful approach to reduce the incidence of restenosis is the introduction of a stent. A stent is a coil of wire that is introduced at the place of the stenosis and expanded to a diameter that is equal to the diameter of the undiseased artery. The stent is expanded with an angioplasty balloon catheter. Because of the rigid structure, stents provide mechanical strength, which minimizes the process of vascular remodeling [25]. As the diameter after stenting is larger than after PTA, the higher tissue growth in and around the stent does not lead to a smaller final inner diameter [26]. Compared to PTA, stenting leads to a decrease in the incidence of restenosis [26-28]. Nevertheless, stented small arteries tend to reocclude more easily than stented large arteries and conditions where excessive smooth muscle cell response occurs (e.g. in diabetics) lead to relatively high in-stent restenosis [26]. Due to a decrease in the incidence of restenosis, stents are nowadays also used in more complex lesions, resulting in an overall in-stent restenosis of 10 to 50% of the stented lesions [29].

Medication

Another approach to decrease the incidence of restenosis is drug administration. Initially drugs that inhibit specific pathways in the development of restenosis were administered systemically. These include drugs that inhibit platelet adhesion and activation (e.g. aspirin and GP IIb/IIIa receptor inhibitors), coagulation (e.g. heparin, hirudin), cell proliferation (e.g. heparin, colchicine, platelet-derived growth factor antagonist) and inflammation (e.g. corticosteroids) [30]. However, none of the systemically administered drugs have clearly demonstrated a reduction of the incidence of restenosis [25]. The main reason for this is the low drug concentration at the site of the lesion. Since increasing the local drug concentration

by using higher doses leads to adverse side effects, other methods have been developed to achieve a more efficient way of delivering the drug to the site of arterial injury.
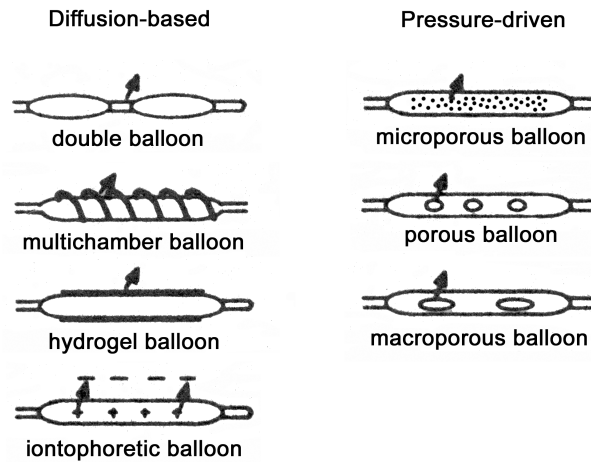
Figure 2.2 *Schematic representation of several types of drug delivery devices, divided in two categories, based on their mode of delivery: diffusion-based and pressure-driven.*

In local intravascular drug delivery, drugs are delivered to the injured arterial wall segment from the luminal side of the artery using several types of drug delivery catheters. These can be divided in two categories, based on their mode of delivery: diffusion-based and pressure-driven (Figure 2.2) [31-33].

Diffusion-based balloon catheters. These were the first balloon catheters used for drug delivery. Diffusion of the drug into the arterial wall takes place from an infusion channel (double balloon), a perfusion canal (multichamber balloon), a hydrogel (hydrogel balloon) or pores (iontophoretic balloon). The latter uses a low-energy electrical field to create a gradient, which causes charged drugs to move. The main disadvantage of diffusion-based delivery devices is the low efficiency of delivery as the penetration depth of the drug is low and therefore, the drug is rapidly washed out by the blood flow.

Pressure-driven balloon catheters. In pressure-driven devices, the drug is forced into the arterial wall using balloon catheters containing pores of different sizes (8 μm: microporous, 25 μm: porous and 75 μm: macroporous). The advantage of pressure-driven devices is that they are more efficient than diffusion-based catheters and can be used for any kind of drug (in contrast to the iontophoretic balloon catheter). An important limitation of the pressure-driven devices is that they may cause additional vessel injury due to jet-like streams. Of the pressure-driven drug delivery catheters, jet formation is lowest for the microporous balloon catheter and hardly any additional trauma to the blood vessel is expected with the use of this balloon catheter.

Although drug delivery using balloon catheters can be accompanied by additional injury to the artery due to the applied pressures, it has the advantage that it can be applied simultaneously with a standard PTA intervention. The first local drug delivery balloon catheters that have been approved for intracoronary drug infusion by the US Food and Drug

Administration (FDA) were the Dispatch delivery catheter (SciMed Inc.) and InfusaSleeve (Localmed, Inc.) in 1996 [16].

Potentially therapeutic drugs have been injected into the arterial wall after PTA via a porous balloon catheter [34]. It was shown that because of blood flow via the vasa vasorum, drugs injected as an aqueous solution had a short residence time in the arterial wall [35,36]. Lipophilic drugs have relatively long residence times when locally delivered to arteries *in vivo* and may therefore be more efficient than hydrophilic substances [37]. Since lipophilic drugs are poorly water-soluble, drug carriers can be used to solubilize the drugs. Due to the slow diffusion of drug carriers in the arterial wall, their residence time is higher than of free drugs [38].

Drug carriers

Drug carriers that have been used for the delivery of drugs to the arterial wall can be divided in micro- and nanoparticles. In general, microparticles can be particles that consist of a more or less homogeneous polymeric matrix, with the drug dispersed throughout the particle matrix. In literature these particles are referred to as microspheres. Microparticles can also be vesicles or microcapsules that consist of an outer barrier layer that includes a drug in a liquid inner phase. For drug delivery to the arterial wall only microspheres have been used.

Microspheres with a diameter of 5 μm have been administered to atherosclerotic rabbit arteries via a porous balloon catheter, as first shown in 1991 by Wilensky *et al.* [38]. These particles were merely introduced to the adventitia and neointima, with hardly any particles present in the media [38]. When fluorescent labeled microparticles of approximately 1 μm were administered to rabbit carotid arteries using a porous balloon catheter, they were mainly present in the media and adventitia, some even up to 4 weeks [36]. Other researchers also found that compared to particles of 4.5 μm particles of 1 μm are mainly present in the media [39]. Particles as large as 11 μm were administered to atherosclerotic rabbit femoral arteries using a porous balloon catheter. The particles were mainly present in the periadventitial microvasculature [40], supporting the idea that the vasa vasorum plays an important role in the transport of particles to the adventitia. The administration efficiency of these particles was approximately 0.15% [40].

The *in vivo* effect of colchicine-loaded biodegradable (PLGA) microparticles (6-8 μm) on restenosis was first studied by Gradus-Pizlo *et al.* in 1995 [41]. Although after drug delivery colchicine was present in the wall of atherosclerotic rabbit arteries, no beneficial effect on restenosis was observed [41]. Dev *et al.* [36] administered colchicine- and dexamethasone-loaded PLA microparticles to rabbit carotid arteries using a porous balloon catheter. Although these particles showed sustained drug release *in vitro* and the particles remained in the arterial wall up to 4 weeks, no reduction in restenosis was observed.

Due to the large size of microparticles, these particles are only introduced into the arterial wall by large tears in the arterial wall caused by the PTA or local drug delivery procedure or

via the vasa vasorum [36,38,40]. Although the formation of large tears facilitates particle administration [39], the particles will only be present in close proximity to the tears in the arterial wall. Furthermore, the formation of large tears can induce additional intimal proliferation [33] and thus increase the incidence of restenosis. As nanoparticles may be introduced to all layers of the arterial wall due to their small size, the administration of biodegradable drug-loaded nanoparticles may be a good alternative to microparticles. Furthermore, in contrast to microparticles, the penetration of nanoparticles into the arterial wall is relatively a-traumatic [39,42] and nanoparticles can be actively taken up by smooth muscle cells [43].

In general, nanoparticles prepared from polymers can be divided in three different categories, depending on their structure. Capsules are the first category. Nanocapsules are vesicular systems in which a liquid core is surrounded by a polymeric membrane [44]. Another example of a vesicular system are the liposomes. In an aqueous environment, phospholipid molecules form a lipid bilayer, resulting in the formation of liposomes. Several types of liposomes can be prepared, including uni-laminar, multi-laminar, and multi-vesicular [45]. The size of liposomes can range from 0.01 to 10 μm for uni-laminar and multi-laminar vesicles, respectively, and from 10 to 100 μm for multi-vesicular liposomes. The disadvantages of liposomes are the unreliable reproducibility of liposomes [44] and exchange of phospholipids with certain blood components [46].

The second category are polymeric micelles. Micelles are amphiphilic in nature and can be composed of low molecular weight surfactants or block copolymers. Low molecular weight surfactants do not form stable micelles that are suited for drug delivery. In the case of block copolymers, micelles are composed of a hydrophobic core surrounded by a hydrophilic shell when placed in an aqueous surrounding [47-51]. This core-shell structure enables the solubilization of hydrophobic drugs in the core. Micelles are spherical and fairly monodisperse in terms of size [49]. The micelles are formed spontaneously above a certain copolymer concentration: the critical micelle concentration (CMC) [52]. The CMC depends on the temperature and the balance of core-forming and shell-forming blocks [53]. The size of the micelles depends on the same factors [54].

The third category of nanoparticles are particles that consist of a more or less homogeneous polymeric matrix. Analogous to microspheres, these particles are generally referred to as nanospheres. These particles are larger than micelles and may be more polydisperse in terms of size [49].

In the preparation of particles for drug delivery systems, biodegradable materials are preferably used to prevent that polymer remains in the body, once the drug has been released. These materials can be roughly divided in two categories: biological and synthetic polymers.

Examples of biological polymers that are used to prepare biodegradable particles are proteins such as albumin [55-62] or gelatin [46,63-66]. An advantage of particles that are based on proteins is that they contain functional COOH- and NH_2-groups [55], which can be used for

mild cross-linking or (surface) modification chemistry [66]. Furthermore, since albumin is not body foreign, no adverse tissue reactions are expected. Although particles based on proteins are suitable for the incorporation of hydrophilic drugs, it is difficult to load them with hydrophobic drugs [46]. Furthermore, although the proteins themselves are biocompatible, potentially antigenic material may be associated with them [44]. Another disadvantage of biodegradable particles based on biological polymers is that tuning of, for instance, mechanical properties or rate of degradation is not straightforward.

Particles based on synthetic polymers offer an interesting alternative, because they possess good stability in biological fluids [44]. Commonly used biodegradable synthetic polymers include polyesters, such as poly(lactic acid) (PLA), poly(hydroxybutyrate) (PHB), poly(lactic-co-glycolic acid) (PLGA) and poly(ε-caprolactone) (PCL). These polyesters are known for their biodegradability and biocompatibility [67-74]. The use of biodegradable polyester copolymers, e.g. PLGA, offers the possibility to tune properties, such as rate of degradation and mechanical characteristics, by changing the molecular weight and/or the molar composition of these copolymers.

Also block copolymers based on poly(ethylene oxide) (PEO) and PLGA (PEO-PLGA) are employed for the preparation of nanoparticles. Depending on the preparation method, PEO will be present at the surface of the particles. The presence of PEO at the surface of particles decreases protein adsorption [75] and prolongs the blood circulation time as it reduces the recognition of the particles by the reticuloendothelial system [76,77]. PEO is an uncharged, highly flexible polymer that has been used because of its outstanding physiochemical properties including solubility in water and in organic solvents [78]. PEO is known to be non-toxic, non-antigenic and non-immunogenic. It has been shown that PEO with a molecular weight less than $6 \cdot 10^3$ g/mol is removed from the circulation via the kidneys [79].

In general, four methods can be distinguished by which nanoparticles that are based on synthetic polymers can be prepared. These are termed the emulsification-evaporation, solvent-displacement, salting-out, and emulsification-diffusion method [44]. In the *emulsification-evaporation method* a water-immiscible solvent, generally dichloromethane or chloroform is used as organic solvent. Solvent evaporation after emulsification results in particle formation [76,80-83]. In the *solvent-displacement method* polymer is dissolved in a semi-polar water-miscible solvent, such as acetone or ethanol. This organic phase is poured or injected into an aqueous phase under magnetic stirring and particles are formed, after which the solvent is removed by evaporation [84,85]. The *salting-out method* consists of the emulsification of polymer dissolved in a water-miscible solvent (e.g. acetone or tetrahydrofuran) in a nearly saturated aqueous salt solution. After emulsification the addition of water results in the formation of particles. The water-miscible solvent is removed by ultracentrifugation or cross-flow filtration [86-91]. The *emulsification-diffusion method* is similar to the salting-out method. Instead of using salt to saturate the aqueous phase, a partially water-soluble solvent (e.g. benzyl alcohol or ethyl acetate) is used to saturate the aqueous phase. After

emulsification the addition of water results in the formation of particles. Depending on the boiling point of the partially water-soluble solvent, it is either removed by evaporation or cross-flow filtration [44,92].

All four methods are suitable for the incorporation of hydrophobic drugs into biodegradable nanoparticles, yet less suitable for the incorporation of hydrophilic drugs. In all four methods, the hydrophobic drug is added to the organic phase and is incorporated in the hydrophobic core of the nanoparticles after removal of the organic solvent.

The salting-out method has some advantages over the other three methods. It is possible to incorporate high amounts of drug, excellent nanoparticle yields can be obtained, no chlorinated solvents are used, and the scaling-up of the process can be easily carried out. Furthermore, this technique is well suited for the incorporation of thermally unstable drugs, since no elevated temperatures are used.

Surface characteristics, such as surface charge, might be important for the introduction of nanoparticles to the arterial wall. In *ex vivo* and *in vivo* studies it was shown that the concentration of positively charged particles in the arterial wall was higher than of negatively charged particles which may be caused by the electrostatic affinity of the positively charged particles for the negatively charged glycosaminoglycans of the arterial wall [93]. Besides the surface charge, specific targeting of particles increases the efficiency of administration of particles to the arterial wall. The use of particles as drug carriers gives the possibility to provide particles with a targeting moiety that has a high affinity for specific cell types that are present in restenotic arterial segments, e.g. activated smooth muscle cells [94,95], macrophages [21], or dysfunctional endothelium [96-98] or to provide particles with targeting moieties that bind to microvasculature (e.g. vasa vasorum and regions of neovascularization) [99].

Biodegradable fluorescent labeled PLGA nanoparticles (165 nm) have been administered to rat carotid arteries using porous balloon catheters and it was concluded that they were successfully introduced to the vessel wall [16]. After 3 h most of the particles were present at the luminal surface of the artery and some in the adventitia. After 24 h, more particles were present in the adventitia, and some in the media, whereas after 3 d, particles were only present in the adventitia in the form of clusters. This can be explained by the transport of particles via the vasa vasorum to the adventitia. Since the vasa vasorum reaches the media, this explains the presence of particles in the media [100]. At day 7, the fluorescent activity decreased, and dropped to zero at day 14. When dexamethasone-loaded PLGA particles were administered in the same experimental setting, a 31 % reduction in restenosis was observed [16].

Banai *et al.* [101] administered biodegradable PLA nanoparticles (130 nm) loaded with a tyrphostin (a low-molecular weight, synthetic compound that blocks specific receptors for smooth muscle cell proliferation as shown by perivascular delivery [102]) to the vessel wall, causing an inhibition of neointimal formation. No data was given on the exact position of the particles in the vessel wall. It was reported, that hardly any inflammatory reaction was

provoked by the PLA particles [101], and that the particles themselves did not interfere with smooth muscle cells and therefore had no effect on smooth muscle cell proliferation [103].

Drug-eluting stents

Since stenting and local drug delivery reduce the incidence of restenosis, the combination of both is expected to reduce the incidence of restenosis even further. This has been demonstrated by the use of polymer-coated, drug-eluting stents [104,105]. Besides as a drug depot, the polymer coating can be used to regulate the drug release rate [104]. It was shown in clinical trials that the use of rapamycin-eluting stents inhibited restenosis completely [104,105], due to the inhibition of vascular smooth muscle cell proliferation [106]. These drug-eluting stents consisted of stents coated with a thin layer of a non-erodable copolymer of *n*-butyl methacrylate and ethylene-vinyl acetate containing rapamycin, which released rapamycin for more than 28 d. Also after 18 months, no delayed restenosis was observed [107].

Although drug-eluting stents inhibited restenosis completely, they are not biodegradable and are thus permanently present, which could lead to long-term adverse tissue reactions. However, no long-term (>18 months) studies on adverse reactions of drug-eluting stents have been performed yet.

CONCLUDING REMARKS

Restenosis is the most important drawback of the techniques that are currently used in the treatment of atherosclerotic lesions, such as balloon angioplasty and stenting. An important step in the process that leads to restenosis is the activation of the migration and proliferation of smooth muscle cells. Therefore, the delivery of drugs that inhibit migration and proliferation of smooth muscle cells seems a promising approach to reduce the incidence of restenosis. As smooth muscle cell migration and proliferation take place in the first 4 weeks after treatment, sustained drug delivery for at least one month is desirable.

As systemic administration of drugs appeared to be inefficient and hampered by toxic side effects, several local drug delivery approaches were studied. The most promising approaches are the use of drug-eluting stents and the local delivery of biodegradable drug-loaded nanoparticles. In the latter approach drug delivery can be combined with a standard balloon angioplasty procedure. The use of biodegradable nanoparticles prevents long-term inflammatory reactions. The aim of this study was therefore to prepare drug-loaded biodegradable nanoparticles by which a sustained release for more than one month of a drug that inhibits the migration and proliferation of smooth muscle cells can be achieved. Consequently, the degradation time of the drug-loaded nanoparticles should exceed one month.

REFERENCES

1. McGill, H.C.; McMahan, C.A.; Malcom, G.T.; Oalmann, M.C. and Strong, J.P., *Arterioscler. Thromb. Vasc. Biol.,* **1997**, *17*, 95-106.

2. Reitsma, J.B. and Bonsel, G.J. *Hart- en vaatziekten in Nederland 2001, cijfers over ziekte en sterfte*; Nederlandse Hartstichting: Den Haag, **2001**.

3. [Online]: http://dukemednews.duke.edu/news/healthtip.php?id=1728, February **2001**.

4. Pathobiological Determinants of Atherosclerosis in Youth (PDAY) Research Group, *Arterioscler. Thromb.,* **1993**, *13*, 1291-1298.

5. Schettler, F.G. and Boyd, G.S. *Atherosclerosis - Pathology, physiology, aetiology, diagnosis and clinical management*; Elsevier: Amsterdam, **1969**.

6. Botti, T.P.; Amin, H.; Hiltscher, L.; Wissler, R.W.; Robertson, A.L.; Strong, J.P.; Cornhill, J.F.; McGill, H.C.; McMahan, C.A.; Oalmann, M.C. *et al.*, *Atherosclerosis,* **1996**, *124*, 191-202.

7. Stevens, A. and Lowe, J.S. *Human histology*; 2nd ed.; Mosby: London, **1997**.

8. Beurskens, H. *De bloedstolling: thrombose, atherosclerose en het hartinfarct*; Natuur en techniek: Diemen, **1979**.

9. Consigny, P.M., *Am. J. Röntgenol.,* **1995**, *164*, 553-558.

10. Ross, R., *Nature,* **1993**, *362*, 801-809.

11. Geary, R.L.; Williams, J.K.; Golden, D.; Brown, D.G.; Benjamin, M.E. and Adams, M.R., *Arterioscler. Thromb. Vasc. Biol.,* **1996**, *16*, 34-43.

12. Mayr, M. and Xu, Q., *Exp. Gerontol.,* **2001**, *36*, 969-987.

13. Libby, P. In *Scientific American,* May **2002**.

14. Rutherford, R.B., *Cardiovasc. Surg.,* **1999**, *7*, 5-12.

15. Johnson, L.L.; Schofield, L.M.; Verdesca, S.A.; Sharaf, B.L.; Jones, R.M.; Virmani, R. and Khaw, B.A., *J. Nucl. Med.,* **2000**, *41*, 1535-1540.

16. Guzman, L.A.; Labhasetwar, V.; Song, C.; Jang, Y.; Lincoff, M.; Levy, R. and Topol, E.J., *Circulation,* **1996**, *94*, 1441-1448.

17. Huehns, T.Y.; Gonschior, P. and Höfling, B., *Heart,* **1996**, *75*, 537-538.

18. Haudenschild, C. and Studer, A., *Eur. J. Clin. Invest.,* **1971**, *2*, 1-7.

19. Lincoff, A.M.; Topol, E.J. and Ellis, S.G., *Circulation,* **1994**, *90*, 2070-2084.

20. Murakami, S.; Toda, Y.; Seki, T.; Munetomo, E.; Kondo, Y.; Sakurai, T.; Furukawa, Y.; Matsuyama, M.; Nagate, T.; Hosokawa, N. *et al.*, *Atherosclerosis,* **2001**, *157*, 361-368.

21. Nagae, T.; Louie, A.Y.; Aizawa, K.; Ishimaru, S. and Wilson, S.E., *J. Cardiovasc. Surg.,* **1998**, *39*, 709-715.

22. Fishbein, I.; Chorny, M.; Rabinovich, L.; Banai, S.; Gati, I. and Golomb, G., *J. Control. Release,* **2000**, *65*, 221-229.

23. Fingerle, J.; Müller, R.M.K.; Kuhn, H.; Pech, M. and Baumgartner, H.R., *Arterioscler. Thromb. Vasc. Biol.,* **1995**, *15*, 1945-1950.

24. Zeymer, U.; Fishbein, M.C.; Forrester, J. and Cercek, B., *Am. J. Pathol.,* **1992**, *141*, 685-690.

25. Chorny, M.; Fishbein, I. and Golomb, G., *Crit. Rev. Ther. Drug Carrier Syst.,* **2000**, *17*, 249-284.

26. Gershlick, A.H., *Atherosclerosis,* **2002**, *160*, 259-271.

27. Serruys, P.W.; De Jaegere, P.; Kiemeneij, F.; Macaya, C.; Rutsch, W.; Heyndrickx, G.; Emanuelsson, H.; Marco, J.; Legrand, V.; Materne, P. *et al.*, *N. Engl. J. Med.,* **1994**, *331*, 489-495.

28. Fischman, D.L.; Leon, M.B.; Baim, D.S.; Schatz, R.A.; Savage, M.P.; Penn, I.; Detre, K.; Veltri, L.; Ricci, D.; Nobuyoshi, M. *et al.*, *N. Eng. J. Med.,* **1994**, *331*, 496-501.

29. Lowe, H.C.; Oesterle, S.N. and Khachigian, L.M., *J. Am. Coll. Cardiol.,* **2002**, *39*, 183-193.

30. Liu, M.W.; Roubin, G.S. and King, S.B., *Circulation,* **1989**, *79*, 1374-1387.

31. Gonschior, P.; Wilensky, R.; March, K. and Höfling, B., *Zeitschrift für Kardiologie,* **1996**, *85*, 155-165.

32. Bailey, S.R., *Prog. Cardiovasc. Dis.,* **1997**, *40*, 183-204.

33. Alfke, H.; Wagner, H.J.; Calmer, C. and Klose, K.J., *Cardiovasc. Intervent. Radiol.,* **1998**, *21*, 50-56.

34. Wolinsky, H. and Thung, S.N., *J. Am. Coll. Cardiol.,* **1990**, *15*, 475-481.

35. Mitchel, J.F.; Fram, D.B.; Palme, D.F.; Foster, R.; Hirst, J.A.; Azrin, M.A.; Bow, L.M.; Eldin, A.M.; Waters, D.D. and McKay, R.G., *Circulation,* **1995**, *91*, 785-793.

36. Dev, V.; Eigler, N.; Fishbein, M.C.; Tian, Y.; Hickey, A.; Rechavia, E.; Forrester, J.S. and Litvack, F., *Cathet. Cardiovasc. Diagn.,* **1997**, *41*, 324-332.

37. Lambert, T.L.; Dev, V.; Rechavia, E.; Forrester, J.S.; Litvack, F. and Eigler, N.L., *Circulation,* **1994**, *90*, 1003-1011.

38. Wilensky, R.L.; March, K.L. and Hathaway, D.R., *Am. Heart J.,* **1991**, *122*, 1136-1140.

39. Nasser, T.K.; Wilensky, R.L.; Mehdi, K. and March, K.L., *Am. Heart J.,* **1996**, *131*, 892-898.

40. Wilensky, R.L.; March, K.L.; Gradus-Pizlo, I.; Schauwecker, D.; Michaels, M.B.; Robinson, J.; Carlson, K. and Hathaway, D.R., *Am. Heart J.,* **1995**, *129*, 852-859.

41. Gradus-Pizlo, I.; Wilensky, R.L.; March, K.L.; Fineberg, N.; Michaels, M.; Sandusky, G.E. and Hathaway, D.R., *J. Am. Coll. Cardiol.,* **1995**, *26*, 1549-1557.

42. Valero, F.; Hamon, M.; Fournier, C.; Meurice, T.; Flautre, B.; Van Belle, E.; Lablanche, J.-M.; Gosselin, B.; Bauters, C. and Bertrand, M., *J. Cardiovasc. Pharm.,* **1998**, *31*, 513-519.

43. Suh, H.; Jeong, B.M.; Liu, F. and Kim, S.W., *Pharm. Res.,* **1998**, *15*, 1495-1498.

44. Quintanar-Guerrero, D.; Allémann, E.; Fessi, H. and Dölker, E., *Drug Dev. Ind. Pharm.,* **1998**, *24*, 1113-1128.

45. Peyman, G.A. and Ganiban, G.J., *Adv. Drug Deliv. Rev.,* **1995**, *16*, 107-123.

46. Cascone, M.G.; Lazzeri, L.; Carmignani, C. and Zhu, Z.H., *J. Mater. Sci. - Mater. Med.,* **2002**, *13*, 523-526.

47. Torchilin, V.P., *J. Microencapsul.,* **1998**, *15*, 1-20.

48. Couvreur, P.; Dubernet, C. and Puisieux, F., *Eur. J. Pharm. Biopharm.,* **1995**, *41*, 2-13.

49. Kwon, G.S., *Crit. Rev. Ther. Drug Carrier Syst.,* **1998**, *15*, 481-512.

50. Magenheim, B. and Benita, S., *S.T.P. Pharma Sci.,* **1991**, *1*, 221-241.

51. Allémann, E.; Gurny, R. and Dölker, E., *Eur. J. Pharm. Biopharm.,* **1993**, *39*, 173-191.

52. Thurmond, K.B.; Kowalewski, T. and Wooley, K.L., *J. Am. Chem. Soc.,* **1997**, *119*, 6656-6665.

53. Hecht, E. and Hoffmann, H., *Colloids Surf. A - Physicochem. Eng. Asp.,* **1995**, *96*, 181-197.

54. Kabanov, A.V.; Nazarova, I.R.; Astafieva, I.V.; Batrakova, E.V.; Alakhov, V.Y.; Yaroslavov, A.A. and Kabanov, V.A., *Macromolecules,* **1995**, *28*, 2303-2314.

55. Lin, W.; Garnett, M.C.; Davies, M.C.; Bignotti, F.; Ferruti, P.; Davis, S.S. and Illum, L., *Biomaterials,* **1997**, *18*, 559-565.

56. Winoto, S. and Müller, W., *Eur. J. Pharm. Biopharm.,* **1995**, *41*, 55-61.

57. Lin, W.; Coombes, A.G.A.; Davies, M.C.; Davis, S.S. and Illum, L., *J. Drug Target.,* **1993**, *1*, 237-243.

58. Müller, B.G.; Leuenberger, H. and Kissel, T., *Pharm. Res.,* **1996**, *13*, 32-37.

59. Lin, W.; Coombes, A.G.A.; Garnett, M.C.; Davies, M.C.; Schacht, E.; Davis, S.S. and Illum, L., *Pharm. Res.,* **1994**, *11*, 1588-1592.

60. Lin, W.; Garnett, M.C.; Ferruti, P.; Davis, S.S. and Illum, L., *J. Control. Release,* **1997**, *48*, 329-331.

61. Nakagawa, Y.; Takayama, K.; Ueda, H.; Machida, Y. and Nagai, T., *Drug Design and Deliv.,* **1987**, *2*, 99-107.

62. Chen, G.Q.; Lin, W.; Coombes, A.G.A.; Davis, S.S. and Illum, L., *J. Microencapsul.,* **1994**, *11*, 395-407.

63. Nahman, N.S.; Drost, W.T.; Bhatt, U.Y.; Sferra, T.J.; Johnson, A.; Gamboa, P.; Hinkle, G.H.; Haynam, A.; Bergdall, V.; Hickey, C. *et al.*, *Biomed. Microdevices,* **2002**, *4*, 189-195.

64. Wang, W.; Antonsen, K. and Nayar, R., *Pharm. Dev. Technol.,* **2002**, *7*, 169-180.

65. Morita, T.; Horikiri, Y.; Suzuki, T. and Yoshino, H., *Int. J. Pharm.,* **2001**, *219*, 127-137.

66. Morimoto, K.; Katsumata, H.; Yabuta, T.; Iwanaga, K.; Kakemi, M.; Tabata, Y. and Ikada, Y., *Eur. J. Pharm. Sci.,* **2001**, *13*, 179-185.

67. Juni, K. and Nakano, M., *Crit. Rev. Ther. Drug Carrier Syst.,* **1987**, *3*, 209-232.

68. Lemoine, D.; Francois, C.; Kedzierewicz, F.; Preat, V.; Hoffman, M. and Maincent, P., *Biomaterials,* **1996**, *17*, 2191-2197.

69. Yamaguchi, K. and Anderson, J.M., *J. Control. Release,* **1993**, *24*, 81-93.

70. Anderson, J.M. and Shive, M.S., *Adv. Drug Deliv. Rev.,* **1997**, *28*, 5-24.

71. Gautier, S.E.; Oudega, M.; Fragoso, M.; Chapon, P.; Plant, G.W.; Bunge, M.B. and Parel, J.M., *J. Biomed. Mater. Res.,* **1998**, *42*, 642-654.

72. Ignatius, A.A. and Claes, L.E., *Biomaterials,* **1996**, *17*, 831-839.

73. Piskin, E., *J. Biomater. Sci. Polym. Ed.,* **1994**, *6*, 775-795.

74. Ronneberger, B.; Kao, W.J.; Anderson, J.M. and Kissel, T., *J. Biomed. Mater. Res.,* **1996**, *30*, 31-40.

75. Gref, R.; Luck, M.; Quellec, P.; Marchand, M.; Dellacherie, E.; Harnisch, S.; Blunk, T. and Muller, R.H., *Colloids Surf. B - Biointerfaces,* **2000**, *18*, 301-313.

76. Gref, R.; Minamitake, Y.; Peracchia, M.T.; Trubetskoy, V.; Torchilin, V. and Langer, R., *Science,* **1994**, *263*, 1600-1603.

77. Allémann, E.; Brasseur, N.; Benrezzak, O.; Rousseau, J.; Kudrevich, S.V.; Boyle, R.W.; Leroux, J.-C.; Gurny, R. and Van Lier, J.E., *J. Pharm. Pharmacol.,* **1995**, *47*, 382-387.

78. Uhrich, K.E.; Cannizzaro, S.M.; Langer, R.S. and Shakesheff, K.M., *Chem. Rev.,* **1999**, *99*, 3181-3198.

79. Shaffer, C.B. and Critchfield, F.H., *Am. J. Pharm. Assoc.,* **1947**, *36*, 152-157.

80. Vandorpe, J.; Schacht, E.; Dunn, S.; Hawley, A.; Stolnik, S.; Davis, S.S.; Garnett, M.C.; Davies, M. and Illum, L., *Biomaterials,* **1997**, *18*, 1147-1152.

81. Gref, R.; Domb, A.; Quellec, P.; Blunk, T.; Müller, R.H.; Verbavatz, J.M. and Langer, R., *Adv. Drug Deliv. Rev.,* **1995**, *16*, 215-233.

82. Peracchia, M.T.; Gref, R.; Minamitake, Y.; Domb, A.; Lotan, N. and Langer, R., *J. Control. Release,* **1997**, *46*, 223-231.

83. Stolnik, S.; Illum, L. and Davis, S.S., *Adv. Drug Deliv. Rev.,* **1995**, *16*, 195-214.

84. Dunn, S.E.; Coombes, A.G.A.; Garnett, M.C.; Davis, S.S.; Davies, M.C. and Illum, L., *J. Control. Release,* **1997**, *44*, 65-76.

85. Fessi, H.; Puisieux, F.; Devissaguet, J.-P.; Ammoury, N. and Benita, S., *Int. J. Pharm.,* **1989**, *55*, R1-R4.

86. Dölker, E.; Bindschädler, C. and Gurny, R., Process for preparing a powder of water-insoluble polymer which can be redispersed in a liquid phase, the resulting powder and utilization thereof, **1990**, EP 0 363 549.

87. Ibrahim, H.; Bindschädler, C.; Dölker, E.; Buri, P. and Gurny, R., *Int. J. Pharm.,* **1992**, *87*, 239-246.

88. Allémann, E.; Gurny, R. and Dölker, E., *Int. J. Pharm.,* **1992**, *87*, 247-254.

89. Allémann, E.; Leroux, J.-C.; Gurny, R. and Dölker, E., *Pharm. Res.,* **1993**, *10*, 1732-1737.

90. De Jaeghere, F.; Allémann, E.; Leroux, J.-C.; Stevels, W.; Feijen, J.; Dölker, E. and Gurny, R., *Pharm. Res.,* **1999**, *16*, 859-866.

91. Rafler, G. and Jobmann, M., *Pharm. Ind.,* **1997**, *59*, 620-624.

92. Quintanar-Guerrero, D.; Fessi, H.; Allémann, E. and Dölker, E., *Int. J. Pharm.,* **1996**, *143*, 133-141.

93. Labhasetwar, V.; Song, C.; Humphrey, W.; Shebuski, R. and Levy, R.J., *J. Pharm. Sci.,* **1998**, *87*, 1229-1234.

94. Pastore, C.J.; Isner, J.M.; Bachc, P.A.; Kearney, M. and Pickering, J.G., *Circ. Res.,* **1995**, *77*, 519-529.

95. Mattar, S.G.; Hanson, S.R.; Pierce, G.F.; Chen, C.; Hughes, J.D.; Cook, J.E.; Shen, C.; Noe, B.A.; Suwyn, C.R.; Scott, J.R. *et al., J. Surg. Res.,* **1996**, *60*, 339-344.

96. Wickham, T.J.; Haskard, D.; Segal, D. and Kovesdi, I., *Cancer Immunol. Immunother.,* **1997**, *45*, 149-151.

97. Hillis, G.S. and Flapan, A.D., *Heart,* **1998**, *79*, 429-431.

98. Giuffre, L.; Cordey, A.-S.; Monai, N.; Tardy, Y.; Schapira, M. and Spertini, O., *J. Cell Biol.,* **1997**, *136*, 945-956.

99. Dashwood, M.R.; Barker, S.G.E.; Muddle, J.R.; Yacoub, M.H. and Martin, J.F., *J. Cardiovasc. Pharm.,* **1993**, *22*, S343-S347.

100. Wolinsky, H. and Glagov, S., *Circ. Res.,* **1967**, *20*, 409-421.

101. Banai, S.; Wolf, Y.; Golomb, G.; Pearle, A.; Waltenberger, J.; Fishbein, I.; Schneider, A.; Gazit, A.; Perez, L.; Huber, R. *et al.*, *Circulation,* **1998**, *97*, 1960-1969.

102. Golomb, G.; Fishbein, I.; Banai, S.; Mishaly, D.; Moscovitz, D.; Gertz, S.D.; Gazit, A.; Poradosu, E. and Levitzki, A., *Atherosclerosis,* **1996**, *125*, 171-182.

103. Cleek, R.L.; Rege, A.A.; Denner, L.A.; Eskin, S.G. and Mikos, A.G., *J. Biomed. Mater. Res.,* **1997**, *35*, 525-530.

104. Rensing, B.J.; Vos, J.; Smits, P.C.; Foley, D.P.; van den Brand, M.; van der Giessen, W.J.; de Feijter, P.J. and Serruys, P.W., *Eur. Heart J.,* **2001**, *22*, 2125-2130.

105. Sousa, J.E.; Costa, M.A.; Abizaid, A.C.; Rensing, B.J.; Abizaid, A.S.; Tanajura, L.F.; Kozuma, K.; Van Langenhove, G.; Sousa, A.; Falotico, R. *et al.*, *Circulation,* **2001**, *104*, 2007-2011.

106. Klugherz, B.D.; Llanos, G.; Lieuallen, W.; Kopia, G.A.; Papandreou, G.; Narayan, P.; Sasseen, B.; Adelman, S.J.; Falotico, R. and Wilensky, R.L., *Coronary Artery Dis.,* **2002**, *13*, 183-188.

107. Tanabe, K.; Degertekin, M.; Regar, E.; Ligthart, J.M.R.; Van der Giessen, W.J. and Serruys, P.W., *Cathet. Cardiovasc. Intervent.,* **2002**, *57*, 65-68.

CHAPTER 3

The preparation of monodisperse biodegradable
polyester nanoparticles with a controlled size[*]

ABSTRACT

In local drug delivery, nanoparticles based on biodegradable polymers can function as vehicles with controlled drug release properties. To achieve a well-controlled drug release profile, control over the particle size is of great importance. Therefore, biodegradable polyester nanoparticles were prepared using the salting-out method. Process variables were varied to study the effect on the particle size. The monodisperse, spherical particles obtained were between 100 and 400 nm in size. It was found that the particle size could be adjusted by varying the process variables of which the polymer concentration had the most pronounced effect.

INTRODUCTION

The ability to deliver drugs locally is of great benefit to the treatment of many diseases. Nano- and microparticles can function as a drug carrier from which controlled delivery of the drug can be achieved. The particle size is an important parameter for the effectiveness of drug delivery. Particles of several microns, for example, get trapped in the lung capillaries [1]. Phagocytosis of particles is highest for particles between 1 and 2 μm in size, and gradually drops as particle size decreases [2]. Phagocytosis is reduced by the presence of poloxamer [3], poly(vinly alcohol) [4] and poly(ethylene oxide) [5] at the particle surface. Also in the local treatment of restenosis by employing nanoparticles as drug delivery vehicles, the particle size is of great importance, as only the delivery of sub-micron particles resulted in a prolonged residence time of the particles in the injured vessel wall [6].

In the preparation of nanoparticles for drug delivery systems, biodegradable polymers are preferably used to prevent that polymer remains in the body, once the drug has been released. FDA approved biodegradable polymers are the homopolymers of DL-lactide (PDLLA) and copolymers of DL-lactide and glycolide (PLGA). These polyesters are known for their biodegradability and biocompatibility [7-11]. Control over the degradation rate can be achieved by adjusting the ratio of DL-lactide and glycolide in the copolymer as hydrolysis increases with increasing glycolide content [12]. The drug release rate from particles is increased when the molecular weight is lowered due to faster drug diffusion [13] and possibly due to higher swelling, as the total number of hydroxyl end groups is higher.

One way to prepare nanoparticles is by dispersion of polymers [14]. The procedures for dispersing polymers are mostly based on multi-phase systems in which water-immiscible organic solvents, like chloroform and dichloromethane, are emulsified in an aqueous phase [15]. These solvents have the advantage of being volatile. However, the main drawback is their potential toxicity, which makes them less suitable for pharmaceutical applications. This can be overcome by applying the salting-out technique, described by Dölker *et al.* [16]. In this technique a water-miscible organic solvent (e.g. acetone) is emulsified in an aqueous phase saturated or nearly saturated with salt. This technique is also well suited for the incorporation of thermally unstable drugs, since no elevated temperatures are used. Furthermore, several other organic solvents (e.g. ethyl acetate and tetrahydrofuran) can be employed, which makes it a versatile technique for the preparation of drug-loaded particles.

The salting-out method has been successfully used in the preparation of particles of methacrylic acid copolymers [17], PDLLA [17-19] and cellulose acetate phthalate [20]. However, this method has never been used to prepare PLGA nanoparticles, nor has the influence of process variables on the size of PDLLA or PLGA particles been studied to elucidate the process variables that give good control over the particle size.

The aim of this work is to prepare biodegradable particles employing low molecular weight polyesters based on DL-lactic acid and glycolic acid, and to study the effect of process variables on the size of the nanoparticles.

MATERIALS AND METHODS

Materials

DL-lactide and glycolide were purchased from Purac Biochem b.v. (Gorinchem, The Netherlands). Stannous octoate and phosphotungstic acid were purchased from Sigma (St. Louis, USA) and used as received. Hexanol (Merck, Darmstadt, Germany) was distilled from calcium hydride (Acros Organics, New Jersey, USA) prior to use. Deuterated chloroform (CDCl₃) and magnesium chloride hexahydrate ($MgCl_2 \cdot 6H_2O$) were purchased from Merck (Darmstadt, Germany) and were used without further purification. Poly(vinyl alcohol) (PVA) ($\overline{M}_n = 2 \cdot 10^3$ g/mol; 75% hydrolyzed from poly(vinyl acetate) and $\overline{M}_n = 22 \cdot 10^3$ g/mol; 88% hydrolyzed from poly(vinyl acetate)) were purchased from Acros Organics (New Jersey, USA), PVA ($\overline{M}_n = 9\text{-}10 \cdot 10^3$ g/mol; 80% hydrolyzed from poly(vinyl acetate)) was purchased from Aldrich (Milwaukee, USA). All solvents used were of analytical grade.

Polymer synthesis

Low molecular weight polymers were synthesized by ring opening polymerizations of DL-lactide with glycolide with hexanol as an initiator and stannous octoate as a catalyst at 130 °C for 24 h.

Typically, a mixture of DL-lactide (10.1 g; 69.8 mmol) and glycolide (5.45 g; 47.0 mmol) with stannous octoate in pentane (5.0 ml; 1.89 g/l) and an appropriate amount of initiator (318 μl hexanol; 2.53 mmol) were transferred to an ampoule. After removal of pentane by applying vacuum, the ampoule was evacuated, vacuum-sealed and subsequently transferred to an oil bath of 130 °C. After 24 h of reaction, the crude product was dissolved in chloroform, precipitated into a ten-fold volume of methanol and dried in vacuo at 40 °C for three days.

Synthesis of high molecular weight polymer was performed in the same manner, with the exception that no initiator was added, and that the polymerization time was 3 days [21].

The synthesized (co)polymers are denoted PDLLA for the low molecular weight homopolymer of DL-lactide, HMW PDLLA for the high molecular weight homopolymer of DL-lactide and PLGAx/y for the copolymer of DL-lactide with glycolide. The symbols x and y denote the molar percentages of lactyl and glycolyl units in the polymer, respectively.

Polymer characterization

The number average molecular weight ($\overline{M}_n$) and the composition of the (co)polymers were determined by ¹H-NMR, performed using a Varian Inova (Varian, Palo Alto, USA) operating at 300 MHz, with CDCl₃ as the solvent.

The $\overline{M}_n$ and the molecular weight distribution of the (co)polymers were determined by gel permeation chromatography (GPC) in chloroform (10 mg/ml) at 25 °C and a flow rate of 1.5 ml/min. The GPC setup consisted of a Waters Model 510 pump, a HP Ti-Series 1050 autosampler, a Waters Model 410 Differential Refractometer, and a Viscotek H502 Viscometer Detector with HR0.5, HR2 and HR4 Waters Ultra-Styragel columns (Waters, Milford, USA) placed in series. For the high molecular weight polymer the same setup was used, with the exception that HR1, HR2, HR4 and HR5 Waters Ultra-Styragel columns (Waters, Milford, USA) were placed in series. Polystyrene standards with narrow molecular weight distributions (PSS, Mainz, Germany) were used for calibration.

The thermal properties of the synthesized materials were evaluated by differential scanning calorimetry (DSC) using a DSC 7 (Perkin-Elmer, Shelton, USA). A heating rate of 10 °C/min was applied, and aluminum pans (Perkin-Elmer) were used. The copolymer samples (5-10 mg) were

heated from –50 °C to 150 °C. Subsequently, the samples were cooled (300 °C/min) to –50 °C and after 5 min, a second scan was recorded. The data presented are from the second scan. The glass transition temperatures (T_g) were taken as the midpoint of the heat capacity change. Indium and gallium were used as standards for temperature calibration.

Nanoparticle preparation

Nanoparticles were prepared using the salting-out method. Because of its pharmaceutical acceptance with regard to toxicity [18] acetone was chosen as the water-miscible organic solvent. The method consists of the addition of the water-soluble PVA in a highly concentrated aqueous salt solution (aqueous phase) to a polymer solution in acetone (organic phase). Although acetone is miscible with pure water in all proportions, the high salt concentration of the aqueous phase prevents mixing of both phases. After emulsification, the addition of pure water in a sufficient quantity causes acetone to diffuse into the aqueous phase, resulting in the formation of nanoparticles. Besides acetone, tetrahydrofuran (THF) and various ratios of acetone to ethyl acetate were used as the organic phase.

In the standard procedure, an acetone solution (5.0 g) containing 2 wt% (co)polymer was emulsified under mechanical stirring (20,500 rpm; 40 s; T25 Ultraturrax equipped with a S25 dispersing tool, Ika-Labortechnik, Staufen, Germany) in an aqueous phase (7.5 g) containing 60 wt% $MgCl_2 \cdot 6H_2O$ as the salting-out agent and 2 wt% PVA as a stabilizer (in a glass beaker; 3.5 cm diameter; 6.6 cm height). After the fast addition (5 s) of pure water (7.5 g) under mechanical stirring (20,500 rpm) causing acetone to diffuse into the water phase, nanoparticles were formed and stirring was continued (20,500 rpm; 20 s).

The nanoparticles were purified by rinsing with water. First, the nanoparticles were separated by ultracentrifugation (65,000×g for 30 min; Centrikon T-2180, Kontron Instruments, Watford, UK) and the supernatant was removed. The nanoparticles were redispersed in water, centrifuged and the supernatant was removed. This procedure was repeated three times.

The yield of the nanoparticles was determined gravimetrically.

Several process variables were varied to determine their influence on the final particle size. These variables include the degree of hydrolysis and concentration of PVA, the stirring speed, the ratio of the amount of aqueous to organic phase (w:o-ratio), and the polymer concentration.

All nanoparticle preparations were performed in duplo, unless stated otherwise.

Particle size analysis

The nanoparticle size was determined by dynamic light scattering (DLS) (Zetasizer 4000, Malvern Instruments Ltd., Malvern, UK) at 25 °C at an angle of 90°, taking the average of three measurements. The particle dispersion was diluted with water to such a degree that the desired number of counts was obtained. The desired number of counts is the number of counts that is high enough to get the highest possible signal to noise ratio, yet small enough to prevent multiple scattering to occur.

First, the polydispersity index (P.I.) is determined by the cumulants method. The P.I. is a dimensionless number indicating the width of the size distribution, and lies between zero and one, being zero for monodisperse particles. If the P.I. is small enough (<0.08), the particle size can be determined by the cumulants method and the size distribution obtained is based on a log normal distribution characterized by a mean and width. For polydispersity indices higher than 0.08, the CONTIN-method is used to determine the particle size. The CONTIN-method, developed by

Provencher *et al.* [22] describes bimodal and smooth distributions without the need for information such as an initial estimate for the particle size.

Zeta-potential measurements

Zeta-potential measurements by laser Doppler electrophoresis were performed on particles redispersed in 10 mM NaCl at the same concentration as used for particle analysis (Zetasizer 2000, Malvern Instruments Ltd., Malvern, UK), taking the average of five measurements.

Thermal properties in the wet state

The thermal properties of the nanoparticles in water were evaluated by differential scanning calorimetry (DSC) on a DSC 7 (Perkin-Elmer, Shelton, USA). A heating rate of 10 °C/min was applied, and stainless steel pans (Perkin-Elmer) were used. Fifty µl of pure water (MilliQ, Molsheim, France) was added to 15-20 mg of nanoparticles and this dispersion was heated from 10 °C to 65 °C. The samples were then cooled (300 °C/min) to 10 °C and after 5 min, a second scan was recorded. The data presented are from the second scan. The T_gs were taken as the midpoint of the heat capacity change. Indium and gallium were used as standards for temperature calibration.

Particle morphology

To examine the shape and morphology of the nanoparticles, samples were analyzed using transmission electron microscopy (TEM) (Philips CM30, Eindhoven, The Netherlands). Nanoparticle samples for TEM examination were prepared by placing a drop of an aqueous particle dispersion (1 mg/ml) on a carbon grid and drying at ambient temperature for 30 min. Staining with 3% (w/v) phosphotungstic acid was performed before analysis with TEM through bright field imaging at 300 kV.

RESULTS AND DISCUSSION

Polymer synthesis

After polymerization the crude product was analyzed by ^{1}H-NMR to determine the conversion, the theoretical and actual composition and $\overline{M}_n$. The $\overline{M}_n$ and polydispersity index (PDI) were determined by GPC and the glass transition temperature (T_g) by DSC. The results are presented in Table 3.1.

The polymer composition is close to the monomer ratio in the feed, with slightly more glycolide than DL-lactide incorporated. The higher reactivity of glycolide in comparison with DL-lactide, as previously reported [12], accounts for the larger fraction of glycolide in the copolymer than in the monomer feed. From the ^{1}H-NMR-results it becomes clear that the theoretical molecular weight is indeed obtained. Furthermore, it can be seen that the polydispersity index ranges from 1.42 to 2.09. Polydispersity indices close to 2 are typical for stannous octoate catalyzed ring-opening polymerizations [23-25] and are indicative for transesterification reactions [26]. The DSC results show that the T_g of the low molecular weight polymers is slightly lower for PLGA than for PDLLA. The T_g of HMW PDLLA is

clearly higher (55 °C), showing the effect of molecular weight on the T_g [27]. No melting peak is detected for any of the (co)polymers, confirming the amorphous nature of the (co)polymers.

Table 3.1 *The composition, number average molecular weight ($\overline{M}_n$), conversion, polydispersity index (PDI) and the glass transition temperature (T_g) of the polymers and of particles in the wet state.*

Polymer	Composition x:y[a]		$\overline{M}_n$ (kg/mol)			PDI[d]	Conversion of lactide (%)	T_g (°C)	T_g (°C)[e]
	feed	polymer	theor[b]	exp[c]	exp[d]				
HMW PDLLA	100:0	100:0	-	-	301	2.09	98	55	-
PDLLA	100:0	100:0	10.1	11.5	14.5	1.42	97	41	39
PLGA80/20	80:20	76:24	10.1	11.6	12.6	1.84	98	42	39
PLGA60/40	60:40	57:43	10.1	11.4	12.8	1.95	98	39	35

[a]x:y denotes the ratio lactyl:glycolyl units in the polymer, determined by ^{1}H-NMR.
[b]the theoretical molecular weight is calculated from the [Monomer]/[Initiator] ratio.
[c]determined by ^{1}H-NMR.
[d]determined by GPC.
[e]T_g of the corresponding nanoparticles in the wet state, determined by DSC.

Influence of preparation parameters on the particle size

An important step in the preparation of nanoparticles is the formation of the emulsion, as the droplet size is directly related to the final nanoparticle size. By applying a homogenizer, which induces high shear forces, emulsion droplets smaller than 0.5 µm are obtained [14] which leads to particles of the same size [17]. The total volume and total viscosity are related to the effectiveness of mixing, whereas the stirring speed relates to the amount of energy put into the system. These parameters are therefore expected to determine the final particle size. Furthermore, the stabilizer that is added in the formulation stabilizes the surface area that is created during emulsification. Changing its properties or concentration will therefore change the total surface area that can be stabilized, and will have an effect on the final particle size.

Several preparation parameters were varied to identify their influence on the particle size, keeping the other parameters as in the standard procedure (2 wt% PVA (80%), 2 wt% polymer, stirring speed 20,500 rpm and a ratio aqueous to organic phase (w:o-ratio) of 1.5). The parameters studied were the degree of hydrolysis of PVA, the PVA concentration in the aqueous phase, the stirring speed, the w:o-ratio before emulsification and the polymer concentration.

The water-soluble PVA functions as a stabilizer. It is commercially available with different molecular weights and degrees of hydrolysis. PVAs with a rather low degree of hydrolysis (75-88%) were used. The reason for this is that PVA with a high degree of hydrolysis leads to unstable particle dispersions, poor redispersibility and therefore low yields [28].

The effect of the degree of hydrolysis and of the molecular weight of the PVA on the particle size is shown in Figure 3.1. An increase of the degree of hydrolysis and the molecular weight leads to larger particles and a small increase in the polydispersity index. The former is caused

by an increase in hydrogen bonding and the latter is caused by the higher viscosity of the PVA-solution [29]. Since reproducible results and a low polydispersity index with PVA with a degree of hydrolysis of 80% were obtained (Figure 3.1), this stabilizer is used further on.
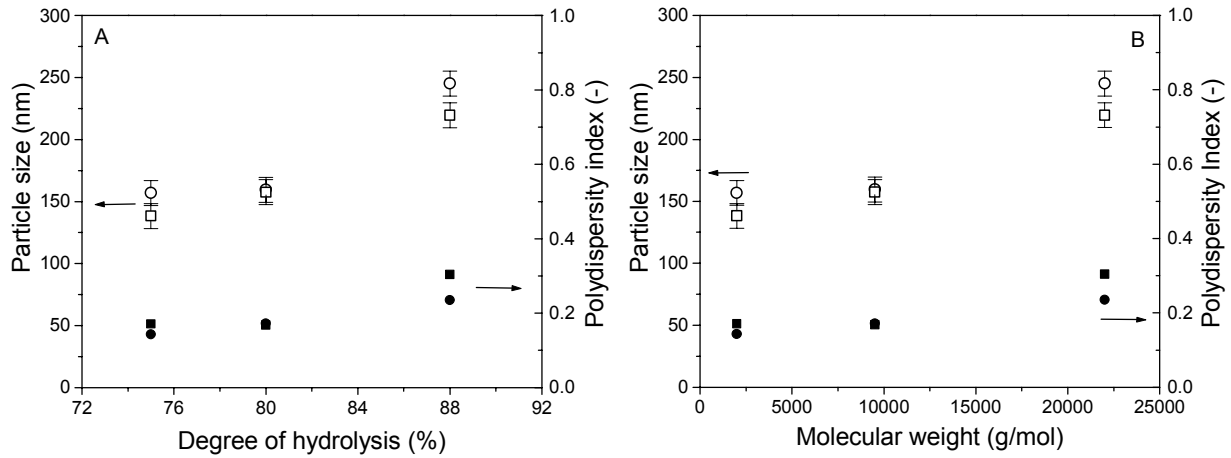
Figure 3.1 *The influence of (A) the degree of hydrolysis of PVA and (B) the molecular weight of PVA on the particle size for PLGA80/20 (○) and PLGA60/40 (□) and its influence on the polydispersity index for PLGA80/20 (●) and PLGA60/40 (■) (n=2). Other parameters were kept constant: polymer concentration (2 wt%), PVA concentration (2 wt%), w:o-ratio (1.5) and stirring speed (20,500 rpm).*

The concentration of this stabilizer was varied to identify its effect on the particle size (Figure 3.2A). With increasing PVA concentration (0-2 wt%) the particle size decreases. After further increase in the concentration (2-5 wt%), the particle size remains almost constant, but increases after further increasing the PVA concentration (5-10 wt%).
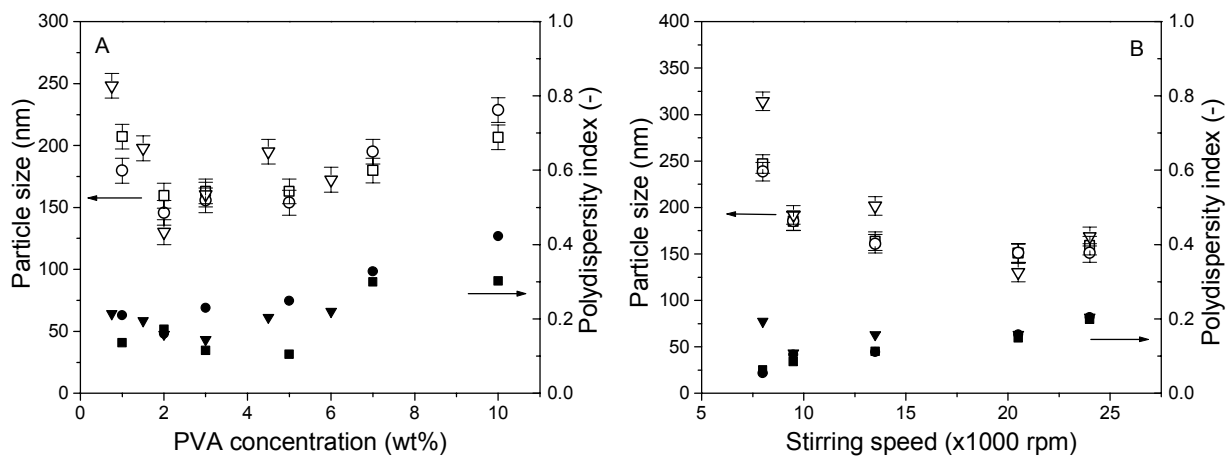
Figure 3.2 *The influence of (A) PVA concentration and (B) stirring speed on the particle size for PDLLA (∇), PLGA80/20 (○) and PLGA60/40 (□) and its influence on the polydispersity index for PDLLA (▼), PLGA80/20 (●) and PLGA60/40 (■) (n=2). Other parameters were kept constant: degree of hydrolysis of PVA (80%), polymer concentration (2 wt%), w:o- ratio (1.5) and (A) stirring speed (20,500 rpm) and (B) PVA concentration (2 wt%).*

Scholes *et al.* [30] have also reported this effect. However, Allémann *et al.* [17] reported a decrease in size for increasing stabilizer concentrations and similar results were obtained by Quintanar-Guerrero *et al.* [31]. Conversely, Benita *et al.* [32] and Vandervoort *et al.* [33] reported increased particle sizes with increased stabilizer concentrations, which was explained in terms of an increased viscosity. Apparently, there is both enhanced stabilization of the emulsion and decreased effectivity of mixing. Under the given settings, the point from where mixing becomes less effective due to the increased viscosity is at a PVA concentration of 5 wt%. The increased viscosity results from the fact that most of the stabilizer stays in the continuous phase, and does not play a significant role, neither in the emulsification nor in the stabilization of the droplets [34]. This is independent of polymer composition.

As a third variable, the effect of the stirring speed on the nanoparticle size was studied (Figure 3.2B). The results in Figure 3.2B clearly show that an increase in the stirring speed leads to a decrease in particle size as a result of smaller droplet formation during emulsification and thus smaller particles after solvent diffusion. This trend is, again, independent of the polymer composition. Although the trend corresponds to the results obtained by others, the relationship is not linear in a log-log plot [31] or to the power −5/6 (referring to the Hinze-Clay relation used in emulsion technology) [17]. The reason for the differences in the power of the relationship is probably due to differences in technique [31] or in the polymer used [17].
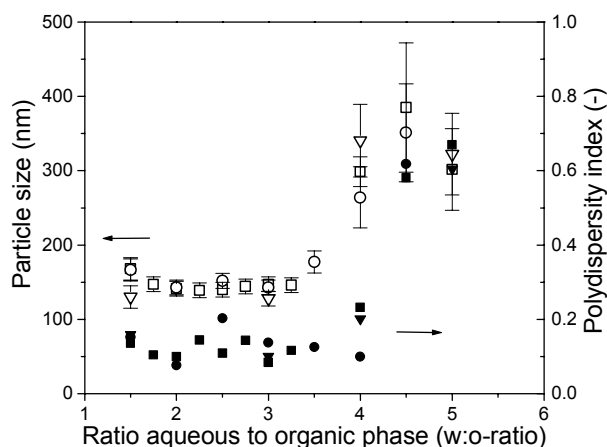
Figure 3.3 *The influence of the w:o-ratio on the particle size for PDLLA (▽), PLGA80/20 (○) and PLGA60/40 (□) and its influence on the polydispersity index for PDLLA (▼), PLGA80/20 (●) and PLGA60/40 (■) (n=2). Other parameters were kept constant: degree of hydrolysis of PVA (80%), PVA concentration (2 wt%), polymer concentration (2 wt%) and stirring speed (20,500 rpm).*

As can be seen in Figure 3.3, the w:o-ratio has a large influence on the particle size. It enables the preparation of monodisperse particles in the range of 100 to 200 nm for a w:o-ratio of 1.5 to 3.5. Larger particles are obtained at ratios higher than 3.5, at which the polydispersity increases significantly as well, indicating that broad size distributions are obtained. The increase in size for increasing w:o-ratio can be explained by a lower mixing effectiveness due to an increasing viscosity of the emulsion and an increase in the total volume, not only leading to larger droplets, and therefore to larger particles after solvent diffusion, but also to a

larger variation in size. This trend is independent of polymer composition. There is a lower limit of the w:o-ratio of 1, below which irregular particles are obtained. This is in accordance with the results of Rafler and co-workers [35].

The last variable studied was the polymer concentration. Its influence on the particle size and the polydispersity index are shown for low molecular weight polymer (Figure 3.4A) and for high molecular weight polymer (Figure 3.4B).
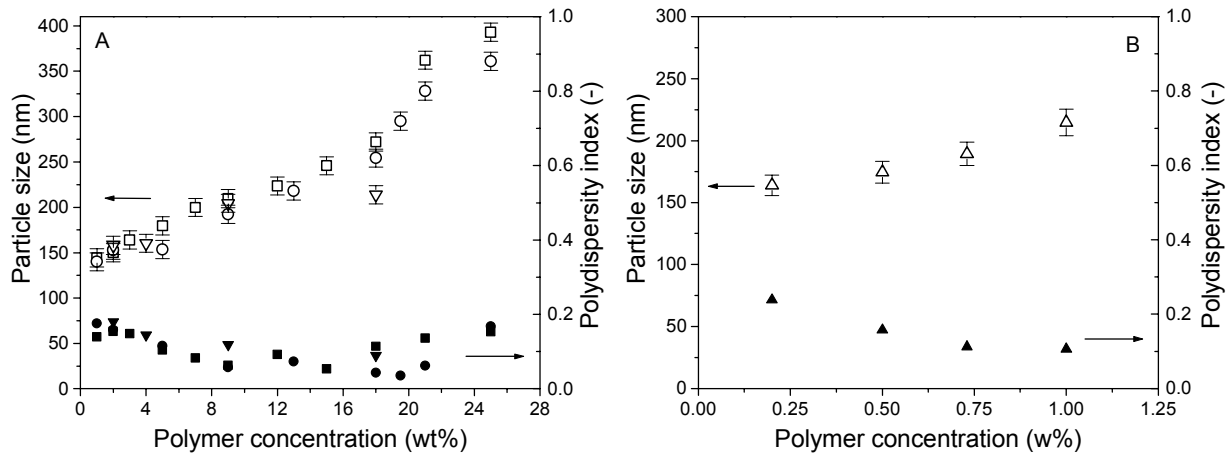
Figure 3.4 *The influence of the polymer concentration on the particle size for (A) PDLLA (∇), PLGA80/20 (○) and PLGA60/40 (□) and (B) HMW PDLLA (△) and its influence on the polydispersity index for (A) PDLLA (▼), PLGA80/20 (●) and PLGA60/40 (■) and (B) HMW PDLLA (▲) (n=2). Other parameters were kept constant: degree of hydrolysis of PVA (80%), w:o-ratio (1.5), PVA concentration (2 wt%) and stirring speed (20,500 rpm).*

The results in Figure 3.4A show that increasing the polymer concentration leads to an increase in the particle size, without affecting the polydispersity index. This means that, by changing the polymer concentration, fairly monodisperse particles can be prepared over a size range of 100-400 nm. This increase in size as a function of the polymer concentration is caused by an increase in viscosity of the organic phase that leads to less effective mixing. Again, there was no apparent relationship between particle size and the copolymer composition.

A similar trend is seen when HMW PDLLA is used (Figure 3.4B). Particles in a similar size range are obtained, yet at far lower concentrations than for the low molecular weight polymers. This is because the viscosity of high molecular weight polymer solutions is similar to the viscosity of low molecular weight polymer solutions at lower polymer concentrations. Though the increase in size with increasing polymer concentration is in accordance with most of the results reported in literature [30,31,36], an opposite effect has also been reported [17].

The discussion on the influence of the various preparation parameters on the particle size given above clearly shows that there is conflicting data in literature. However, it becomes also clear that it is possible to set the process variables in such a way that the particle size can be precisely tuned, e.g. by changing the polymer concentration or the stirring speed.

The yield of nanoparticles was determined for particles prepared from PLGA60/40 at three

different polymer concentrations: 9, 11 and 13 wt%. The yield of nanoparticles is independent of the polymer concentration, being higher than 93% for all three concentrations.

To demonstrate that not only acetone, but also other solvents having different physical properties such as polarity and solubility parameter, can be employed, particles were prepared using THF and acetone/ethyl acetate combinations as the organic solvent (Table 3.2).

Table 3.2 *Particle sizes and polydispersity indices (P.I.) obtained by changes in the solvent (n=2).*

Polymer	Solvent*	Size (nm)	P.I. (-)
PLGA80/20	Acetone	144.2 ± 1.5	0.12 ± 0.003
PLGA80/20	10% ethyl acetate/90% acetone	174.3 ± 1.5	0.17 ± 0.01
PLGA80/20	20% ethyl acetate/80% acetone	154.9 ± 0.2	0.11 ± 0.02
PLGA80/20	30% ethyl acetate/70% acetone	143.1 ± 1.6	0.10 ± 0.02
PLGA60/40	Acetone	157.5 ± 1.1	0.17 ± 0.02
PLGA60/40	THF	185.7 ± 2.1	0.22 ± 0.04

*the percentages are wt%.

Exchanging up to 30 wt% of acetone by ethyl acetate did not result in major changes in particle size. The same holds when acetone is replaced by THF. This shows that the method is very versatile in terms of choice of organic solvent, and therefore is expected to be very suitable for the incorporation of various drugs.

The particle size is determined directly after preparation, and after purification. These results are shown in Table 3.3. The particles can be easily redispersed with hardly any size difference before and after purification, indicating that stable particle dispersions were obtained.

Zeta-potential measurements

To get insight in the surface characteristics of the nanoparticles of the three different polymers, the zeta-potential was determined (Table 3.3). From Table 3.3 it becomes clear that the zeta-potential of the particles is slightly negative and independent of the polymer composition. It is independent of the polymer composition since a small amount of PVA is tightly adhered to the surface after purification [37]. The small amount of PVA adsorbed to the surface also results in a less negative zeta-potential than the zeta-potential of bare PLGA particles (-56 mV; in 1 mM NaCl) [38], as it shifts the hydrodynamic surface of shear [39].

Table 3.3 *Zeta-potential after and size before and after purification for particles of three polymers prepared according to the standard procedure (n=2).*

Polymer	Zeta-potential (mV)	Size (nm) before	Size (nm) after
PDLLA	-5.4 ± 1.1	130 ± 1	123 ± 1
PLGA80/20	-2.3 ± 0.6	144 ± 2	129 ± 11
PLGA60/40	-5.4 ± 1.2	151 ± 9	120 ± 9

Particle morphology

A TEM picture of PLGA60/40 nanoparticles is shown in Figure 3.5. The particle size as determined by DLS (200.7 ± 1.9 nm) is a hydrodynamic diameter, whereas the particle size as determined by TEM (approximately 160 nm) represents the actual size in the dry state. This difference in size indicates that swelling of the particles occurs (ca. 95%), which is higher than the 11% swelling as gravimetrically determined by Quellec *et al.* for PLA nanoparticles [38]. Furthermore, TEM confirms that the nanoparticles are spherical and monodisperse in size.
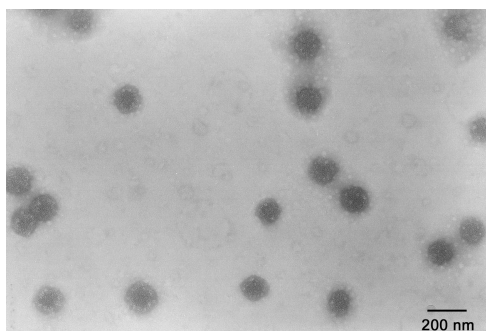
Figure 3.5 *PLGA60/40 nanoparticles as visualized by TEM through bright field imaging at 300 kV.*

CONCLUSIONS

This study demonstrates that monodisperse PDLLA, HMW PDLLA and PLGA nanoparticles can be prepared in high yields using the salting-out method avoiding the use of toxic chlorinated solvents. It is shown that the particle size is influenced by changes in the process variables and can be best controlled by adjusting the polymer concentration. This enables the preparation of monodisperse particles of PDLLA, PLGA and HMW PDLLA from 100 to 400 nm. Furthermore, various organic solvents can be used, making this technique suitable for the incorporation of various drugs. It is shown that changes in the polymer composition do not influence the particle size. This implies that the rate of degradation of the copolymers can be varied by changing the composition without losing control over the particle size.

ACKNOWLEDGEMENTS

REFERENCES

1. Illum, L.; Davis, S.S.; Wilson, C.G.; Frier, M.; Hardy, J.G. and Thomas, N.W., *Int. J. Pharm.,* **1982**, *12*, 135-146.
2. Tabata, Y. and Ikada, Y., *Biomaterials,* **1988**, *9*, 356-362.

3. Moghimi, S.M.; Porter, C.J.H.; Muir, I.S.; Illum, L. and Davis, S.S., *Biochem. Biophys. Res. Commun.,* **1991**, *177*, 861-866.

4. Tabata, Y. and Ikada, Y., *J. Biomed. Mater. Res.,* **1988**, *22*, 837-858.

5. Gref, R.; Miralles, G. and Dellacherie, E., *Polym. Int.,* **1999**, *48*, 251-256.

6. Song, C.X.; Labhasetwar, V.; Murphy, H.; Qu, X.; Humphrey, W.R.; Shebuski, R.J. and Levy, R.J., *J. Control. Release,* **1997**, *43*, 197-212.

7. Juni, K. and Nakano, M., *Crit. Rev. Ther. Drug Carrier Syst.,* **1987**, *3*, 209-232.

8. Yamaguchi, K. and Anderson, J.M., *J. Control. Release,* **1993**, *24*, 81-93.

9. Anderson, J.M. and Shive, M.S., *Adv. Drug Deliv. Rev.,* **1997**, *28*, 5-24.

10. Ignatius, A.A. and Claes, L.E., *Biomaterials,* **1996**, *17*, 831-839.

11. Piskin, E., *J. Biomater. Sci. Polym. Ed.,* **1994**, *6*, 775-795.

12. Gilding, D.K. and Reed, A.M., *Polymer,* **1979**, *20*, 1459-1464.

13. Liggins, R.T. and Burt, H.M., *Int. J. Pharm.,* **2001**, *222*, 19-33.

14. Quintanar-Guerrero, D.; Allémann, E.; Fessi, H. and Dölker, E., *Drug Dev. Ind. Pharm.,* **1998**, *24*, 1113-1128.

15. Allémann, E.; Gurny, R. and Dölker, E., *Eur. J. Pharm. Biopharm.,* **1993**, *39*, 173-191.

16. Dölker, E.; Bindschädler, C. and Gurny, R., Process for preparing a powder of water-insoluble polymer which can be redispersed in a liquid phase, the resulting powder and utilization thereof, **1990**, EP 0 363 549.

17. Allémann, E.; Gurny, R. and Dölker, E., *Int. J. Pharm.,* **1992**, *87*, 247-254.

18. Allémann, E.; Leroux, J.-C.; Gurny, R. and Dölker, E., *Pharm. Res.,* **1993**, *10*, 1732-1737.

19. Leroux, J.-C.; Allémann, E.; De Jaeghere, F.; Dölker, E. and Gurny, R., *J. Control. Release,* **1996**, *39*, 339-350.

20. Ibrahim, H.; Bindschädler, C.; Dölker, E.; Buri, P. and Gurny, R., *Int. J. Pharm.,* **1992**, *87*, 239-246.

21. Pêgo, A.P.; Poot, A.A.; Grijpma, D.W. and Feijen, J., *J. Mater. Sci. - Mater. Med.,* **2002**, submitted.

22. Provencher, S.W.; Hendrix, J. and De Maeyer, L., *J. Chem. Phys.,* **1978**, *69*, 4273-4276.

23. Schwach, G.; Coudane, J.; Engel, R. and Vert, M., *Polym. Bull.,* **1996**, *37*, 771-776.

24. Tracy, M.A.; Ward, K.L.; Firouzabadian, L.; Wang, Y.; Dong, N.; Qian, R. and Zhang, Y., *Biomaterials,* **1999**, *20*, 1057-1062.

25. Wang, N.; Wu, X.S.; Chao, L. and Mei, F.F., *J. Biomater. Sci. Polym. Ed.,* **2000**, *11*, 301-318.

26. Kricheldorf, H.R.; Kreiser-Saunders, I. and Stricker, A., *Macromolecules,* **2000**, *33*, 702-709.

27. Jamshidi, K.; Hyon, S.H. and Ikada, Y., *Polymer,* **1988**, *29*, 2229-2234.

28. Murakami, H.; Kawashima, Y.; Niwa, T.; Hino, T.; Takeuchi, H. and Kobayashi, M., *Int. J. Pharm.,* **1997**, *149*, 43-49.

29. Briscoe, B.; Luckham, P. and Zhu, S., *Polymer,* **2000**, *41*, 3851-3860.

30. Scholes, P.D.; Coombes, A.G.A.; Illum, L.; Davis, S.S.; Vert, M. and Davies, M.C., *J. Control. Release,* **1993**, *25*, 145-153.

31. Quintanar-Guerrero, D.; Fessi, H.; Allémann, E. and Dölker, E., *Int. J. Pharm.,* **1996**, *143*, 133-141.

32. Benita, S.; Benoit, J.P.; Puisieux, F. and Thies, C., *J. Pharm. Sci.,* **1984**, *73*, 1721-1724.

33. Vandervoort, J. and Ludwig, A., *Pharmazie,* **2001**, *56*, 484-488.

34. Jalil, R. and Nixon, J.R., *J. Microencapsul.,* **1990**, *7*, 25-39.

35. Rafler, G. and Jobmann, M., *Pharm. Ind.,* **1997**, *59*, 620-624.

36. Kwon, H.Y.; Lee, J.Y.; Choi, S.W.; Jang, Y.S. and Kim, J.H., *Colloids Surf. A - Physicochem. Eng. Asp.,* **2001**, *182*, 123-130.

37. Murakami, H.; Kobayashi, M.; Takeuchi, H. and Kawashima, Y., *Int. J. Pharm.,* **1999**, *187*, 143-152.

38. Quellec, P.; Gref, R.; Perrin, L.; Dellacherie, E.; Sommer, F.; Verbavatz, J.M. and Alonso, M.J., *J. Biomed. Mater. Res.,* **1998**, *42*, 45-54.

39. Coombes, A.G.A.; Tasker, S.; Lindblad, M.; Holmgren, J.; Hoste, K.; Toncheva, V.; Schacht, E.; Davies, M.C.; Illum, L. and Davis, S.S., *Biomaterials,* **1997**, *18*, 1153-1161.

CHAPTER 4

Biodegradable polyester nanoparticles without stabilizer

ABSTRACT

Nanoparticles of poly(ethylene oxide)-poly(DL-lactic-co-glycolic acid) diblock copolymers (PEO-PLGA) were prepared without additional stabilizer using the salting-out method. The PEO content in the nanoparticles was varied by applying different weight ratios of PEO_3-$PLGA_8$ to $PLGA_{11}$ (the numbers denote the molecular weight of the block in kg/mol). The surface of the nanoparticles in the wet state was analyzed by zeta-potential measurements and nuclear magnetic resonance spectroscopy. Surface enrichment with PEO was observed above a total PEO content of 13 wt%. At lower PEO contents, particle aggregation was observed. The surface in the dry state was also analyzed by time-of-flight secondary ion mass spectroscopy and X-ray photoelectron spectroscopy. A negligible surface enrichment with PEO in the dry state was observed, possibly due to rearrangements upon drying of the nanoparticles. This study demonstrates that stable PEO-PLGA nanoparticle dispersions can be prepared without an additional stabilizer. This approach also allows the preparation of PEO-PLGA nanoparticles with specific surface chemistry for targeting purposes.

INTRODUCTION

For the preparation of nanoparticles to be used for local drug delivery systems, biodegradable polymers are preferably used to prevent that polymer remains in the body, once the drug has been released. Biodegradable polymers approved by the Food and Drug Administration include homopolymers of DL-lactide (PDLLA) and copolymers of DL-lactide and glycolide (PLGA). These polyesters are known for their biodegradability and biocompatibility [1-7].

The surface characteristics of nanoparticles are important with respect to the stability of the particles in dispersion, but also regarding the recognition by the reticuloendothelial system (RES) [8-10] as well as the targeting to the tissue of interest [11].

Stability of PLGA nanoparticle dispersions is achieved by the application of an external stabilizer in the nanoparticle preparation. Common stabilizers are poly(vinyl alcohol) (PVA) and poly(ethylene oxide)-poly(propylene oxide) block copolymers (PEO-PPO). Although most of the stabilizer is removed upon purification of the nanoparticles, a small amount remains present at the surface [12]. This has the disadvantage that the stabilizer might affect biological interaction and targeting of the nanoparticles. In addition, PVA is suspected to be carcinogenic [13].

Some investigators have tried to overcome this problem by preparing surfactant-free PLGA nanoparticles [14-16], in which the carboxyl end groups of the PLGA are used for stabilization. As long as enough of these end groups are present at the surface, this may provide electrostatic repulsion between particles resulting in stabilized dispersions. However, the stability of the dispersion decreases with increasing electrolyte concentration [15] and aggregation occurred at sodium sulfate concentrations similar to the ionic strength at physiological conditions [15]. Furthermore, these nanoparticles aggregated upon freeze-drying and could not be redispersed [16].

An alternative approach to obtain stabilized polyester nanoparticles is the use of PEO-PLGA block copolymers. The presence of PEO at the surface of nanoparticles decreases protein adsorption [17] and prolongs the blood circulation time as it reduces recognition by RES [18,19]. The use of PEO-PLGA also offers the possibility to obtain particles with functional groups at the surface. This can be achieved by preparing particles from end-functionalized PEO-PLGA. Functional groups at the surface can be used for further modification or coupling reactions.

When the molecular weight of the hydrophilic PEO block exceeds the molecular weight of the hydrophobic PLGA block, PEO-PLGA diblock copolymers tend to self-assemble into micelles in aqueous environment above the critical micelle concentration [20]. Upon self-assembly, the hydrophobic PLGA blocks form the core, whereas the hydrophilic PEO-chains are oriented towards the aqueous phase, thereby forming the shell of the micelles.

If the molecular weight of the PEO block is lower than the molecular weight of the PLGA block, larger colloids such as nanoparticles are formed [20]. However, in this case a strict phase separation of the two blocks is uncertain in contrast to the phase separation in micelles

[20]. In addition, it is not known what the minimum PEO content should be to obtain stable nanoparticles. This probably explains that an additional stabilizer is still added in PEO-PLGA nanoparticle preparations [21], and therefore the stabilizer might affect the surface properties.

The aim of this study is to prepare PEO-PLGA nanoparticles without the use of an additional stabilizer. It has been shown that PEO with a molecular weight lower than $6 \cdot 10^3$ g/mol can be removed from the circulation via the kidneys [22]. Therefore, a PEO block with a molecular weight of $3 \cdot 10^3$ g/mol was used. The ratio of PEO_3-$PLGA_8$ to $PLGA_{11}$ (the numbers denote the molecular weight of the block in kg/mol) in the particle preparation was varied to determine the minimum PEO content to prepare stable polyester based particles under the conditions used.

The surface characteristics of these particles in the wet state were analyzed by means of ^{1}H-NMR and zeta-potential measurements. Two techniques, namely time-of-flight-secondary ion mass spectroscopy (ToF-SIMS) and X-ray photoelectron spectroscopy (XPS) were applied to characterize the surface of the nanoparticles in the dry state. ToF-SIMS provides information on the chemical composition of the top 10 Å surface layer [12], while XPS yields information on the surface chemistry of the top 70-100 Å layer [12].

MATERIALS AND METHODS

Materials

DL-lactide and glycolide (Purac Biochem b.v., Gorinchem, The Netherlands), stannous octoate (Sigma, St. Louis, USA) and monomethoxy poly(ethylene glycol) (MPEG) ($\overline{M}_n = 3.0 \cdot 10^3$ g/mol, Shearwater Polymers, Huntsville, USA) were used as received. Hexanol (Merck, Darmstadt, Germany) was distilled from calcium hydride (Acros Organics, New Jersey, USA) prior to use. Deuterated chloroform ($CDCl_3$), deuterated water (D_2O) and magnesium chloride hexahydrate ($MgCl_2 \cdot 6H_2O$) were purchased from Merck (Darmstadt, Germany) and used without further purification. PVA ($\overline{M}_n = 9$-$10 \cdot 10^3$ g/mol; 80% hydrolyzed from poly(vinyl acetate)) was purchased from Aldrich (Milwaukee, USA). The phosphate buffer used for particle analysis was an aqueous solution of sodium dihydrogenphosphate (Merck) and disodium hydrogenphosphate (Merck) (1 mM; pH 7.4). The solvents used were of analytical grade (Biosolve, Valkenswaard, The Netherlands).

Polymer synthesis

A mixture of DL-lactide (10.1 g; 69.8 mmol) and glycolide (5.45 g; 47.0 mmol) with stannous octoate in pentane (5.0 ml; 1.89 g/l) and an appropriate amount of initiator (318 μl hexanol or 7.59 g MPEG; 2.53 mmol) were transferred to an ampoule. After removal of the pentane by applying vacuum, the ampoule was purged three times with argon, evacuated, vacuum-sealed and subsequently transferred to an oil bath at 130 °C. After 24 h of reaction, the crude product was dissolved in chloroform, precipitated into a ten-fold volume of methanol and dried in vacuo at 40 °C for three days.

The synthesized (co)polymers are denoted as PLGA for the copolymers of DL-lactide and glycolide and as PEO-PLGA for the diblock copolymer based on poly(ethylene oxide) and PLGA.

Polymer characterization

The number average molecular weight ($\overline{M}_n$) and the composition of the (co)polymers were determined by nuclear magnetic resonance (^{1}H-NMR) spectroscopy performed using a Varian Inova (Varian, Palo Alto, USA) operating at 300 MHz, with CDCl$_3$ as the solvent.

The $\overline{M}_n$ and the molecular weight distribution of the (co)polymers were determined by gel permeation chromatography (GPC) using chloroform (10 mg/ml) as an eluent at 25 °C at a flow rate of 1.5 ml/min. The GPC setup consisted of a Waters Model 510 pump, a HP Ti-Series 1050 autosampler, a Waters Model 410 Differential Refractometer, and a Viscotek H502 Viscometer Detector with HR0.5, HR2 and HR4 Waters Ultra-Styragel columns (Waters, Milford, USA) placed in series. Polystyrene standards with narrow molecular weight distributions (PSS, Mainz, Germany) were used for calibration.

The thermal properties of the synthesized materials were evaluated by differential scanning calorimetry (DSC) using a DSC 7 (Perkin-Elmer, Shelton, USA). A heating rate of 10 °C/min was applied, and aluminum pans (Perkin-Elmer) were used. The copolymer samples (5-10 mg) were heated from –50 °C to 150 °C. The samples were then cooled (300 °C/min) to –50 °C and after 5 min, a second scan was recorded. The data presented are from the second scan. The glass transition temperatures (T_g) were taken as the midpoint of the heat capacity change. Indium and gallium were used as standards for temperature calibration.

Nanoparticle preparation

Nanoparticles were prepared using the salting-out method [23]. Because of its pharmaceutical acceptance with regard to toxicity [24] acetone was chosen as the water-miscible organic solvent. The method consists of the addition of a highly concentrated salt solution in water (aqueous phase) to a polymer solution in acetone (organic phase). Although acetone is miscible with pure water in all ratios, the high salt concentration of the aqueous phase prevents mixing of both phases. After emulsification, the addition of pure water in a sufficient quantity causes acetone to diffuse into the aqueous phase, resulting in the formation of nanoparticles.

Typically, an acetone solution (5.0 g) containing 2 wt% copolymer was emulsified under mechanical stirring (20,500 rpm; 40 s; T25 Ultraturrax equipped with a S25 dispersing tool, Ika-Labortechnik, Staufen, Germany) in an aqueous phase (7.5 g) containing 60 wt% MgCl$_2$·6H$_2$O as the salting-out agent (in a glass beaker; 3.5 cm diameter; 6.6 cm height). After the fast addition (5 s) of pure water (7.5 g) under mechanical stirring (20,500 rpm) causing acetone to diffuse into the water phase, nanoparticles were formed and stirring was continued (20,500 rpm; 20 s).

PEO-PLGA and PLGA nanoparticles with PVA as a stabilizer were prepared as well. The same procedure as described above was followed, except that the aqueous phase also contained 2 wt% PVA. The nanoparticles were purified by rinsing with water. First, the nanoparticles were separated by ultracentrifugation (65,000×g for 30 min.; Centrikon T-2180, Kontron Instruments, Watford, UK) and the supernatant was removed. The nanoparticles were redispersed in water, centrifuged and the supernatant was removed. This procedure was repeated three times.

All nanoparticle preparations were performed in duplo, unless stated otherwise.

Particle size analysis

The nanoparticle size was determined by dynamic light scattering (DLS) (Zetasizer 4000, Malvern Instruments Ltd., Malvern, UK) at 25 °C at an angle of 90°, taking the average of three measurements. The particle dispersion was diluted with 10 mM NaCl to such a degree that the desired number of counts was obtained. The desired number of counts is the number of counts that is high enough to get the highest possible signal to noise ratio, yet small enough to prevent multiple scattering to occur.

First, the polydispersity index (P.I.) is determined by the cumulants method. The P.I. is a dimensionless number indicating the width of the size distribution, and has a value between zero and one, being zero for monodisperse particles. If the P.I. is small enough (<0.08), the particle size can be determined by the cumulants method and the size distribution obtained is based on a log normal distribution characterized by a mean and width. For polydispersity indices higher than 0.08, the CONTIN-method is used to determine the particle size. The CONTIN-method, developed by Provencher *et al.* [25] describes bimodal and smooth distributions without the need for information such as an initial estimate for the particle size.

To examine the size of the nanoparticles in the dry state, samples were analyzed by scanning electron microscopy (SEM) using a LEO 1500 (LEO Electron Microscopy Ltd., Cambridge, UK). Silicon substrates (∅ 15 mm) were cleaned ultrasonically, successively in isopropanol (10 min, two times), in methanol (10 min, two times) and in acetone (10 min, two times). The nanoparticle samples were prepared in two different ways. The first way was by dropping an aqueous particle dispersion on a freshly cleaned silicon substrate, after which it was allowed to dry for 2 h at 25 °C. The second way was by placing freeze-dried particles onto an Indium foil by applying gentle pressure. SEM analysis was performed at 1 kV at magnifications ranging from 2000× to 15000×. The particle size in the dry state was determined by averaging the size of 35 particles.

Surface analysis of nanoparticles in the wet state

Nanoparticles were redispersed in phosphate buffer (1 mM; pH 7.4) at the concentration used for DLS (Zetasizer 2000, Malvern Instruments Ltd., Malvern, UK). The zeta-potential of the nanoparticles was determined by measuring the velocity of particles moving through the phosphate buffer solution resulting from an applied electric field, taking the average of five measurements. The measurements were performed within the stationary layer to ensure that the measured velocity was due to electrophoresis only. Measurements were carried out at a temperature of 25 °C with a cell drive voltage of 120 V and a modulator frequency of 250 Hz.

After the last purification step, PEO-PLGA nanoparticles were redispersed in D_2O. ^{1}H-NMR spectra of the PEO-PLGA nanoparticles in D_2O were recorded using a Varian Inova (Varian, Palo Alto, USA) operating at 300 MHz.

Surface analysis of nanoparticles in the dry state

For time-of-flight-secondary ion mass spectroscopy (ToF-SIMS) analysis, nanoparticle samples were prepared in two different ways as described above for the SEM analysis. Indium was chosen as the substrate, as this is recorded as a clear, single peak and therefore less likely interferes with peaks arising from the material of interest. As a reference, powdered PLGA, PEO-PLGA, PEO and PVA polymer were placed onto an Indium foil by applying gentle pressure. Analysis of the samples was performed using a TRIFT II instrument (Physical Electronics, Eden Prairie, MN, USA) employing a

15 keV Ga[+] ion source. The 2 nA DC primary ion beam was pulsed at a 11 kHz frequency with a pulse width of 12 ns. A low energy electron beam was used for charge compensation. Emitted secondary ions were analyzed with respect to their mass/charge (m/z) ratio, yielding positive and negative ToF-SIMS spectra. PVA-enrichment on the top 10 Å nanoparticle surface layer of PLGA and PEO-PLGA nanoparticles was determined by comparing ToF-SIMS spectra of PVA with ToF-SIMS spectra of PLGA and PEO-PLGA, respectively. PEO-enrichment on the top 10 Å nanoparticle surface layer was determined by comparing ToF-SIMS spectra of PEO with ToF-SIMS spectra of PEO-PLGA. To be able to compare, characteristic peaks in the negative ToF-SIMS spectra of the nanoparticles and of the PVA, PLGA and PEO-PLGA polymers were used. Since the choice of peaks had an influence on the final result, several peaks (in total eight, namely at m/z = 43, 58, 59, 71, 87, 89, 103 and 105) were used. The sum of the intensity of these eight peaks in individual spectra was set to 100 % and the relative intensity of each peak was calculated. The relative intensity of these peaks in the nanoparticle spectra was compared to the relative intensity of these peaks in the spectra of the polymer (either PLGA or PEO-PLGA) and in the spectra of the stabilizing block (either PVA or PEO). The PVA-enrichment and the PEO-enrichment were calculated from the best least squared fit.

For X-ray photoelectron spectroscopy (XPS) analysis, polymer samples and nanoparticle samples were prepared as described above for the ToF-SIMS analysis. Spectra of PLGA, PEO-PLGA, PEO, PVA polymer and the nanoparticle samples were obtained using a Quantum 2000 Scanning ESCA Microprobe (Physical Electronics, Eden Prairie, MN, USA) using monochromatized Al Kα (25 W) X-rays and an electron take-off angle of 45°. The X-ray spot size was 100 μm for all spectra. A detailed scan of the C1*s* regions (278-298 eV) was performed for each sample on three different spots using a pass energy of 29.35 eV, after which a single survey spectrum (0-1100 eV) was recorded on each sample on the same three spots employing a pass energy of 187.85 eV. Every scan had an acquisition time of 5 min. Charge neutralization was performed using a 1 eV electron source and a 5 eV ion source. Although under the given conditions, no degradation due to X-ray radiation is expected [21], a degradation study on PLGA powder was carried out by performing four C1*s* scans on one and the same spot, each scan having an acquisition time of 2.5 min.

RESULTS AND DISCUSSION

Polymer synthesis

The characteristics of the synthesized polymers are presented in Table 4.1. The theoretical and actual copolymer composition, number average molecular weight ($\overline{M}_n$) and monomer conversion are determined by ^{1}H-NMR, the polydispersity index (PDI) by GPC and the glass transition temperature (T_g) by DSC.

The actual molar composition of the PLGA copolymer (lactyl:glycolyl 57:43) is close to the theoretical molar composition (60:40). The higher reactivity of glycolide in comparison with DL-lactide, as previously reported [26], accounts for the larger fraction of glycolide in the copolymer than in the monomer feed. The somewhat larger deviation of the actual composition for PEO-PLGA is probably caused by the lower DL-lactide conversion. The ^{1}H-NMR and GPC results confirm that the desired molecular weight is indeed obtained.

Furthermore, it can be seen that the molecular weight distribution is rather broad as indicated by the polydispersity indices of 1.95 and 1.24, respectively. Polydispersity indices close to 2 are typical for stannous octoate catalyzed ring-opening polymerizations [27-29] and are indicative for transesterification reactions [30].

The T_gs of the two copolymers differ considerably, with the T_g of PLGA being higher than body temperature. However, when applied *in vivo* the T_g of both copolymers will be below 37 °C as the presence of water lowers the T_g due to a plasticizing effect [31].

Table 4.1 *The composition, number average molecular weight ($\overline{M}_n$) and conversion, the polydispersity index (PDI) and the glass transition temperature (T_g) of the (co)polymers.*

Polymer	Composition x:y[b]		$\overline{M}_n$ (kg/mol)			PDI[e]	Conversion of lactide (%)	T_g (°C)[f]
	feed	polymer	theor[c]	exp[d]	exp[e]			
PLGA	60:40	57:43	10.1	11.4	12.8	1.95	98	39
PEO-PLGA[a]	60:40	52:48	11.9	11.2	9.9	1.24	94	3

[a] $\overline{M}_{n,PEO} = 3 \cdot 10^3$ g/mol.
[b] x:y denotes the ratio lactyl:glycolyl units of the PLGA block, determined by ^{1}H-NMR.
[c] the theoretical molecular weight is calculated from the [Monomer]/[Initiator] ratio.
[d] determined by ^{1}H-NMR.
[e] determined by GPC.
[f] determined by DSC.

Particle size analysis

Nanoparticles of PEO-PLGA, PLGA and of mixtures of both polymers using different weight fractions of PEO-PLGA (WF$_{PEO-PLGA}$) were prepared without stabilizer (see Table 4.2). PEO-PLGA and PLGA particles with stabilizer were also prepared (marked as [a] in Table 4.2). It was not possible to obtain PLGA particles without stabilizer, as upon mixing of the two phases precipitation of the polymer occurred instantaneously. All formulations in which PEO was present (WF$_{PEO-PLGA}$ 0.1-1) resulted in particles that could be easily redispersed after each purification step without change in particle size. The particle size and zeta-potential of the particles obtained after the purification procedure are shown in Table 4.2.

As can be seen in Table 4.2, there is a tendency of increasing particle size with decreasing PEO-PLGA weight fraction. This can be explained by the fact that less surface can be covered by the PEO present, leading to larger particles. The increasing particle size can also be caused by an increasing PLGA concentration, as previously shown [23]. The higher polydispersity indices for formulations with WF$_{PEO-PLGA}$ less than 0.4 are caused by partial aggregation of the particles as a bimodal size distribution is observed. Therefore, the minimal WF$_{PEO-PLGA}$ to prepare PEO-PLGA/PLGA nanoparticles without aggregation under the conditions used in this study is 0.4, which corresponds to a PEO content in the nanoparticles of 13 wt%.

After lyophilization of nanoparticles that do not contain PVA, a large increase in particle diameter and polydispersity is observed (data not shown). The reason for the change in diameter and polydispersity could be that during the freeze-drying procedure the PEO had crystallized, resulting in an intermolecular interaction between the crystallized PEO-chains and therefore also between the PLGA-chains. This causes a decrease in the ability to rehydrate the particles after freeze-drying. This can be solved by the addition of a cryoprotector, such as trehalose [32] or sucrose [33].

Table 4.2 Particle size, polydispersity index (P.I.) and zeta potential of nanoparticles of PEO-PLGA, PLGA and mixtures of these polymers with different weight fractions of PEO-PLGA (WF$_{PEO-PLGA}$).

Code	WF$_{PEO-PLGA}$	Particle size (nm)	P.I. (-)	Zeta-potential (mV)
PEO-PLGA 1[a]	1	135 ± 11	0.27 ± 0.07	−6.6 ± 5
PEO-PLGA 1	1	231 ± 30	0.16 ± 0.05	−14.1 ± 0.3
PEO-PLGA 0.9	0.9	254 ± 19	0.32 ± 0.04	-
PEO-PLGA 0.8	0.8	262 ± 10	0.25 ± 0.05	−21.4 ± 0.1
PEO-PLGA 0.7	0.7	268 ± 26	0.26 ± 0.10	-
PEO-PLGA 0.6	0.6	261 ± 44	0.16 ± 0.06	−20.9 ± 0.9
PEO-PLGA 0.5	0.5	300 ± 13	0.31 ± 0.02	-
PEO-PLGA 0.4	0.4	333 ± 23	0.28 ± 0.09	−22.2 ± 0.5
PEO-PLGA 0.3	0.3	553 ± 354	0.52 ± 0.36[c]	-
PEO-PLGA 0.2	0.2	397 ± 19	0.54 ± 0.17[c]	−23.7 ± 0.1
PEO-PLGA 0.1	0.1	490 ± 84	0.71 ± 0.22[c]	-
PEO-PLGA 0	0	n.p.[b]	-	-
PEO-PLGA 0[a]	0	124 ± 20	0.20 ± 0.02	+2.0 ± 0.7

[a]PVA used as stabilizer.

[b]n.p. = no particles, as precipitation of the polymer occurred during particle preparation.

[c]bimodal size distributions were observed.

To determine if all PEO chains can be present at the surface of a PEO-PLGA nanoparticle, the core-shell model used to describe micellar systems [34] was applied. Thereby it is assumed that the shell of the particles consists of hydrophilic PEO chains solely and that the particle core consists of hydrophobic PLGA chains. Based on the measured hydrodynamic radius of the particles and the thickness of a PEO shell reported in literature, the radius of the PLGA core (r_{core}) is calculated. The shell thickness of PEO chains in PEO$_5$-PLA$_{15}$ (the numbers denote the molecular weight of the block in kg/mol) micelles was 9-11 nm, determined by modeling using the mean-field theory and by rheology measurements [35]. The thickness of immobilized PEO$_{1.9}$ chains onto a silicon substrate is reported to be 10 nm [36]. Therefore, 10 nm is taken as the shell thickness of PEO$_3$ in the calculations below.

From r_{core}, the number of PEO chains at the surface (N_{PEO}) can be calculated [34]:

$$N_{PEO} = 4\pi r_{core}^2 / A \qquad (4.1)$$

in which A is the area per PEO molecule. The minimal area that one PEO chain ($\overline{M}_w = 3\cdot10^3$ g/mol) occupies is reported to be 0.45 nm^2 based on compression of a PEO monolayer [37]. By further compression the monolayer collapsed [37].

Subsequently, for nanoparticles prepared from PEO-PLGA, the number of PLGA chains (N_{PLGA}) is equal to the number of PEO chains:

$$N_{PLGA} = N_{PEO} \qquad (4.2)$$

The density of the PLGA core (ρ_{core}) consisting of N_{PLGA} chains is expressed as [34]

$$\rho_{core} = \frac{3\overline{M}_{w,PLGA} N_{PLGA}}{4\pi N_A (r_{core})^3} \qquad (4.3)$$

N_A is Avogadro's constant ($6.02\cdot10^{23}$) and $\overline{M}_{w,PLGA}$ is the weight average molecular weight of the PLGA block in PEO-PLGA (which is $1.24\cdot(11.2-3)\cdot10^3$ (Table 4.1) = $10.2\cdot10^3$ g/mol). From the particle size of PEO-PLGA nanoparticles, ρ_{core} is determined to be 1.05 g/cm^3. Since this value is much smaller than the density of PLGA (=1.37 g/cm^3 (calculated from the densities of amorphous poly(DL-lactide) and poly(glycolide) [38])) and the water-uptake of PLGA is lower than 10% [39], the core does not only consist of PLGA chains, but also of PEO chains. Apparently, there is no strict phase separation of the two blocks, but enough PEO chains are present at the surface to stabilize the particles.

Zeta-potential measurements

The zeta-potential of the nanoparticles becomes less negative with increasing PEO content (Table 4.2), which is in accordance with literature [40]. This is an indication of an increased surface coverage of nanoparticles by the PEO groups with increasing PEO content, which can only occur when the surface is not yet fully covered at low PEO contents. The zeta-potential of PEO-PLGA nanoparticles prepared with PVA as an additional stabilizer was even less negative than the nanoparticles prepared without PVA and had the same value as found by De Jaeghere *et al.* [41]. Indeed, the presence of residual PVA is known to result in less negative zeta-potential values [42,43]. The presence of flexible chains at the surface results in a shift of the hydrodynamic surface of shear (surface separating the moving particles, ions and solvent from the stationary phase) to greater distances from the surface of the solid nanoparticle core and consequently in a less negative zeta-potential [44]. In addition, the presence of PEO might result in a lower preferential adsorption of negatively charged ions present in the medium.

^{1}H-NMR-analysis of nanoparticles in dispersion

In the ^{1}H-NMR spectrum of PEO-PLGA nanoparticles dispersed in D$_2$O, two major peaks are observed (Figure 4.1), corresponding to PEO (δ=3.6 ppm) and DOH (δ=4.7 ppm).

The large DOH peak is due to the substantial amount of water present in the nanoparticles after ultracentrifugation. The fact that only small peaks corresponding to PLGA (δ 1.5 ppm) are detected, indicates that the majority of the PLGA protons are in a solid environment and not detected in the ^{1}H-NMR-spectrum, because the equipment was configured for normal liquid-state ^{1}H-NMR. Since the PEO is observed as a symmetric singlet, it must be fully solvated [45]. This supports the results obtained by the zeta-potential measurements that PEO is present at the surface and confirms the observation that stable particle dispersions are formed when sufficient PEO is present.
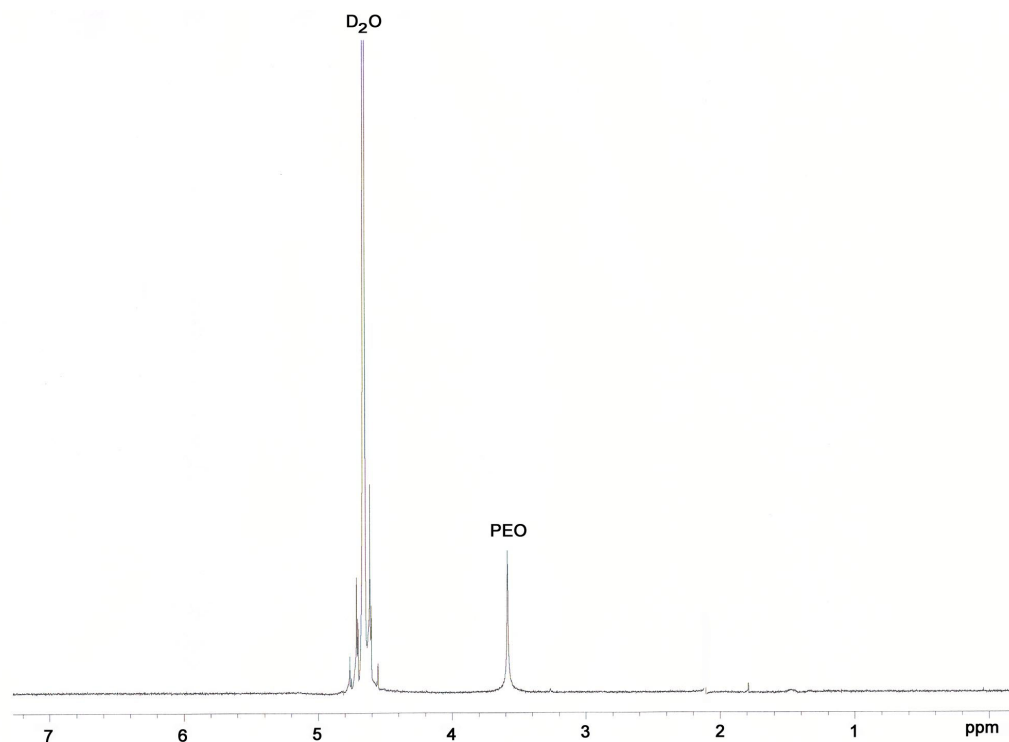
Figure 4.1 *^{1}H-NMR spectrum of PEO-PLGA nanoparticles dispersed in D$_2$O.*

Electron microscopy

PLGA and PEO-PLGA nanoparticles were analyzed by SEM to determine the morphology and the nanoparticle size in the dry state (Figure 4.2).

As can be seen in Figure 4.2 spherical particles were obtained. Especially in the case of the PLGA nanoparticles, the size distribution is very narrow. The PEO-PLGA nanoparticles have a somewhat broader size distribution.

The average size of these PLGA particles as determined by DLS (124 nm) is a hydrodynamic diameter, whereas the particle size as determined by SEM (approximately 105 nm; Figure 4.2A) is the actual size in the dry state. This difference in size indicates that considerable swelling (65%) of the particles occurs. Since the particle size distribution of PEO-PLGA nanoparticles observed by SEM is broader than determined by DLS, aggregation of particles occurred, probably during drying of PEO-PLGA nanoparticles prior to the SEM-analysis. The

fact that the hydrodynamic diameter of PEO-PLGA nanoparticles as determined by DLS (268 nm) is larger than the particle size observed by SEM (approximately 220 nm; Figure 4.2B) is caused by aggregation as well as swelling.
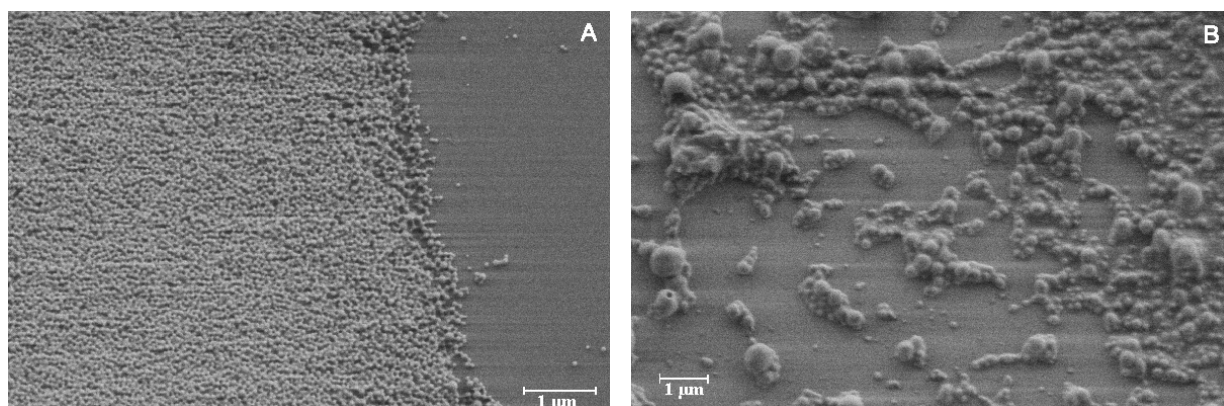
Figure 4.2 *Scanning electron microscopy image of (A) PLGA nanoparticles with PVA and (B) PEO-PLGA nanoparticles without PVA on a silicon substrate obtained by air-drying an aqueous dispersion (10 mg/ml) for 2 h at 25 °C.*

The zeta-potential measurements and ^{1}H-NMR-analysis give an indication of the surface characteristics of the nanoparticles in an aqueous environment. To determine the surface characteristics of the particles in the dry state, XPS and ToF-SIMS were conducted. To 'preserve' the wet state, nanoparticle formulations were freeze-dried and subsequently analyzed. Besides nanoparticle formulations, the constituents PLGA, PEO, PEO-PLGA and PVA were also analyzed.

XPS-analysis

To determine possible damage of the surface by the XPS-analysis, 4 sequential C1*s* scans of 2.5 min each were conducted on one spot. No change in composition in time was observed. As the acquisition time for analysis of the nanoparticles was 5 min, it was concluded that no degradation due to the X-ray exposure takes place during the measurement. This is in accordance with the observations by Shakesheff *et al.* [21].

From the survey scan the surface atomic composition was determined and the C/O-ratio of the polymers was calculated (Table 4.3). No significant amounts (less than 0.4%) of elements other than C and O were detected. Except for the PLGA copolymer, the C/O-ratio of all polymers as calculated from the measured atomic composition is close to the theoretical C/O-ratio. The deviation for PLGA could be caused by a slight enrichment of lactide-units at the surface, as the C/O-value is closer to poly(lactide) (1.50) than to poly(glycolide) (1.00).

Deconvolution of the C1*s* scans was performed after referencing chemical shifts to the O-$\underline{\text{C}}$=O peak (289.00 eV), because the commonly used $\underline{\text{C}}$-C/H peak was not always clearly identifiable. The individual carbon environments were selected from the chemical formula of the polymers. This is exemplified for PEO-PLGA and PVA in Figure 4.3.
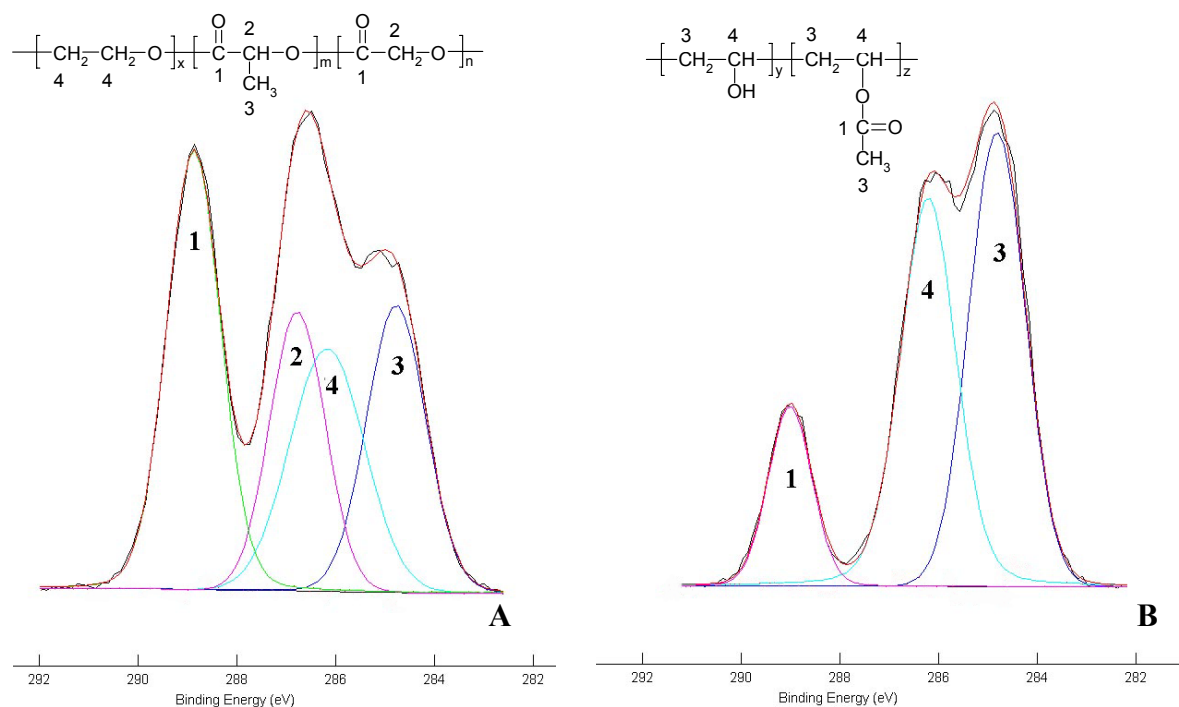
Figure 4.3 *C1s regions of XPS spectra of (A) PEO-PLGA and (B) PVA. The bold lines show the XPS spectrum. The numbered curves show the calculated fit resulting from deconvolution. The numbers in the curves correspond to the numbers in the chemical formula.*

The atom percentages of carbon atoms in different binding states of the polymers are summarized in Table 4.3. The theoretical values are based on the molar composition of the polymer, whereas the experimental values are obtained by deconvolution of the C1*s* peaks.

The C1*s* peak of PLGA was deconvoluted into three peaks, corresponding to O-C=O (peak 1; 289.0 eV), C-O-C=O (peak 2; 286.8 eV) and C-C/H (peak 3; 284.8 eV). The C1s peak of PEO-PLGA (Figure 4.3A) was deconvoluted into four peaks: peak 1 to 3 for PLGA and an additional peak corresponding to the ether C-O-C (peak 4; 286.2 eV), as observed for PEO. It is noted, that the methine group in the PLGA is shifted +0.6 eV compared to the ether group of PEO, caused by the adjacent ester [46].

For PVA, the best fit was obtained using three main peaks corresponding to O-C=O (peak 1; 289.0 eV), C-O-H (peak 4; 286.2 eV) and C-C/H (peak 3; 284.8 eV) (Figure 4.3B).

The deconvolution results described above correspond to deconvolution results described in literature [46]. The atom percentages of carbon atoms in different binding states show some deviation from theory. On one hand this may be caused by reorganization within the sample and on the other hand this may be due to the accuracy of the XPS analysis not being high enough.

The C/O-ratios of the polymers and the data obtained from deconvolution are used to estimate the contributions of each polymer to the nanoparticle surface. The denotation of the nanoparticles corresponds to the denotation used in Table 4.2.

PEO-PLGA 0 FD[*] is characterized by a C/O-ratio in between the C/O-ratio of the PLGA (1.31) and PVA (2.00) polymers (Table 4.3). This indicates that PVA is present at the surface. Either only part of the analyzed surface is covered with PVA or the depth of analysis is larger than the thickness of the PVA layer. The lower atom percentages of carbon atoms in ester and methine groups when compared to PLGA alone also show that PVA is present at the surface.
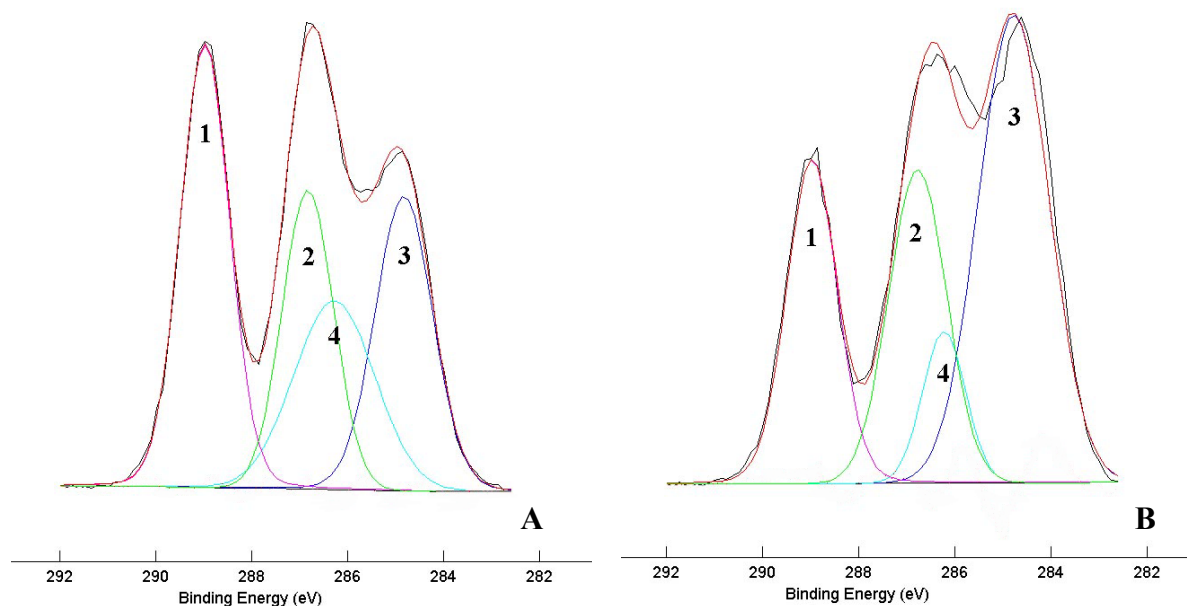
Figure 4.4 *C1s regions of XPS spectra of (A) lyophilized PEO-PLGA nanoparticles without PVA and (B) lyophilized PEO-PLGA nanoparticles with PVA. The bold lines show the XPS spectrum. The numbered curves show the calculated fit resulting from deconvolution. The numbers in the curves correspond to the numbers in Figure 4.3.*

PVA is also present at the surface of PEO-PLGA 1 FD[*] (Figure 4.4B), as the C-C/H-percentage is clearly higher than for PEO-PLGA and for PEO-PLGA nanoparticles without PVA (Figure 4.4A). This explains why the C/O-value of PEO-PLGA 1 FD[*] is approximately the same as the C/O-value of PEO-PLGA 0 FD[*]. The same conclusion can be drawn for PEO-PLGA 0 AD[*]. PVA is present at the surface of these particles as the C/O-value is higher than the value for PLGA. For PEO-PLGA 1 AD[*] it is difficult to draw a conclusion based on the data. The C/O-ratio is less than PEO-PLGA and the presence of a (small) C-O-C/H-peak (Table 4.3) can be due to either PEO or PVA present, or a combination of both.

The C/O-value of the freeze-dried PEO-PLGA nanoparticles based on different ratios of PEO-PLGA and PLGA is slightly higher when relatively more PEO-PLGA is used to prepare the nanoparticles and lies slightly above the C/O-value of PEO-PLGA (1.50). This indicates that some PEO-enrichment takes place, which is highest when more PEO-PLGA is present. For corresponding air-dried nanoparticles samples, the C/O-values and the compositions are shifted towards values more resembling PLGA and no PEO-enrichment was observed. This might be caused by rearrangements upon drying of the samples, as the hydrophobic PLGA tends to migrate to the air-particle interface.

Table 4.3 XPS and ToF-SIMS results of PLGA, PEO, PEO-PLGA and PVA used in the nanoparticle preparation. XPS and ToF-SIMS results of PLGA and PEO-PLGA nanoparticles with PVA and of nanoparticles of different weight fractions of PEO-PLGA/PLGA without PVA.

Code	C/O	C1s (atom%)				Enrichment of PVA (%)[‡]	Enrichment of PEO (%)[‡]
		<u>C</u>-C/H	<u>C</u>-O-C/H	<u>C</u>-O-C=O	O-<u>C</u>=O		
PLGA (theor)	1.31	22	-	39	39	-	-
PLGA	1.43	29	-	35	36	-	-
PEO (theor)	2.00	-	100	-	-	-	-
PEO	1.96	-	100	-	-	-	-
PEO-PLGA (theor)	1.50	15	27	29	29	-	-
PEO-PLGA	1.50	14	36	26	24	-	-
PVA (theor)	2.00	50	42	-	8	-	-
PVA	2.07	49	40	-	11	-	-
PEO-PLGA 0 FD[*][†]	1.56	33	23	19	25	92	-
PEO-PLGA 1 FD[*][†]	1.55	44	9	24	23	23	-
PEO-PLGA 1 FD[†]	1.52	30	20	21	29	-	6.0
PEO-PLGA 0.7 FD[†]	1.51	22	29	20	29	-	0.4
PEO-PLGA 0.4 FD[†]	1.50	24	23	22	31	-	0.2
PEO-PLGA 0 AD[*][†]	1.35	27	3	36	34	36	-
PEO-PLGA 1 AD[*][†]	1.38	31	7	33	29	43	-
PEO-PLGA 1 AD[†]	1.48	28	7	34	31	-	−1.8
PEO-PLGA 0.7 AD[†]	-	19	30	19	32	-	−1.0
PEO-PLGA 0.4 AD[†]	1.47	23	23	23	31	-	−0.3

[*]PVA added as a stabilizer.

[†]FD stands for freeze-dried nanoparticles, AD for air-dried nanoparticles and the numbers denote the weight fraction of PEO-PLGA in the PEO-PLGA/PLGA nanoparticles.

[‡]values derived from the negative ToF-SIMS spectra.

ToF-SIMS-analysis

Negative and positive ToF-SIMS spectra of the polymers were obtained. As an example, the negative spectrum of PEO-PLGA is shown in Figure 4.5. In this spectrum m/z-ratios corresponding to fractions related to n lactyl units (nLA), n glycolyl units (nGA) and n EO units (nEO) are observed. Polymer fragments plus or minus a hydrogen atom (as the fractions are ionized), denoted as "±H" and plus or minus an oxygen atom (+O or −O) were identified. Characteristic peaks are observed at m/z = 71, 73, 87, 89, 143, 145, 159 and 161 (nLA±H (+O)), at m/z = 59, 73, 75, 115, 117, 131 and 133 (nGA±H (+O)), at m/z = 172 (LA+2GA−O) and at m/z = 43, 45, 58, 59, 61, 87, 89, 103 and 105 (nEO±H (+O) (+CH$_2$)).

In the positive PEO-PLGA spectrum (data not shown) peaks at m/z = 55, 71, 73, 127, 143 and 145 (nLA±H (−O)), at m/z = 43, 57, 59, 101, 115, 117 and 159 (nGA±H (−O)) and at m/z = 43, 45, 71, 73, 87, 89, 101, 103, 115, 117, 131, 133, 145 and 147 (nEO±H (−O)) are observed. The negative and positive PLGA ToF-SIMS spectra display peaks corresponding to nLA and/or nGA ±H and +O or −O, and the PEO spectrum of nEO±H and +O or −O.
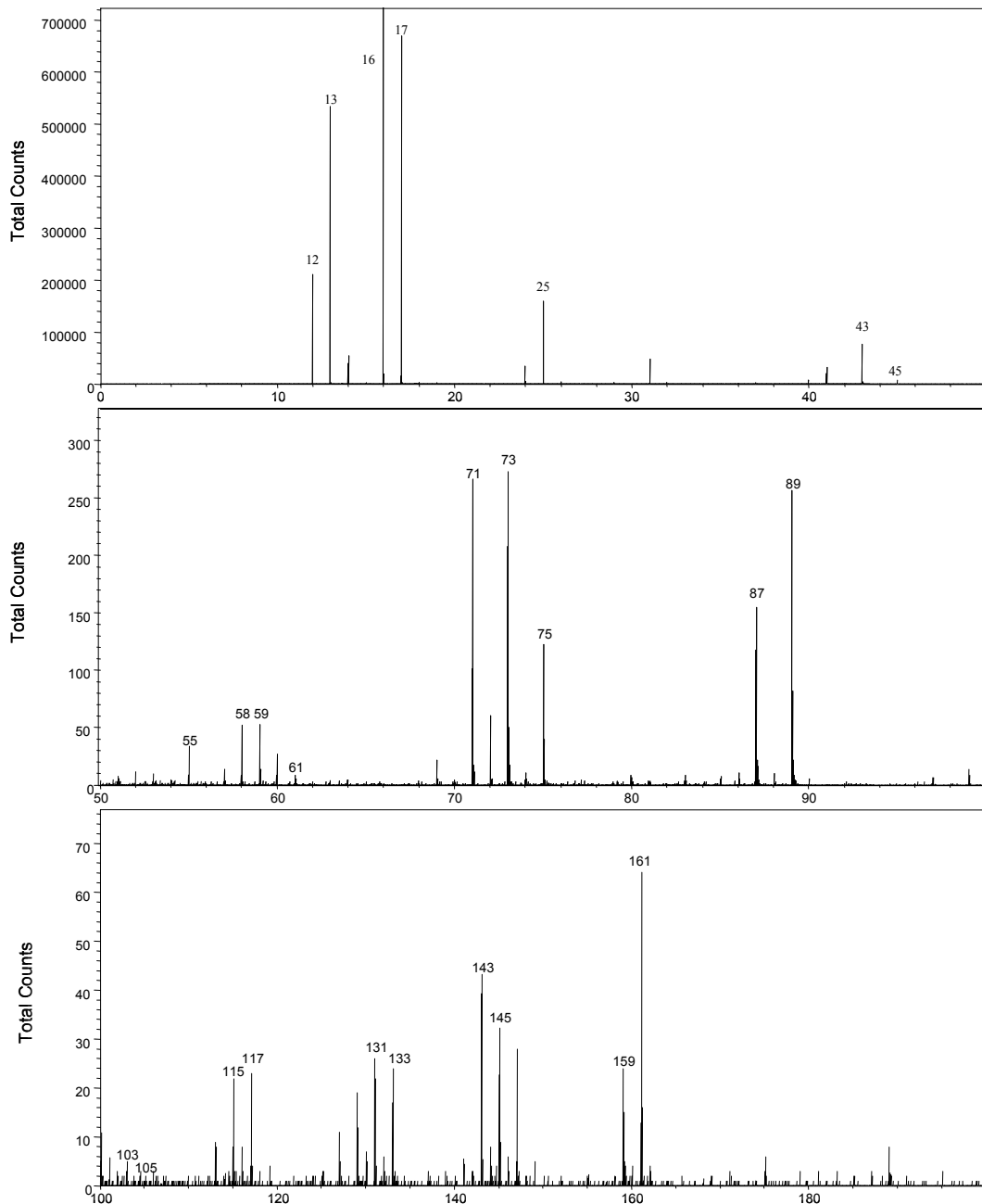
Figure 4.5 *Negative ToF-SIMS spectrum of PEO-PLGA for m/z-ratios from 0 until 200, split in three m/z-intervals.*

Only a few peaks are detected in the negative and the positive spectrum of PVA, mainly arising from the poly(vinyl acetate) component. The dominant peak of PVA in the negative spectrum is located at $m/z = 59$ (O-CO-CH$_3$) and in the positive spectrum at $m/z = 43$ (CO-CH$_3$).

From characteristic peaks in the negative ToF-SIMS spectra of the nanoparticles and polymers, PVA- and PEO-enrichment were calculated (Table 4.3). The denotation of the nanoparticles corresponds to the denotation used in the XPS-analysis. In accordance with the XPS-analysis, it is seen that the surface of PEO-PLGA 0 FD[*], PEO-PLGA 1 FD[*], PEO-PLGA 0 AD[*] and PEO-PLGA 1 AD[*] is partly covered with PVA (92, 23, 36 and 43%,

respectively) (Table 4.3). The fact that the percentage of PVA is smaller for PEO-PLGA 1 FD[*] than for PEO-PLGA 0 FD[*] may be caused by the presence of PEO at the surface, that decreases the amount of PVA needed to stabilize the surface. This difference is not seen in the air-dried (AD) nanoparticles and could be due to surface reorganization during sample preparation.

From the analysis of freeze-dried nanoparticles prepared with PEO-PLGA fractions 0.4-1, it seems that some PEO-surface enrichment takes place and that the surface enrichment is highest when more PEO-PLGA is present. However, as for the XPS-results, the surface enrichment is less than what is expected from the results in the hydrated state.

For the air-dried nanoparticles prepared with different PEO-PLGA fractions, there does not seem to be a PEO-surface enrichment, as indicated by the negative value determined from ToF-SIMS. This is in agreement with the results obtained with XPS-analysis and is probably caused by rearrangements during sample preparation.

CONCLUSIONS

It has been shown that spherical PEO-PLGA nanoparticles can be prepared without stabilizer using different ratios of PEO-PLGA to PLGA. From ^{1}H-NMR-analysis and zeta-potential measurements it is concluded that in the hydrated state PEO is preferentially present at the surface, resulting in stable nanoparticle dispersions. The amount of PEO was varied by using different ratios of PEO-PLGA to PLGA in the nanoparticle preparation. It is concluded that for the PEO-PLGA and PLGA compositions of this study, at least 13 wt% of PEO needs to be present to obtain stable nanoparticle dispersions. However, the combination of particle size and zeta-potential analysis showed that PEO is not exclusively present at the particle surface. This is confirmed by high swelling of the particles (80%). From ToF-SIMS- and XPS-analysis of nanoparticles in the dry state, no PEO-enrichment on the nanoparticle surface was determined. Apparently, reorganization of the polymer chains occurs during preparation of the nanoparticle samples.

ACKNOWLEDGEMENTS

REFERENCES

1. Juni, K. and Nakano, M., *Crit. Rev. Ther. Drug Carrier Syst.,* **1987**, *3*, 209-232.
2. Lemoine, D.; Francois, C.; Kedzierewicz, F.; Preat, V.; Hoffman, M. and Maincent, P., *Biomaterials,* **1996**, *17*, 2191-2197.

3. Yamaguchi, K. and Anderson, J.M., *J. Control. Release,* **1993**, *24*, 81-93.

4. Anderson, J.M. and Shive, M.S., *Adv. Drug Deliv. Rev.,* **1997**, *28*, 5-24.

5. Gautier, S.E.; Oudega, M.; Fragoso, M.; Chapon, P.; Plant, G.W.; Bunge, M.B. and Parel, J.M., *J. Biomed. Mater. Res.,* **1998**, *42*, 642-654.

6. Ignatius, A.A. and Claes, L.E., *Biomaterials,* **1996**, *17*, 831-839.

7. Piskin, E., *J. Biomater. Sci. Polym. Ed.,* **1994**, *6*, 775-795.

8. Allémann, E.; Gurny, R. and Dölker, E., *Eur. J. Pharm. Biopharm.,* **1993**, *39*, 173-191.

9. Moghimi, S.M., *Biochim. Biophys. Acta,* **1997**, *1336*, 1-6.

10. Araujo, L.; Lobenberg, R. and Kreuter, J., *J. Drug Target.,* **1999**, *6*, 373-385.

11. Moghimi, S.M.; Hunter, A.C. and Murray, J.C., *Pharmacol. Rev.,* **2001**, *53*, 283-318.

12. Scholes, P.D.; Coombes, A.G.A.; Illum, L.; Davis, S.S.; Watts, J.F.; Ustariz, C.; Vert, M. and Davies, M.C., *J. Control. Release,* **1999**, *59*, 261-278.

13. Hueper, W.C., *A.M.A. Arch. Pathol.,* **1959**, *67*, 589-617.

14. Carrio, A.; Schwach, G.; Coudane, J. and Vert, M., *J. Control. Release,* **1995**, *37*, 113-121.

15. Stolnik, S.; Garnett, M.C.; Davies, M.C.; Illum, L.; Bousta, M.; Vert, M. and Davis, S.S., *Colloids Surf. A - Physicochem. Eng. Asp.,* **1995**, *97*, 235-245.

16. Jeong, Y.I.; Cho, C.S.; Kim, S.H.; Ko, K.S.; Kim, S.I.; Shim, Y.H. and Nah, J.W., *J. Appl. Polym. Sci.,* **2001**, *80*, 2228-2236.

17. Gref, R.; Luck, M.; Quellec, P.; Marchand, M.; Dellacherie, E.; Harnisch, S.; Blunk, T. and Muller, R.H., *Colloids Surf. B - Biointerfaces,* **2000**, *18*, 301-313.

18. Gref, R.; Minamitake, Y.; Peracchia, M.T.; Trubetskoy, V.; Torchilin, V. and Langer, R., *Science,* **1994**, *263*, 1600-1603.

19. Allémann, E.; Brasseur, N.; Benrezzak, O.; Rousseau, J.; Kudrevich, S.V.; Boyle, R.W.; Leroux, J.-C.; Gurny, R. and Van Lier, J.E., *J. Pharm. Pharmacol.,* **1995**, *47*, 382-387.

20. Kwon, G.S., *Crit. Rev. Ther. Drug Carrier Syst.,* **1998**, *15*, 481-512.

21. Shakesheff, K.M.; Evora, C.; Soriano, I. and Langer, R., *J. Colloid Interface Sci.,* **1997**, *185*, 538-547.

22. Shaffer, C.B. and Critchfield, F.H., *Am. J. Pharm. Assoc.,* **1947**, *36*, 152-157.

23. Zweers, M.L.T.; Grijpma, D.W.; Engbers, G.H.M. and Feijen, J., *J. Biomed. Mater. Res. - Appl. Biomat.,* **2002**, submitted.

24. Rabiant, J., *S.T.P. Pharma,* **1991**, *1*, 278-283.

25. Provencher, S.W.; Hendrix, J. and De Maeyer, L., *J. Chem. Phys.,* **1978**, *69*, 4273-4276.

26. Gilding, D.K. and Reed, A.M., *Polymer,* **1979**, *20*, 1459-1464.

27. Schwach, G.; Coudane, J.; Engel, R. and Vert, M., *Polym. Bull.,* **1996**, *37*, 771-776.

28. Tracy, M.A.; Ward, K.L.; Firouzabadian, L.; Wang, Y.; Dong, N.; Qian, R. and Zhang, Y., *Biomaterials,* **1999**, *20*, 1057-1062.

29. Wang, N.; Wu, X.S.; Chao, L. and Mei, F.F., *J. Biomater. Sci. Polym. Ed.,* **2000**, *11*, 301-318.

30. Kricheldorf, H.R.; Kreiser-Saunders, I. and Stricker, A., *Macromolecules,* **2000**, *33*, 702-709.

31. Aucejo, S.; Marco, C. and Gavara, R., *J. Appl. Polym. Sci.,* **1999**, *74*, 1201-1206.

32. De Jaeghere, F.; Allémann, E.; Feijen, J.; Kissel, T.; Dölker, E. and Gurny, R., *Pharm. Dev. Technol.,* **2000**, *5*, 473-483.

33. Zambaux, M.F.; Bonneaux, F.; Gref, R.; Dellacherie, E. and Vigneron, C., *J. Biomed. Mater. Res.,* **1999**, *44*, 109-115.

34. Kabanov, A.V.; Nazarova, I.R.; Astafieva, I.V.; Batrakova, E.V.; Alakhov, V.Y.; Yaroslavov, A.A. and Kabanov, V.A., *Macromolecules,* **1995**, *28*, 2303-2314.

35. Heald, C.R.; Stolnik, S.; De Matteis, C.; Garnett, M.C.; Illum, L.; Davis, S.S. and Leermakers, F.A.M., *Colloids Surf. A - Physicochem. Eng. Asp.,* **2001**, *179*, 79-91.

36. Gölander, C.-G.; Herron, J.N.; Lim, K.; Claesson, P.; Stenius, P. and Andrade, J.D., Properties of immobilized PEG films and the interaction with proteins - Experiments and modeling, In *Poly(ethylene*

glycol) chemistry - Biotechnical and biomedical applications; Harris, J.M., Ed.; Plenum Press: New York, **1992**.

37. Myrvold, R.; Hansen, F.K. and Balinour, B., *Colloids Surf. A - Physicochem. Eng. Asp.,* **1996**, *117*, 27-36.

38. Brandrup, J.; Immergut, E.H. and Grulke, E.A. *Polymer handbook*; 4th ed.; John Wiley & Sons, Inc.: New York, **1999**.

39. Schmitt, E.A.; Flanagan, D.R. and Linhardt, R.J., *Macromolecules,* **1994**, *27*, 743-748.

40. Li, Y.-P.; Pei, Y.-Y.; Zhang, X.-Y.; Gu, Z.-H.; Zhou, Z.-H.; Yuan, W.-F.; Zhou, J.-J.; Zhu, J.-H. and Gao, X.-J., *J. Control. Release,* **2001**, *71*, 203-211.

41. De Jaeghere, F.; Allémann, E.; Feijen, J.; Kissel, T.; Dölker, E. and Gurny, R., *J. Drug Target.,* **2000**, *8*, 143-154.

42. Gref, R.; Domb, A.; Quellec, P.; Blunk, T.; Müller, R.H.; Verbavatz, J.M. and Langer, R., *Adv. Drug Deliv. Rev.,* **1995**, *16*, 215-233.

43. Quintanar-Guerrero, D.; Fessi, H.; Allémann, E. and Dölker, E., *Int. J. Pharm.,* **1996**, *143*, 133-141.

44. Coombes, A.G.A.; Tasker, S.; Lindblad, M.; Holmgren, J.; Hoste, K.; Toncheva, V.; Schacht, E.; Davies, M.C.; Illum, L. and Davis, S.S., *Biomaterials,* **1997**, *18*, 1153-1161.

45. Ribeiro, A.A. and Dennis, E.A.J., *J. Colloid Interface Sci.,* **1976**, *55*, 94-101.

46. Beamson, G. and Briggs, D. *High resolution XPS of organic polymers - The scientific ESCA300 database*; John Wiley & Sons: Chichester, UK, **1992**.

CHAPTER 5

In vitro degradation of nanoparticles prepared from polymers based on DL-lactide, glycolide and poly(ethylene oxide)

ABSTRACT

Nanoparticles of poly(DL-lactic acid) (PDLLA), poly(DL-lactic-co-glycolic acid) (PLGA) and poly(ethylene oxide)-PLGA diblock copolymer (PEO-PLGA) were prepared by the salting-out method. The in vitro degradation of PDLLA, PLGA and PEO-PLGA nanoparticles in PBS (pH 7.4) at 37 °C was studied. The particle size, molecular weight of the nanoparticles and the amount of lactic and glycolic acid formed were followed in time. PDLLA nanoparticles gradually degraded over a period of two years and retain their size during that period. A faster degradation was observed for PLGA nanoparticles, which was nearly complete after ten weeks. PLGA nanoparticles retained their size during that period. In PEO-PLGA nanoparticles, the ester bond connecting the PEO and the PLGA segments was preferentially cleaved, which led to a relatively fast decrease in molecular weight and to (partial) aggregation, as multimodal size distributions were observed. PEO-PLGA nanoparticles were almost completely degraded within eight weeks.

INTRODUCTION

Block copolymers based on poly(ethylene oxide) (PEO) and poly(DL-lactic-co-glycolic acid) (PLGA) have been applied for the preparation of nanoparticles for drug delivery. The use of PEO-PLGA block copolymers enables the preparation of non-aggregating particles without the need of an additional stabilizer such as poly(vinyl alcohol) (PVA) [1].

PEO is an uncharged, highly flexible polymer that is known to decrease protein adsorption and cell interactions when present at the surface [2]. PEO has outstanding physiochemical and biological properties including solubility in water and in organic solvents [3]. Furthermore, it is non-toxic, non-antigenic and non-immunogenic [3]. It has been shown that PEO with a molecular weight less than $6 \cdot 10^3$ g/mol is passively excreted by the kidney [4].

PLGA copolymers are known for their biodegradability and biocompatibility [5-9]. The final degradation products are lactic and glycolic acid, which are either excreted by the kidneys or enter the Krebs cycle to be eventually eliminated as carbon dioxide and water [10].

The term degradation is used to describe the chain scission of the polymer, whereas erosion is used to describe mass loss [11]. Depending on relative rates of water diffusion into the polymer matrix and degradation of the polymer, two degradation processes can be distinguished. When polymer degradation is faster than diffusion of water into the matrix, degradation and erosion become a surface phenomenon. In the opposite case, where diffusion of water into the matrix is faster than polymer degradation, the whole matrix is affected by degradation and subsequent erosion [11].

PLGA is known to undergo bulk degradation [12], as water diffusion into the matrix is faster than polymer degradation [11]. This process is characterized by random hydrolytic scission of the polyester backbone. The rate of degradation increases with increasing glycolide content in the polymer [13,14] due to a higher amount of bound, reactive water [15], being highest for copolymers with 70 mol% of glycolide [5]. The degradation rate of PEO-PLGA copolymers is higher than of PLGA copolymers [16] due to increased hydrophilicity [17] as characterized by an increased water-uptake [18]. Oligomers of PLGA with a molecular weight less than approximately $1 \cdot 10^3$ g/mol are soluble in water [19]. Oligomers with more monomeric units can still be solubilized when they are connected to PEO [20]. Consequently, earlier mass loss will be encountered for the degradation of PEO-PLGA as compared to PLGA for similar PLGA composition and molecular weight.

Numerous investigations have dealt with the *in vitro* degradation of PLGA. However, the results often differ because the samples used for the degradation studies vary in size and shape. It has been reported that the degradation rate increases with increasing thickness of the sample [21]. The main reason for this phenomenon is the occurrence of autocatalysis caused by the carboxylic end groups formed by chain cleavage [22]. Autocatalysis is more pronounced for thicker samples because of the longer pathway for diffusion of oligomers to the surface [21] and for hydroxide ions into the matrix [23]. This results in accumulation of oligomers in the bulk, and therefore in an increased concentration of carboxylic end groups

which cannot be neutralized by buffer ions, leading to a faster degradation rate in the inside than the outside of the sample. This will result in a bimodal molecular weight distribution in time [21]. It has been observed that thick films or plates develop a skin of approximately 200 μm in which degradation is much slower than in the bulk [21]. On the basis of these results it can be expected that when the thickness of the samples is decreased the contribution of faster bulk degradation to the degradation process of the whole sample will be diminished [21]. This corresponds with the fact that microparticles degrade slower than millimeter-sized beads [21] and that an even slower degradation was found for nanoparticles [24].

There is abundant information on the degradation behavior of poly(DL-lactic acid) (PDLLA) and PLGA microparticles [6,14,16,21,24-37], but only a few studies on the degradation of nanoparticles prepared from PDLLA [38,39], PLGA [19,24,40] or PEO-PLGA [41] are available. The influence of temperature [38] and pH [39] on the degradation of PDLLA nanoparticles has been studied. At neutral pH at 37 °C, the molecular weight half-life of PDLLA nanoparticles was more than 150 days in both studies [38,39]. However, in one study, this conclusion was drawn based on only two time points [39]. In one paper, the *in vitro* degradation of PLGA nanoparticles (530 ± 300 nm) was studied. The particles were totally degraded after 150 days and it was concluded that autocatalysis occurred [24]. In a degradation study of drug-loaded PLGA nanoparticles, no substantial decrease in molecular weight was observed. However, the molecular weight was only monitored for 60 h [40]. In the degradation study of PEO-PLGA nanoparticles, copolymers with constant PEO length ($\overline{M}_n = 5\cdot10^3$ g/mol) and various PLGA lengths ($\overline{M}_n = 7$-$68\cdot10^3$ g/mol) were used [41]. PEO was preferentially cleaved and it was stated that these drug-loaded particles degraded by surface erosion. This conclusion was based on the occurrence of mass loss without a decrease in molecular weight. However, the molecular weight was only measured for 7 days [41]. Comparison of these studies is hampered due to differences in particle preparation conditions and molecular weights of the polymers.

To avoid these problems, nanoparticles of PDLLA, PLGA and PEO-PLGA of similar (relatively low) molecular weights were prepared and their degradation in PBS at pH 7.4 and 37 °C was studied.

MATERIALS AND METHODS

Materials

DL-lactide and glycolide were purchased from Purac Biochem b.v. (Gorinchem, The Netherlands). Stannous octoate, L-lactic acid and sodium azide (NaN$_3$) were purchased from Sigma (St. Louis, USA) and used as received. Hexanol (Merck, Darmstadt, Germany) was distilled from calcium hydride (Acros Organics, New Jersey, USA) prior to use. Monomethoxy poly(ethylene glycol) (MPEG) ($\overline{M}_n = 3.0\cdot10^3$ g/mol) was purchased from Shearwater Polymers (Huntsville, USA). Deuterated chloroform (CDCl$_3$), magnesium chloride hexahydrate (MgCl$_2\cdot$6H$_2$O) and glycolic acid were purchased from Merck and poly(vinyl alcohol) (PVA) ($\overline{M}_n = 9$-$10\cdot10^3$ g/mol; 80% hydrolyzed from poly(vinyl acetate)) was purchased from Aldrich (Milwaukee, USA) and used as received. Phosphate

buffered saline (PBS; pH 7.4) (NPBI, Emmer Compascuum, The Netherlands) was used as received. All solvents used were of analytical grade (Biosolve, Valkenswaard, The Netherlands).

Polymer syntheses

A mixture of DL-lactide (10.1 g; 69.8 mmol) and glycolide (5.45 g; 47.0 mmol) with stannous octoate in pentane (5.0 ml; 1.89 g/l) and an appropriate amount of initiator (318 μl hexanol or 7.59 g MPEG; 2.53 mmol) were transferred to an ampoule. After removal of the pentane by applying vacuum, the ampoule was evacuated, vacuum-sealed and subsequently transferred to an oil bath at 130 °C. After 24 h of reaction, the crude product was dissolved in chloroform, precipitated into a ten-fold volume of methanol, filtered and dried in vacuo at 40 °C for three days.

The synthesized (co)polymers are denoted as PDLLA for the homopolymer of DL-lactide, as PLGA for the copolymer of DL-lactide and glycolide and as PEO-PLGA for the block copolymer of poly(ethylene oxide) and PLGA.

Polymer characterization

The number average molecular weight ($\overline{M}_n$) and the composition of the (co)polymers were determined by proton nuclear magnetic resonance (^{1}H-NMR) with CDCl$_3$ as the solvent. The sequence lengths of monomeric units in PLGA were determined by ^{13}C-NMR from copolymer solutions in CDCl$_3$ (100 mg/ml). Average sequence lengths were calculated from the dyad splitting of the carbonyl signals [42]. NMR spectra were obtained using a Varian Inova (Varian, Palo Alto, USA) operating at 300 MHz.

The $\overline{M}_n$ and molecular weight distribution of the (co)polymers were determined by gel permeation chromatography (GPC) at 25 °C using chloroform as an eluent at a flow rate of 1.5 ml/min. The GPC system consisted of a Waters Model 510 pump, a HP Ti-Series 1050 autosampler, a Waters Model 410 Differential Refractometer, and a Viscotek H502 Viscometer Detector with HR0.5, HR2 and HR4 Waters Ultra-Styragel columns (Waters, Milford, USA) placed in series. Polystyrene standards with narrow molecular weight distributions (PSS, Mainz, Germany) were used for calibration.

Nanoparticle preparation

Nanoparticles were prepared using the salting-out method [1,43] in which acetone was chosen as the water-miscible organic solvent, because of its pharmaceutical acceptance with regard to toxicity [44]. The method consists of the addition of a water-soluble PVA in a highly concentrated salt solution in water (aqueous phase) to a polymer solution in acetone (organic phase). Although acetone is miscible with pure water in all ratios, the high salt concentration of the aqueous phase prevents mixing of the phases. After emulsification, the addition of pure water in a sufficient quantity causes acetone to diffuse into the aqueous phase, resulting in the formation of nanoparticles.

Typically, an acetone solution (5.0 g) containing 2 wt% (co)polymer was emulsified under mechanical stirring (20,500 rpm; 40 s; T25 Ultraturrax equipped with a S25 dispersing tool, Ika-Labortechnik, Staufen, Germany) in an aqueous phase (7.5 g) containing 60 wt% MgCl$_2$·6H$_2$O as the salting-out agent and 2 wt% PVA as a stabilizer (in a glass beaker; 3.5 cm diameter; 6.6 cm height). After the fast addition (5 s) of pure water (7.5 g) under mechanical stirring (20,500 rpm) causing acetone to diffuse into the water phase, nanoparticles were formed and stirring was continued for 20 s at 20,500 rpm. PEO-PLGA nanoparticles were prepared in the same manner, but no PVA was used [1].

The nanoparticles were purified by rinsing with water. First, the nanoparticles were separated by ultracentrifugation (65,000×g for 30 min; Centrikon T-2180, Kontron Instruments, Watford, UK) and the supernatant was removed. The nanoparticles were redispersed in water, centrifuged and the supernatant was removed. This procedure was repeated three times.

In vitro degradation of nanoparticles

PDLLA, PLGA and PEO-PLGA nanoparticles were redispersed in PBS containing 0.02% (w/v) NaN$_3$, at a known concentration of approximately 4 mg/ml. Subsequently, the dispersions were transferred to ultracentrifugation tubes, closed and placed in an oven at 37 °C. At different time points, the particle size was determined. At the same time, nanoparticles were separated from the medium by ultracentrifugation (65,000×g for 40 min). The supernatant was analyzed by HPLC to determine the amount of lactic and glycolic acid and the pH of the supernatant was measured at 25 °C. The sediment was lyophilized and subsequently analyzed with respect to the molar composition and $\overline{M}_n$ of the polymer.

Particle size analysis

The nanoparticle size was determined by dynamic light scattering (DLS) (Zetasizer 4000, Malvern Instruments Ltd., Malvern, UK) at 25 °C at an angle of 90°, taking the average of three measurements. The particle dispersion was diluted with PBS to such a degree that the desired number of counts was obtained. The desired number of counts is the number of counts that is high enough to obtain a good signal to noise ratio, yet small enough to prevent multiple scattering to occur.

First, the polydispersity index (P.I.) is determined by the cumulants method. The P.I. is a dimensionless number indicating the width of the size distribution, and has a value between zero and one, being zero for monodisperse particles. If the P.I. is small enough (<0.08), the particle size can be determined by the cumulants method and the size distribution obtained is based on a log normal distribution characterized by a mean and width. For polydispersity indices higher than 0.08, the CONTIN-method is used to determine the particle size. The CONTIN-method, developed by Provencher *et al.* [45] describes bimodal and smooth distributions without the need for information such as an initial estimate for the particle size.

Thermal analysis of nanoparticles

The thermal properties of the nanoparticles in PBS were evaluated by differential scanning calorimetry (DSC) using a DSC 7 (Perkin-Elmer, Shelton, USA). A heating rate of 10 °C/min was applied, and stainless steel pans (Perkin-Elmer) were used. PBS (50 μl) was added to nanoparticle samples (10-15 mg) obtained after ultracentrifugation and removal of the supernatant. The samples were heated from −10 °C to 70 °C. The samples were then cooled (300 °C/min) to −10 °C and after 5 min, a second scan was recorded. The data presented are from the second scan. The glass transition temperatures (T$_g$) were taken as the midpoint of the heat capacity change. Indium and gallium were used as standards for temperature calibration.

Determination of lactic and glycolic acid concentration in the supernatant

The supernatant of the samples after ultracentrifugation was analyzed by high-performance liquid chromatography (HPLC) to determine the amount of lactic and glycolic acid formed. The supernatant (50 μl) was injected (Injector 50 μl loop Valco) on an Inertsil ODS-3 column (250×4.6 mm; 5 μm;

Chrompack, Bergen op Zoom, The Netherlands). UV-treated 0.1 M $NH_4H_2PO_4$ (pH 2.5) (Merck, Darmstadt, Germany) was used as an eluent at a flow rate of 1 ml/min (Varian HPLC pump 2510). Detection of lactic and glycolic acid was performed at 210 nm using a Varian variable λ detector 2550 and compared to a calibration curve for lactic and glycolic acid. Glycolic acid eluted after 3.7 min and lactic acid after 6.1 min at the used conditions.

RESULTS AND DISCUSSION

After polymerization, the crude product was analyzed by ^{1}H-NMR to determine the actual composition and the number average molecular weight ($\overline{M}_n$). The $\overline{M}_n$ and polydispersity index (PDI) were determined by GPC. The results are presented in Table 5.1.

Table 5.1 *The molar composition, number average molecular weight ($\overline{M}_n$), polydispersity index (PDI) and average sequence lengths of the synthesized (co)polymers.*

Polymer	Composition x:y[b]		$\overline{M}_n$ (kg/mol)			PDI[e]	$\overline{L}_L$[f]	$\overline{L}_G$[f]
	feed	polymer	theor[c]	exp[d]	exp[e]			
PDLLA	100:0	100:0	10.1	11.5	14.5	1.42		
PLGA	60:40	57:43	10.1	11.4	12.8	1.95	3.1	2.1
PEO-PLGA[a]	60:40	52:48	11.9	11.2	9.9	1.24	2.4	1.8

[a] $\overline{M}_{n,PEO} = 3 \cdot 10^3$ g/mol.
[b] x:y denotes the ratio of lactyl:glycolyl units of the PLGA block, determined by ^{1}H-NMR.
[c] the theoretical $\overline{M}_n$ is calculated from the [Monomer]/[Initiator] ratio.
[d] determined by ^{1}H-NMR.
[e] determined by GPC.
[f] the average sequence length of lactyl ($\overline{L}_L$) and glycolyl ($\overline{L}_G$) units of the PLGA block, determined by ^{13}C-NMR and calculated from Eq. (5.1) and (5.2), respectively.

The polymer composition is close to the monomer ratio in the feed, with slightly more glycolide than DL-lactide incorporated. The higher reactivity of glycolide in comparison with DL-lactide, as previously reported [46], accounts for the larger fraction of glycolide in the copolymer than in the monomer feed. From ^{1}H-NMR it becomes clear that molecular weights close to the theoretical molecular weight have been obtained. The polydispersity indices range from 1.24 to 1.95. Polydispersity indices close to 2 are typical for stannous octoate catalyzed ring-opening polymerizations of lactide and glycolide [27,47,48] and are indicative of transesterification reactions [49]. The molecular weights of the three polymers as determined by ^{1}H-NMR are comparable. The $\overline{M}_n$ values obtained from GPC measurements are slightly different. The lactyl to glycolyl ratio is similar for the PLGA and PEO-PLGA polymers.
The average sequence lengths of lactyl and glycolyl units in the PLGA block were determined by ^{13}C-NMR [42]. The integrals of the carbonyl peaks of lactyl next to glycolyl (I_{LG}; δ=171.67

ppm) and of lactyl next to lactyl (I_{LL}; δ=171.42 ppm) were used to calculate the average sequence length of lactyl units ($\overline{L}_L$) (Eq. (5.1)).

$$\overline{L}_L = \frac{I_{LL}}{I_{LG} + I_{LL}}$$ (5.1)

The integrals of the carbonyl peaks of glycolyl next to lactyl (I_{GL}; δ=168.63 ppm) and of glycolyl next to glycolyl (I_{GG}; δ=168.64 ppm) were used to calculate the average sequence length of glycolyl units ($\overline{L}_G$) (Eq. (5.2)).

$$\overline{L}_G = \frac{I_{GG}}{I_{GL} + I_{GG}}$$ (5.2)

The average sequence lengths calculated from Eq. (5.1) and (5.2) are given in Table 5.1. The fact that the lactyl and glycolyl sequence lengths are similar suggests that in the PEO-PLGA and PLGA copolymers the monomers are equally distributed.

Aqueous dispersions of PDLLA, PLGA and PEO-PLGA nanoparticles were prepared and characterized with respect to T_g (aqueous suspension) and particle size (Table 5.2). The T_g of the PDLLA nanoparticles is higher than 37 °C, which indicates that these particles are initially in a glassy state in an aqueous environment at body temperature. This is in contrast to the PLGA and PEO-PLGA nanoparticles, which are in the rubbery state under the same conditions. This might have consequences for the rate of degradation, as above the T_g the mobility of the polymer chains is higher and therefore, water diffusion proceeds faster. As water lowers the T_g due to a plasticizing effect [50], the T_g (aqueous suspension) is lower than the T_g (polymer) [1,43]. Furthermore, PDLLA and PLGA nanoparticles have approximately the same size, whereas the PEO-PLGA nanoparticles are smaller (Table 5.2). The smaller the particles, the more autocatalysis is expected to be diminished [21]. However, since water-uptake is high [1], diffusion of buffer ions into and of water-soluble oligomers out of the particles is probably rapid and autocatalysis is not likely to occur for any of the nanoparticles. This means that the difference in size probably will not affect the degradation rate.

Table 5.2 *The T_g, size and polydispersity index (P.I.) of the nanoparticles in PBS before in vitro degradation.*

Nanoparticle	T_g (°C)	Particle size (nm)	P.I. (-)
PDLLA	39	248	0.04
PLGA	35	230	0.09
PEO-PLGA	2	139	0.19

PDLLA nanoparticles had a size of approximately 250 nm at the start of the degradation and a P.I. of 0.04. The $\overline{M}_n$ of the PDLLA decreases in time and the particle size increases slightly (Figure 5.1A). No solid material was visible anymore at week 104. The increase in size can be explained by a higher swelling of the particles due to the formation of carboxylic acid and hydroxyl groups. The P.I. remains below 0.1 until 60 weeks, and does not exceed 0.2 even up

to 98 weeks, which demonstrates that the particles do not aggregate upon degradation. This can be explained by the presence of PVA. It has previously been shown, that after several purification steps up to 10% of PVA can remain present in or on the particles [44]. During degradation, PVA might remain present at the surface to stabilize the particles. Moreover, the increasing number of end groups might contribute to stabilization of the particles.

The small decrease in $\overline{M}_n$ during the first 5 weeks coincides with negligible lactic acid formation (Figure 5.1B) and no change in pH. After week 5 a linear increase of lactic acid formation in time is observed, resulting in a gradual decrease in the pH. The relative amount of lactic acid determined in the medium at week 104 is approximately 15% of the total lactic acid units initially present. The pH was 6.4 at week 104, which is clearly higher than the pK_a of lactic acid (3.8 at 25 °C [39]). The fact that only 15% of total lactic acid units available in the polymer were converted to free lactic acid indicates that large amounts of water-soluble oligomers are present and are not detected. The onset of lactic acid formation for 0.3 mm thick films or microparticles (125-250 µm) is reported to be 10 weeks [21]. This indicates that diffusion of lactic acid from the nanoparticles is faster than from films or microparticles and that the penetration of buffer in nanoparticles is more rapid than in films of microparticles. This implies that accumulation of oligomers containing carboxylic end groups that could catalyze the hydrolysis is less likely to occur in the case of nanoparticles when compared to films or microparticles. Correspondingly, the time needed to completely degrade PDLLA nanoparticles (approximately 100 weeks) is longer than the time needed to completely degrade PDLLA films or PDLLA microparticles (approximately 50 weeks) [21] and corresponds to results on the degradation of PDLLA nanoparticles of others [38,39].
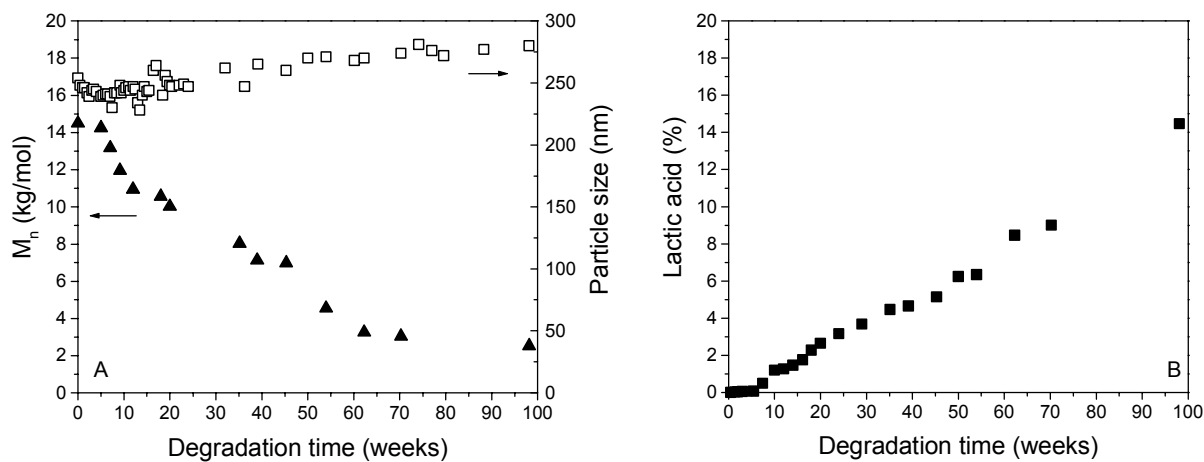
Figure 5.1 *(A) The $\overline{M}_n$ (▲) and the particle size (□) of PDLLA nanoparticles as a function of the degradation time at 37 °C in PBS (pH 7.4). (B) Relative amount of lactic acid in the degradation medium as a function of the degradation time for PDLLA nanoparticles at 37 °C in PBS (pH 7.4), presented as a percentage of the total amount of lactic acid units initially present in the nanoparticles.*

In Figure 5.2, the $\overline{M}_n$, size and relative amount of lactic and glycolic acid formed as a function of degradation time of PLGA nanoparticles is depicted. The $\overline{M}_n$ gradually decreases, reaching 20% of its initial value after 8 weeks. As in the case of PDLLA particles, the particle

size increases slightly in time, with a P.I. lower than 0.2. This indicates that the PLGA nanoparticles do not aggregate upon degradation, which can be explained by the presence of PVA or the increase in number of end groups, as was the case for PDLLA nanoparticles. The degradation of PLGA nanoparticles clearly proceeds more rapidly than the degradation of PDLLA nanoparticles and is complete in 18 weeks.

During degradation of the copolymer, water-soluble oligomers and their corresponding monomeric units, lactic and glycolic acid, are formed. From the first day on, both acids can be detected in the degradation medium (Figure 5.2B). The initial formation of glycolic acid is faster than the formation of lactic acid, as reported before by others [11]. The reason for this is that the glycolic ester bond is more susceptible to hydrolysis [15]. Therefore, there is preferential cleavage at the glycolic-glycolic and glycolic-lactic bonds, resulting in faster release of glycolic acid. This is confirmed by a shift in the copolymer composition towards higher lactide contents increasing from 57 mol% initially to 68 mol% at week 7 as determined by ^{1}H-NMR. The pH gradually decreased in time, being 6.2 after 18 weeks. After 18 weeks, a plateau in the level of acids is reached, and the relative amount of acids corresponds to the percentage of the monomeric units initially present in the nanoparticles (Figure 5.2B). This indicates that PLGA nanoparticles were completely degraded into lactic and glycolic acid after 18 weeks, as also observed by Dunne *et al.* [24]. The fact that lactic and glycolic acid released from the PLGA nanoparticles is seen from day one on indicates that rapid degradation takes place and that degradation products rapidly diffuse into the medium. This also implies that accumulation of oligomers containing carboxylic end groups that could catalyze the hydrolysis is minimal or even absent.
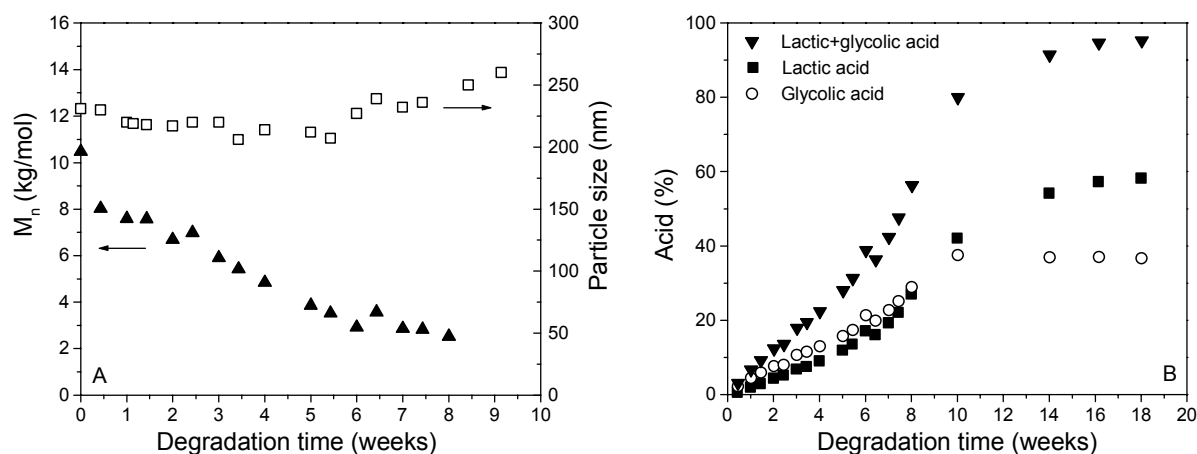
Figure 5.2 *(A) The $\overline{M}_n$ (▲) and the particle size (□) of PLGA nanoparticles as a function of the degradation time at 37 °C in PBS (pH 7.4). (B) Relative amount of lactic and glycolic acid in the degradation medium as a function of the degradation time for PLGA nanoparticles at 37 °C in PBS (pH 7.4), presented as a percentage of the total units initially present in the nanoparticles.*

The results of the degradation of PEO-PLGA nanoparticles that do not contain PVA are presented in Figure 5.3. The $\overline{M}_n$ decreases during the first two weeks, was stable during the next few weeks and then further decreases (Figure 5.3A). The decrease in the first two weeks

is caused by a rapid hydrolysis of ester bonds connecting PEO as can be concluded from the decrease of the molar content of PEO in the resulting polymer as determined by ^{1}H-NMR (32 mol% initially while 12 mol% at week 2), which is in correspondence to the results of Avgoustakis *et al.* [41]. After 4 weeks, the $\overline{M}_n$ decreases further and reaches a value below $2 \cdot 10^3$ g/mol after 7 weeks. However, in contrast to the PDLLA and PLGA nanoparticles, the particle size and the P.I. increase rapidly in time. The P.I. even reaches a value of 1 after three weeks due to aggregation as concluded from multimodal size distributions detected with DLS. This aggregation is caused by the release of PEO upon hydrolysis of PLGA. As observed for PLGA nanoparticles, lactic and glycolic acid are detected in the medium from day one on and more glycolic acid than lactic acid is formed (Figure 5.3B). This is confirmed by a shift in the copolymer composition towards higher lactide contents as determined by ^{1}H-NMR: the molar ratio of lactyl:glycolyl increases from 52:48 initially to 68:32 at week 8. The pH gradually decreased in time, reaching a value of 6.4 after 10 weeks.

After the fast release of PEO, the particles are mainly composed of PLGA. Still, the decrease in $\overline{M}_n$ is faster than observed for PLGA solely. The reason for this is that the amount of PEO still present (8 mol% as determined by ^{1}H-NMR) results in a higher water-uptake, resulting in higher hydrolysis rates [18].
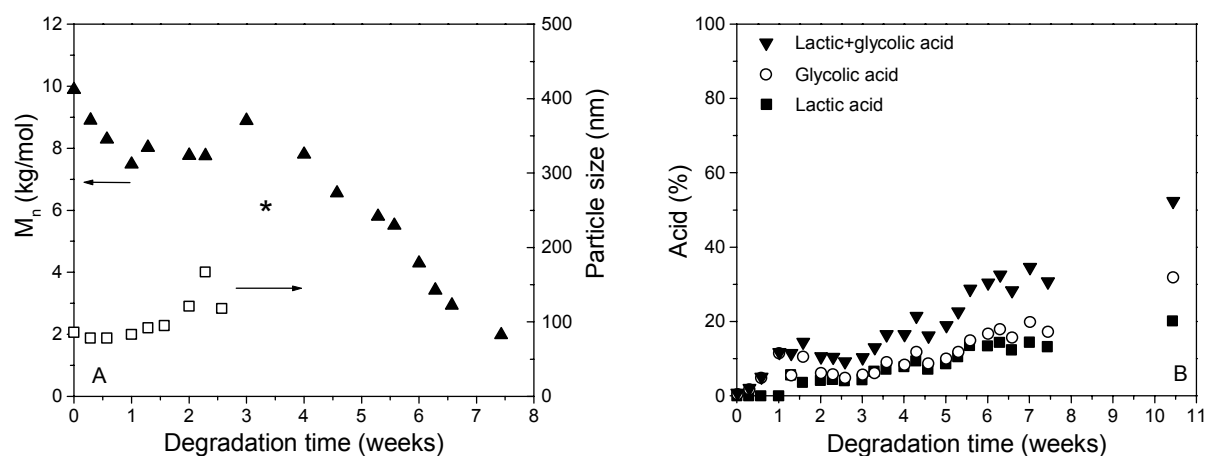
Figure 5.3 *(A) The $\overline{M}_n$ (▲) and the particle size (□) of PEO-PLGA nanoparticles as a function of the degradation time at 37 °C in PBS (pH 7.4). The * indicates the time point from which multiple size distributions were observed. (B) Relative amount of lactic and glycolic acid in the degradation medium as a function of the degradation time for PEO-PLGA nanoparticles at 37 °C in PBS (pH 7.4), presented as a percentage of the total units initially present in the nanoparticles.*

The *in vitro* degradation of PDLLA and related aliphatic polyesters involves the generation of carboxylic end groups that are able to catalyze the hydrolysis [51]. However, the fact that fast acid formation is observed indicates that degradation products rapidly diffuse into the medium. This implies that accumulation of oligomers containing carboxylic end groups that could catalyze the hydrolysis is not likely to occur. This is confirmed by GPC, since no bimodal molecular weight distributions were observed at any time point, for any of the different nanoparticles.

CONCLUSIONS

The *in vitro* degradation rate of PLGA-based nanoparticles is dependent on the composition of the copolymer. PDLLA nanoparticles gradually degrade over a period of 2 years. A faster degradation was observed for PLGA, which was nearly complete after 10 weeks. Both PDLLA and PLGA nanoparticles maintained their size until they were totally degraded, without noticeable aggregation. In PEO-PLGA nanoparticles, the ester bond connecting the PEO and the PLGA segments was preferentially cleaved, which led to a relatively fast decrease in molecular weight and to (partial) aggregation, as multimodal size distributions were observed. The overall degradation rate of PEO-PLGA particles was slightly higher than of PLGA particles. In contrast to the heterogeneous *in vitro* degradation of devices based on copolymers of lactide and glycolide as described in literature, PDLLA, PLGA and PEO-PLGA nanoparticles appear to degrade homogeneously in time, without autocatalysis.

ACKNOWLEDGEMENTS

REFERENCES

1. Chapter 4 of this thesis.
2. Uhrich, K.E.; Cannizarro, S.M.; Langer, R.S. and Shakesheff, K.M., *Chem. Rev.,* **1999**, *99*, 3181-3198.
3. Harris, J.M., Introduction to biotechnical and biomedical applications of poly(ethylene glycol), In *Poly(ethylene glycol) chemistry, biotechnical and biomedical applications*; Harris, J.M., Ed.; Plenum Press: New York, **1992**.
4. Shaffer, C.B. and Critchfield, F.H., *Am. J. Pharm. Assoc.,* **1947**, *36*, 152-157.
5. Juni, K. and Nakano, M., *Crit. Rev. Ther. Drug Carrier Syst.,* **1987**, *3*, 209-232.
6. Yamaguchi, K. and Anderson, J.M., *J. Control. Release,* **1993**, *24*, 81-93.
7. Anderson, J.M. and Shive, M.S., *Adv. Drug Deliv. Rev.,* **1997**, *28*, 5-24.
8. Gautier, S.E.; Oudega, M.; Fragoso, M.; Chapon, P.; Plant, G.W.; Bunge, M.B. and Parel, J.M., *J. Biomed. Mater. Res.,* **1998**, *42*, 642-654.
9. Ignatius, A.A. and Claes, L.E., *Biomaterials,* **1996**, *17*, 831-839.
10. Wu, X.S., Synthesis and properties of biodegradable lactic/glycolic acid polymers, In *Encyclopedic Handbook of Biomaterials and Bioengineering, Part A: Materials*; Wise, D.L., Trantolo, D.J., Altobelli, D.E., Yaszemski, M.J., Gresser, J.D., Schwartz, E.R., Eds.; Marcel Dekker, Inc.: New York, **1995**.
11. Göpferich, A., *Eur. J. Pharm. Biopharm.,* **1996**, *42*, 1-11.
12. Lu, L.; Garcia, C.A. and Mikos, A.G., *J. Biomed. Mater. Res.,* **1999**, *46*, 236-244.
13. O'Hagan, D.T.; Jeffery, H. and Davis, S.S., *Int. J. Pharm.,* **1994**, *103*, 37-45.
14. Park, T.G., *Biomaterials,* **1995**, *16*, 1123-1130.
15. Schmitt, E.A.; Flanagan, D.R. and Linhardt, R.J., *Macromolecules,* **1994**, *27*, 743-748.
16. Bittner, B.; Witt, C.; Mader, K. and Kissel, T., *J. Control. Release,* **1999**, *60*, 297-309.
17. Ronneberger, B.; Kao, W.J.; Anderson, J.M. and Kissel, T., *J. Biomed. Mater. Res.,* **1996**, *30*, 31-40.

18. Quellec, P.; Gref, R.; Perrin, L.; Dellacherie, E.; Sommer, F.; Verbavatz, J.M. and Alonso, M.J., *J. Biomed. Mater. Res.,* **1998**, *42*, 45-54.
19. Yoo, H.S.; Oh, J.E.; Lee, K.H. and Park, T.G., *Pharm. Res.,* **1999**, *16*, 1114-1118.
20. Batycky, R.P.; Hanes, J.; Langer, R. and Edwards, D.A., *J. Pharm. Sci.,* **1997**, *86*, 1464-1477.
21. Grizzi, I.; Garreau, H.; Li, S. and Vert, M., *Biomaterials,* **1995**, *16*, 305-311.
22. Li, S., *J. Biomed. Mater. Res.,* **1999**, *48*, 342-353.
23. Siepmann, J. and Göpferich, A., *Adv. Drug Deliv. Rev.,* **2001**, *48*, 229-247.
24. Dunne, M.; Corrigan, O.I. and Ramtoola, Z., *Biomaterials,* **2000**, *21*, 1659-1668.
25. Giunchedi, P.; Conti, B.; Scalia, S. and Conte, U., *J. Control. Release,* **1998**, *56*, 53-62.
26. Park, T.G., *J. Control. Release,* **1994**, *30*, 161-173.
27. Tracy, M.A.; Ward, K.L.; Firouzabadian, L.; Wang, Y.; Dong, N.; Qian, R. and Zhang, Y., *Biomaterials,* **1999**, *20*, 1057-1062.
28. Carrio, A.; Schwach, G.; Coudane, J. and Vert, M., *J. Control. Release,* **1995**, *37*, 113-121.
29. Garcia, J.T.; Farina, J.B.; Munguia, O. and Llabres, M., *J. Microencapsul.,* **1999**, *16*, 83-94.
30. Spenlehauer, G.; Vert, M.; Benoit, J.P. and Boddaert, A., *Biomaterials,* **1989**, *10*, 557-563.
31. Zhu, J.H.; Shen, Z.R.; Wu, L.T. and Yang, S.L., *J. Appl. Polym. Sci.,* **1991**, *43*, 2099-2106.
32. Menei, P.; Daniel, V.; Monteromenei, C.; Brouillard, M.; Pouplardbarthelaix, A. and Benoit, J.P., *Biomaterials,* **1993**, *14*, 470-478.
33. Reich, G., *Drug Dev. Ind. Pharm.,* **1997**, *23*, 1177-1189.
34. Delgado, A.; Evora, C. and Llabres, M., *Int. J. Pharm.,* **1996**, *140*, 219-227.
35. Sansdrap, P. and Moes, A.J., *J. Control. Release,* **1997**, *43*, 47-58.
36. Viswanathan, N.B.; Patil, S.S.; Pandit, J.K.; Lele, A.K.; Kulkarni, M.G. and Mashelkar, R.A., *J. Microencapsul.,* **2001**, *18*, 783-800.
37. Witt, C. and Kissel, T., *Eur. J. Pharm. Biopharm.,* **2001**, *51*, 171-181.
38. Coffin, M.D. and McGinity, J.W., *Pharm. Res.,* **1992**, *9*, 200-205.
39. Belbella, A.; Vauthier, C.; Fessi, H.; Devissaguet, J.-P. and Puisieux, F., *Int. J. Pharm.,* **1996**, *129*, 95-102.
40. Niwa, T.; Takeuchi, H.; Hino, T.; Kunou, N. and Kawashima, Y., *J. Pharm. Sci.,* **1994**, *83*, 727-732.
41. Avgoustakis, K.; Beletsi, A.; Panagi, Z.; Klepetsanis, P.; Karydas, A.G. and Ithakissios, D.S., *J. Control. Release,* **2002**, *79*, 123-135.
42. Kricheldorf, H.R.; Jonte, J.M. and Berl, M., *Macromol. Chem.,* **1985**, *12*, 25-38.
43. Zweers, M.L.T.; Grijpma, D.W.; Engbers, G.H.M. and Feijen, J., *J. Biomed. Mater. Res. - Appl. Biomat.,* **2002**, submitted.
44. Allémann, E.; Leroux, J.-C.; Gurny, R. and Dölker, E., *Pharm. Res.,* **1993**, *10*, 1732-1737.
45. Provencher, S.W.; Hendrix, J. and De Maeyer, L., *J. Chem. Phys.,* **1978**, *69*, 4273-4276.
46. Gilding, D.K. and Reed, A.M., *Polymer,* **1979**, *20*, 1459-1464.
47. Schwach, G.; Coudane, J.; Engel, R. and Vert, M., *Polym. Bull.,* **1996**, *37*, 771-776.
48. Wang, N.; Wu, X.S.; Chao, L. and Mei, F.F., *J. Biomater. Sci. Polym. Ed.,* **2000**, *11*, 301-318.
49. Kricheldorf, H.R.; Kreiser-Saunders, I. and Stricker, A., *Macromolecules,* **2000**, *33*, 702-709.
50. Aucejo, S.; Marco, C. and Gavara, R., *J. Appl. Polym. Sci.,* **1999**, *74*, 1201-1206.
51. Pitt, C.G.; Gratzl, M.M.; Kimmel, G.L.; Surles, J. and Schindler, A., *Biomaterials,* **1981**, *2*, 215-220.

CHAPTER 6

*Poly(ethylene oxide)-poly(DL-lactic-co-glycolic acid)
nanoparticles for targeted drug delivery*

ABSTRACT

Block copolymers of poly(ethylene oxide) and poly(DL-lactic-co-glycolic acid) with carboxylic acid groups at the PEO-chain end (PLGA-PEO-COOH) were synthesized. Stable nanoparticle dispersions of PLGA-PEO-COOH were prepared using the salting-out method without stabilizer. The diamine 1,8-diamino-3,6-dioxaoctane was coupled to carboxylic acid groups at the nanoparticle surface after pre-activation of the carboxylic end groups. This diamine serves as a model for amine-containing targeting units (e.g. antibody, peptide) and results in free amine groups at the surface that can be readily quantified. It is shown that 80% of the carboxylic acid groups reacted with the diamine. This study demonstrates that PLGA-PEO nanoparticles with functional carboxylic acid groups at the surface can be prepared, enabling the coupling of targeting units under mild conditions in aqueous media applying carbodiimide chemistry.

INTRODUCTION

Poly(ethylene oxide) (PEO) has been widely used in the surface modification of nanoparticles. The PEO molecules at the surface decrease protein adsorption upon contact with blood [1] and thus play a crucial role in establishing long circulation times of nanoparticles avoiding recognition by the reticuloendothelial system (RES) [2-4]. Surface modification with PEO can be achieved by the adsorption of PEO-poly(propylene oxide) (PEO-PPO) block copolymers onto the nanoparticle surface [5]. Biodegradable 'stealth' particles have also been prepared by the adsorption of poly(lactic acid)-PEO diblock copolymers (PLA-PEO) onto the nanoparticle surface [6]. Furthermore, the PEO molecules at the particle surface prevent aggregation of the particles in aqueous dispersions [7]. However, in a physiological environment the block copolymer molecules that are adsorbed onto the particle surface may be displaced by proteins [1]. This can be overcome by preparing nanoparticles based on different ratios of poly(DL-lactic-co-glycolic acid) (PLGA) and PLGA-PEO, without the use of an external stabilizer [7]. For effective delivery of drug-loaded nanoparticles, two routes can be envisaged. The first route is by passive targeting, e.g. in the case of tumor cells. Particles that exhibit long circulation times, such as PEO-containing nanoparticles, accumulate spontaneously inside tumor tissue by diffusion through the tiny ruptures in the endothelium of the tumor's blood vessels [8], the so-called "enhanced permeability and retention (EPR) effect" [9]. The second route is by targeting the particles.

In the design of particles for targeted drug delivery, the ideal nanoparticle surface would be a surface with targeting units (e.g. antibodies or peptides) surrounded by an inert background, for instance immobilized onto functional PEO chains. Targeting molecules can be coupled onto PEO-containing particles via functional groups present at PEO chain ends. Effective functional groups for coupling of proteins or peptides under mild conditions are carboxylic acid or amine groups.

Three possible routes to prepare PLGA-PEO block copolymers with functional groups at PEO chain ends are depicted in Scheme 6.1. The first route is the sequential anionic ring-opening polymerization of ethylene oxide and DL-lactide or glycolide, initiated by a functional group containing initiator of which the functional group does not participate in the ring-opening polymerization. This route has been used in the preparation of poly(DL-lactic acid)-PEO (PDLLA-PEO) with a sugar unit [10], an acetal-group [11] or an aldehyde-group [12] at the PEO chain end. However, this route may not be applicable for the synthesis of PLGA-PEO block copolymers with a functionalized PEO chain end as glycolide polymerization proceeds faster than lactide polymerization. This would result in a blocky PLGA copolymer rather than in a more or less random PLGA copolymer. Furthermore, it involves the polymerization of the toxic ethylene oxide, which has to be performed in an inert atmosphere.

The second route is the ring-opening polymerization of DL-lactide and glycolide using a bifunctional PEO as initiator in which one functional group is protected (Scheme 6.1). This has the advantage that it is a one-step synthesis. However, the choice of functional groups is

limited. The protection of a carboxylic acid group, for instance, proceeds through formation of an ester or through complexation with a metal [13]. In the former, the deprotection step involves cleavage of the ester, which may also result in cleavage of the PLGA chain. In the latter case, the metal complex competes with stannous octoate, which is used as a catalyst. In addition, the protection of an amine often leads to protection of the hydroxyl group used in the polymerization as well [13].

Route 1

Route 2

Route 3

R = unreactive group

R' = H_3C ⌒⌒⌒

R" = coupling unit

F = functional group

prot = protecting group

Scheme 6.1 *Reaction schemes describing three routes to prepare PLGA-PEO with a functional group (F) containing PEO chain end. Route 1 is the sequential anionic ring-opening polymerization of ethylene oxide and DL-lactide and glycolide. Route 2 is the ring-opening polymerization of DL-lactide and glycolide using a bifunctional PEO in which one functional group is either unreactive or protected by a protecting group (prot). If a protecting group is used, the functional polymer is obtained after deprotection. Route 3 involves the coupling of a bifunctional PEO to PLGA that is obtained by ring-opening polymerization of DL-lactide and glycolide initiated by a low molecular weight alcohol.*

The third route presented is the most suitable route. It involves the ring-opening polymerization of DL-lactide and glycolide initiated by a low molecular weight alcohol (e.g. hexanol), after which a commercially available bifunctional PEO is coupled to the PLGA block (Scheme 6.1). The coupling reaction involves activation of the hydroxyl group of PLGA, after which the bifunctional PEO reacts at one end (R"; e.g. OH or NH$_2$) with the activated group to form a diblock copolymer.

Several bifunctional PEOs are commercially available. HO-PEO-COOH was selected to illustrate the approach, because i) the two functionalities are not the same, which makes selective coupling via one of the reactive groups possible; ii) by reacting the acid chloride group of PLGA (by reacting the hydroxyl group of PLGA with succinic anhydride followed by reaction with oxalyl chloride) with the hydroxyl group of the PEO, free carboxylic acid groups will form the chain end of the diblock copolymer. The carboxylic acid group can be used for immobilizing targeting units under mild conditions. A detailed description of the coupling of HO-PEO-COOH to PLGA is depicted in Scheme 6.2A.
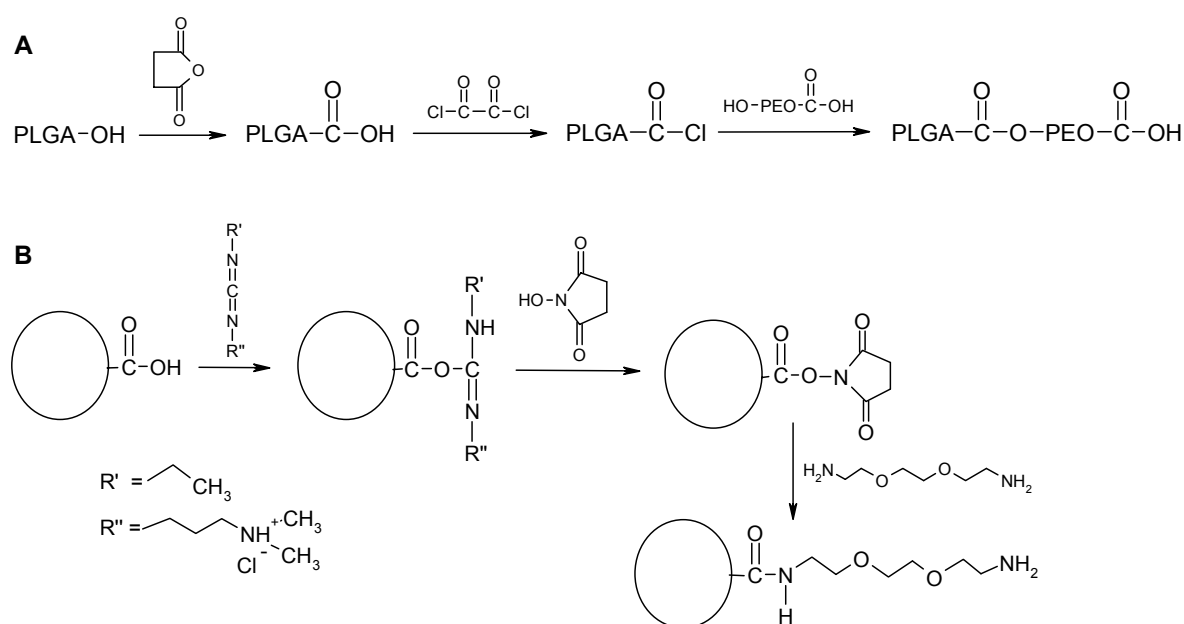
Scheme 6.2 *Detailed reaction schemes of (A) the coupling of a bifunctional PEO to PLGA and (B) the activation of carboxylic acid groups present at the nanoparticle surface by EDC/NHS prior to reaction with 1,8-diamino-3,6-dioxaoctane.*

The aim of this study was to prepare nanoparticles derived from PLGA-PEO block copolymers containing functional groups at the PEO chain end allowing nanoparticle surface modification for targeting purposes. Carboxylic acid groups were chosen to couple targeting units by applying mild carbodiimide chemistry in aqueous media (Scheme 6.2B). Nanoparticles were prepared from PLGA-PEO-COOH copolymers and the coupling of 1,8-diamino-3,6-dioxaoctane (as a model compound for targeting units) to carboxylic acid groups present at the surface was studied.

MATERIALS AND METHODS

Materials

DL-lactide and glycolide (Purac Biochem b.v., Gorinchem, The Netherlands) and α-carboxy-ω-hydroxy-poly(ethylene oxide) (HOOC-PEO-OH) ($\overline{M}_n$ = 3.4·10^3 g/mol, Shearwater Polymers, Huntsville, USA) were used as received. Hexanol (Merck, Darmstadt, Germany) and dichloromethane (Biosolve, Valkenswaard, The Netherlands) were distilled from calcium hydride (Acros Organics, New Jersey, USA) prior to use. A 2 M solution of oxalyl chloride in dichloromethane was purchased from Aldrich (Milwaukee, USA) and 2,4,6-trinitrobenzene sulfonic acid solution (TNBS; 1 M) from Fluka (Buchs, Switzerland). Magnesium sulfate, (2-[N-morpholino]ethanesulfonic acid) hydrate (MES), N-(3-dimethylaminopropyl)-N'-ethylcarbodiimide hydrochloride (EDC) and stannous octoate were purchased from Sigma (St. Louis, USA). The phosphate buffer used for particle analysis was an aqueous solution of sodium dihydrogenphosphate and disodium hydrogenphosphate (1 mM; pH 7.4). The solvents used were of analytical grade (Biosolve). All other reagents were obtained from Merck.

Polymer synthesis

PLGA was synthesized by ring-opening polymerization. Typically, a mixture of DL-lactide (10.1 g; 69.8 mmol) and glycolide (5.45 g; 47.0 mmol) with stannous octoate in pentane (5.0 ml; 1.89 g/l) were transferred to an ampoule. After removal of the pentane by applying vacuum, hexanol (318 µl; 2.53 mmol) was added, the ampoule was purged three times with argon, vacuum-sealed and subsequently transferred to an oil bath at 130 °C. After 24 h of reaction, the crude product was dissolved in chloroform, precipitated into a ten-fold volume of methanol and dried in vacuo at 40 °C for three days. The synthesized copolymer is denoted as PLGA-OH.

Conversion of the hydroxyl end group of PLGA-OH into carboxylic end group

Succinic anhydride (60 mg; 6·10^{-4} mol), triethylamine (84 µl; 6·10^{-4} mol) and 4-(dimethylamino)-pyridine (0.3 g; 10 wt%) were added to a solution of PLGA-OH (3.0 g; 3·10^{-4} mol) in dichloromethane (50 ml). After 4 h of reaction at 25 °C under continuous stirring, the organic phase was washed with water (twice), 1 N HCl (twice) and water (twice). Subsequently, the organic phase was dried over magnesium sulfate, filtered and dried in vacuo at room temperature until constant weight [14]. The resulting copolymer is denoted as PLGA-COOH.

Covalent coupling of HO-PEO-COOH to PLGA-COOH

A PLGA-COOH (2.0 g; ≈2·10^{-4} mol) solution in dichloromethane (30 ml) was added drop-wise to an oxalyl chloride solution in dichloromethane (0.2 ml; 4·10^{-4} mol) that was kept at 0 °C while being stirred. After 10 min, the reaction mixture was warmed up to 25 °C to drive the reaction to completion. Subsequently, a HO-PEO-COOH (1.0 g; 3·10^{-4} mol) solution in dichloromethane (20 ml) containing triethylamine (56 µl; 4·10^{-4} mol) was added drop-wise to the reaction mixture. The reaction was allowed to proceed for 30 min at 25 °C under continuous stirring. The crude product was precipitated into a ten-fold volume of methanol, filtered and dried in vacuo at 40 °C until constant weight. The resulting block copolymer is denoted as PLGA-PEO-COOH.

Preparation of PLGA-PEO-COOH nanoparticles

Nanoparticles were prepared using the salting-out method [7]. Because of its pharmaceutical acceptance with regard to toxicity [15] acetone was chosen as the water-miscible organic solvent. The method consists of the addition of a highly concentrated salt solution in water (aqueous phase) to a polymer solution in acetone (organic phase). Although acetone is miscible with pure water in all proportions, the high salt concentration of the aqueous phase prevents mixing of the two phases. After emulsification, the addition of pure water in a sufficient quantity causes acetone to diffuse into the aqueous phase, resulting in the formation of nanoparticles.

Typically, an acetone solution (5.0 g) containing 2 wt% block copolymer was emulsified under mechanical stirring (20,500 rpm; 40 s; T25 Ultraturrax equipped with a S25 dispersing tool, Ika-Labortechnik, Staufen, Germany) in an aqueous phase (7.5 g) containing 60 wt% $MgCl_2 \cdot 6H_2O$ as the salting-out agent (in a glass beaker; 3.5 cm diameter; 6.6 cm height). After rapid addition (5 s) of pure water (7.5 g) under mechanical stirring (20,500 rpm) causing acetone to diffuse into the water phase, nanoparticles were formed and stirring was continued (20,500 rpm; 20 s).

The nanoparticles were purified by rinsing with water. First, the nanoparticles were separated by ultracentrifugation (65,000×g for 30 min.; Centrikon T-2180, Kontron Instruments, Watford, UK) and the supernatant was removed. The nanoparticles were redispersed in water, centrifuged and the supernatant removed. This procedure was repeated three times.

Coupling of 1,8-diamino-3,6-dioxaoctane to PLGA-PEO-COOH nanoparticles

To allow the coupling reaction of 1,8-diamino-3,6-dioxaoctane to PLGA-PEO-COOH nanoparticles, the carboxylic groups of PLGA-PEO-COOH nanoparticles were pre-activated with EDC/NHS (molar ratio 4:1) [16]. The reactions were performed in MES buffer (0.05 M adjusted to pH 5.4 by the addition of 1 N NaOH). An EDC solution in MES buffer (200 μl; 1 M) and an N-hydroxysuccinimide (NHS) solution in MES buffer (200 μl; 0.25 M) were added to a dispersion of nanoparticles (15 mg; $9.2 \cdot 10^{-7}$ mol -COOH) in 1.6 ml MES buffer. As a control, the same reaction without EDC was performed. After 10 min of reaction at 25 °C under continuous shaking, the nanoparticles were separated by ultracentrifugation (25 °C; 65,000×g for 30 min). After removal of the supernatant, the nanoparticles were redispersed in a 1,8-diamino-3,6-dioxaoctane solution in water (2 ml; 0.1 M). After 2 h of reaction at 25 °C under continuous shaking, the nanoparticles were separated by ultracentrifugation and the supernatant was removed. The particles were rinsed twice with water: the particles were redispersed in water, separated by ultracentrifugation and the supernatant was removed. The resulting surface-modified nanoparticles are denoted as PLGA-PEO-NH_2 nanoparticles.

Determination of amino-group concentration at the nanoparticle surface

The determination of the number of free amine groups present on the surface of PLGA-PEO-NH_2 nanoparticles was based on the depletion of TNBS and was performed in duplicate. Briefly, PLGA-PEO-NH_2 nanoparticles were dispersed in 1 ml of water, to which 4 ml of borate buffer (0.1 M; pH 8.5) and 400 μl TNBS (10 mM in water) were added. The mixture was allowed to react for 2 h at 37 °C. Subsequently, the nanoparticles were separated by ultracentrifugation and the supernatant was collected.

The amount of TNBS in the supernatant was determined using the quantitative reaction of TNBS with an excess of 1,8-diamino-3,6-dioxaoctane: 0.2 ml of the supernatant was added to 0.1 ml of a

1,8-diamino-3,6-dioxaoctane solution (3 mM in water) and 2.7 ml of borate buffer (0.1 M; pH 8.5). As a blank, 1,8-diamino-3,6-dioxaoctane was replaced by water. The reaction was allowed to proceed for 40 min at 37 °C and then the mixture was cooled down to room temperature.

For the calibration curve, 0.2 ml of known amounts of TNBS (1, 0.8, 0.6, 0.4, 0.2 and 0.1 mM, respectively) were added to 0.1 ml of a 1,8-diamino-3,6-dioxaoctane solution (3 mM in water) and 2.7 ml of borate buffer (0.1 M; pH 8.5). As a blank, 1,8-diamino-3,6-dioxaoctane was replaced by water. The reaction was allowed to proceed for 40 min at 37 °C and then the mixture was cooled down to room temperature.

The absorbance at 421 nm was determined using a UV spectrophotometer (CARY 300 BIO UV visible spectrophotometer, Varian, Middelburg, The Netherlands) and the amine group concentration was calculated using the calibration curve.

Polymer characterization

The number average molecular weight ($\overline{M}_n$) and the composition of the copolymers were determined by proton nuclear magnetic resonance spectroscopy (^{1}H-NMR) using a Varian Inova (Varian, Palo Alto, USA) operating at 300 MHz, with $CDCl_3$ as the solvent.

The $\overline{M}_n$ and the molecular weight distribution of the PLGA copolymer was determined by gel permeation chromatography (GPC) using chloroform (10 mg/ml) at 25 °C at a flow rate of 1.5 ml/min. The GPC setup consisted of a Waters Model 510 pump, a HP Ti-Series 1050 autosampler, a Waters Model 410 Differential Refractometer, and a Viscotek H502 Viscometer Detector with HR0.5, HR2 and HR4 Waters Ultra-Styragel columns (Waters, Milford, USA) placed in series. Polystyrene standards with narrow molecular weight distributions (PSS, Mainz, Germany) were used for calibration.

Particle size analysis

The nanoparticle size was determined by dynamic light scattering (DLS) (Zetasizer 4000, Malvern Instruments Ltd., Malvern, UK) at 25 °C at an angle of 90°, taking the average of three measurements. The particle dispersion was diluted with phosphate buffer (1 mM; pH 7.4) to such a degree that the desired number of counts was obtained. The desired number of counts is the number of counts that is high enough to get the highest possible signal to noise ratio, yet small enough to prevent multiple scattering to occur.

First, the polydispersity index (P.I.) is determined by the cumulants method. The P.I. is a dimensionless number indicating the width of the size distribution, and lies between zero and one, being zero for monodisperse particles. If the P.I. is small enough (<0.08), the particle size can be determined by the cumulants method and the size distribution obtained is based on a log normal distribution characterized by a mean and width. For polydispersity indices higher than 0.08, the CONTIN-method is used to determine the particle size. The CONTIN-method, developed by Provencher *et al.* [17] describes bimodal and smooth distributions without the need for information such as an initial estimate for the particle size.

Zeta-potential measurements

Nanoparticles were redispersed in phosphate buffer (1 mM; pH 7.4) at the same concentration used for DLS (Zetasizer 2000, Malvern Instruments Ltd., Malvern, UK). The zeta-potential of the nanoparticles

was determined by measuring the velocity of particles moving through phosphate buffer resulting from an applied electric field, taking the average of five measurements. The measurements were performed within the stationary layer to ensure that the measured velocity was due to electrophoresis only. Measurements were carried out at a temperature of 25 °C with a cell drive voltage of 120 V and a modulator frequency of 250 Hz.

RESULTS AND DISCUSSION

Polymer synthesis

The characteristics of the prepared copolymer and block copolymers were determined by ^{1}H-NMR and GPC. The monomer conversion was almost complete. Unreacted glycolide could not be detected by ^{1}H-NMR, whereas the DL-lactide conversion was 98%. The actual molar composition of the PLGA copolymer (lactyl:glycolyl 57:43) is close to the theoretical molar composition (60:40). The higher reactivity of glycolide in comparison with DL-lactide, as previously reported [18], accounts for the larger fraction of glycolide in the copolymer than in the monomer feed. The molecular weight determination by ^{1}H-NMR ($\overline{M}_n = 11.4 \cdot 10^3$ g/mol) and GPC ($\overline{M}_n = 12.8 \cdot 10^3$ g/mol) is in good agreement with the expected molecular weight as calculated from the monomer over initiator ratio ($\overline{M}_n = 10.1 \cdot 10^3$ g/mol). Furthermore, the polydispersity index of 1.95 indicates that the molecular weight distribution is rather broad. Polydispersity indices close to 2 are typical for stannous octoate catalyzed ring-opening polymerizations of lactide and glycolide [19-21] and are indicative of transesterification reactions [22].

Conversion of the hydroxyl end group of PLGA-OH into carboxylic end group

Reaction of PLGA-OH with succinic anhydride resulted in the formation of PLGA-COOH. Besides peaks corresponding to lactyl units (m, 3H, δ=1.4-1.65 ppm (A); m, 1H, δ=5.1-5.3 ppm (D)) and glycolyl units (m, 2H, δ=4.6-4.9 ppm (C)), the end group (OOC-C$\underline{H}_2$-C$\underline{H}_2$-COOH) (t, 4H, δ=2.75 ppm (B)) resulting from the reaction with succinic anhydride is observed. The percentage of hydroxyl end groups that had reacted with succinic anhydride is calculated from the ratio of the integral of the end group peak (B) over the integral of one of the polymer peaks (C) and resulted in 80% (Figure 6.1). No peaks of triethylamine (δ=1.0 and 2.4 ppm), unreacted succinic anhydride (δ=3.0 ppm) or 4-(dimethylamino)-pyridin (δ=3.0, 6.4 and 8.2 ppm) are observed (Figure 6.1), which means that these compounds have been completely removed in the purification procedure.
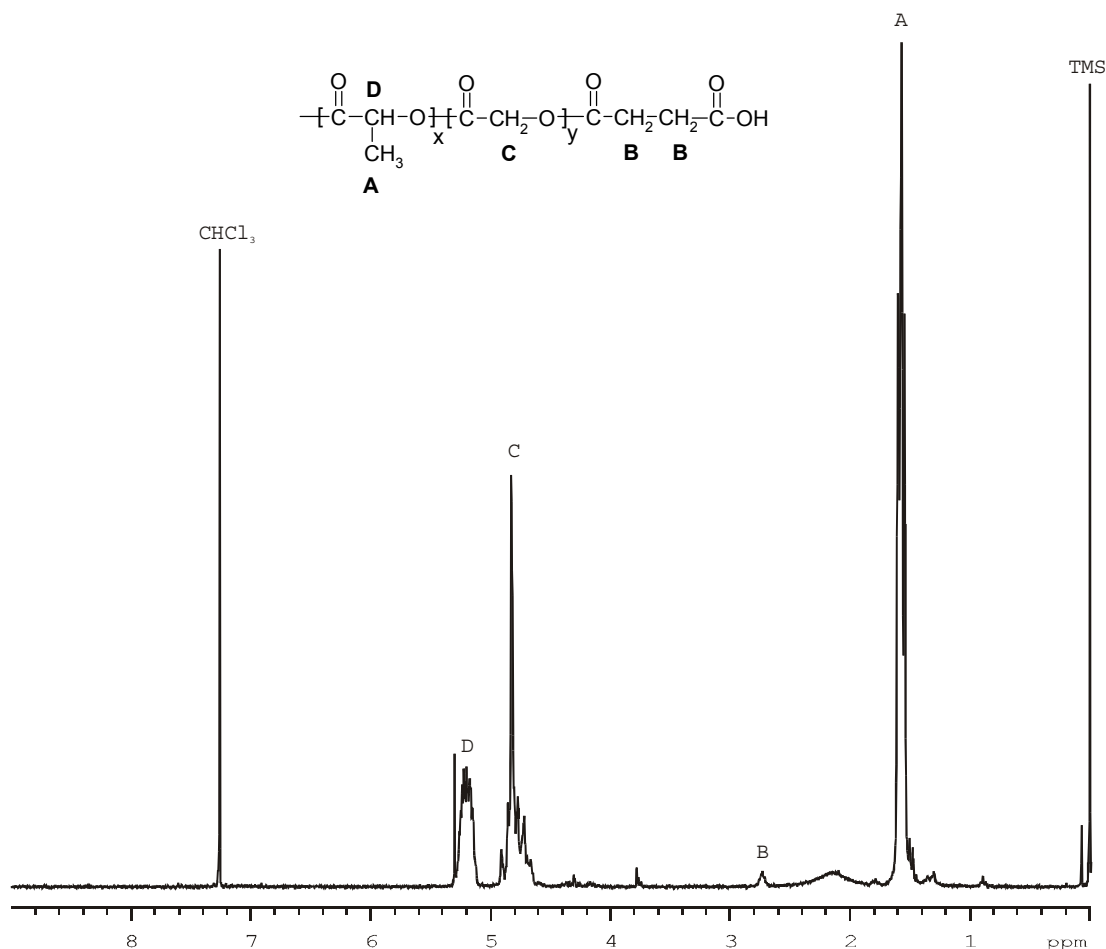
Figure 6.1 *^{1}H-NMR-spectrum of PLGA-COOH in CDCl$_3$. The letters in the spectrum correspond to the letters in the chemical formula.*

Covalent coupling of HO-PEO-COOH to PLGA-COOH

After the formation of PLGA-COCl by reacting PLGA-COOH with oxalyl chloride, HO-PEO-COOH was coupled to PLGA-COCl to form PLGA-PEO-COOH.

Besides peaks corresponding to lactyl units (m, 3H, δ=1.4-1.65 ppm (A); m, 1H, δ=5.1-5.3 ppm (E)), glycolyl units (m, 2H, δ=4.6-4.9 ppm (D)) and the OOC-C$\underline{H}_2$-C$\underline{H}_2$-COO group (t, 4H, δ=2.75 ppm (B)), protons of PEO (t, 4H, δ=3.6 ppm (C)) are observed (Figure 6.2). The relative number of PEO chains coupled to PLGA was calculated from the ratio of the integral of the PEO peak (C) over the integral of one of the polymer peaks (D) and resulted in 70% (Figure 6.2).
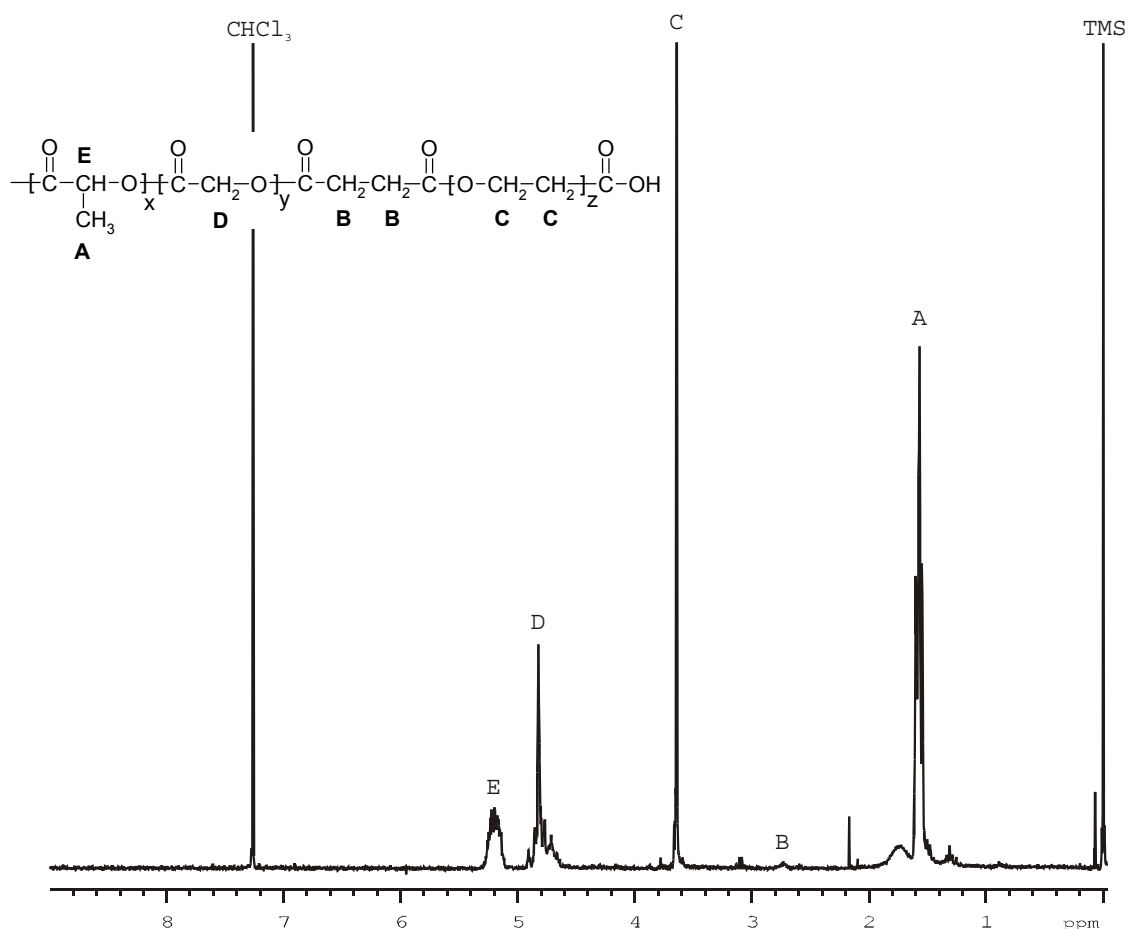
Figure 6.2 *^{1}H-NMR-spectrum of PLGA-PEO-COOH in CDCl$_3$. The letters in the spectrum correspond to the letters in the chemical formula.*

PLGA-PEO-COOH nanoparticle formation and modification with 1,8-diamino-3,6-dioxaoctane

After preparing nanoparticles of PLGA-PEO-COOH, EDC and NHS were added to pre-activate the carboxylic acid group. Subsequently, 1,8-diamino-3,6-dioxaoctane was coupled to the pre-activated carboxylic acid groups present at the surface of the particles. The resulting particles are denoted as PLGA-PEO-NH$_2$ nanoparticles. The particle size and zeta-potential of PLGA-PEO-COOH and PLGA-PEO-NH$_2$ nanoparticles are shown in Table 6.1.

Table 6.1 *Average particle size, polydispersity index (P.I.) and zeta-potential of PLGA-PEO-COOH and PLGA-PEO-NH$_2$ nanoparticles in phosphate buffer (1 mM; pH 7.4) at 25 °C.*

	Average particle size (nm)	P.I. (-)	Zeta-potential (mV)
PLGA-PEO-COOH	328	0.25	−52
PLGA-PEO-NH$_2$	330	1 [a]	−45

[a]Multiple size fractions were observed.

The particle size of PLGA-PEO-NH$_2$ particles is similar to the size of PLGA-PEO-COOH particles. In principle, the coupling of 1,8-diamino-3,6-dioxaoctane could lead to a higher hydrophilicity, and swelling and thus a larger size. However, it is expected that the effect will be small, as 1,8-diamino-3,6-dioxaoctane is similar to two ethylene oxide monomeric units, which is far less than the 77 ethylene oxide monomeric units of the PEO block of the copolymer. A P.I. of 1 is measured for the PLGA-PEO-NH$_2$ particles as a result of aggregation. The reason could be that during immobilization a small fraction of the 1,8-diamino-3,6-dioxaoctane reacts with COOH groups of two different particles, leading to bridging between two particles.

The zeta-potential of PLGA-PEO-COOH nanoparticles is far more negative than PLGA-PEO nanoparticles without carboxylic acid groups (–14 mV) [7], indicating that carboxylic acid groups are present at the surface, as these are negatively charged at pH 7.4. The zeta-potential of PLGA-PEO-NH$_2$ particles is slightly less negative than of PLGA-PEO-COOH particles, which could indicate that reaction with carboxylic acid groups has occurred.

The number of free amine groups present at the surface of PLGA-PEO-NH$_2$ particles was determined by reaction with TNBS. In the control sample, EDC was left out in the activation step. The number of amine groups at the surface of the particles when no EDC was added was 10% of the initial number of carboxylic acid groups. The fact that a small amount of TNBS has reacted although the carboxylic acid groups were not activated indicates that some complexation of the diamine with the carboxylic acid group occurs or that, despite the washing procedure, a small amount of unreacted 1,8-diamino-3,6-dioxaoctane is still present.

In the case of PLGA-PEO-NH$_2$ nanoparticles, the number of amine groups is 80 ± 10% of the number of carboxylic acid groups initially present. This high coupling efficiency indicates that it is possible to couple an amino group containing targeting unit to the surface of PLGA-PEO-COOH nanoparticles.

Several reasons for the fact that the immobilization efficiency was less than 100% can be given: i) part of the carboxylic acid groups were not activated as part of the PEO is located within the particle [7]; ii) some deactivation takes place during ultracentrifugation and iii) bridging between particles (as observed by DLS (Table 6.1)) does not result in free amine groups. Optimizing the reaction conditions can increase the efficiency of coupling of the diamine to the carboxylic acid groups.

CONCLUSIONS

It is demonstrated that nanoparticle dispersions of PLGA-PEO with functionalized PEO chain ends can be prepared without an external stabilizer. It is shown that 80% of the carboxylic acid end groups present at the surface reacted with a model compound (1,8-diamino-3,6-dioxaoctane) under mild conditions in aqueous media. PLGA-PEO-COOH particles are therefore suited for the immobilization of targeting units. After immobilization, these particles can be used for targeting to tissues of interest.

ACKNOWLEDGEMENTS

REFERENCES

1. Gref, R.; Luck, M.; Quellec, P.; Marchand, M.; Dellacherie, E.; Harnisch, S.; Blunk, T. and Muller, R.H., *Colloids Surf. B - Biointerfaces,* **2000**, *18*, 301-313.
2. Allémann, E.; Gurny, R. and Dölker, E., *Eur. J. Pharm. Biopharm.,* **1993**, *39*, 173-191.
3. Moghimi, S.M., *Biochim. Biophys. Acta,* **1997**, *1336*, 1-6.
4. Araujo, L.; Lobenberg, R. and Kreuter, J., *J. Drug Target.,* **1999**, *6*, 373-385.
5. Stolnik, S.; Daudali, B.; Arien, A.; Whetstone, J.; Heald, C.R.; Garnett, M.C.; Davis, S.S. and Illum, L., *Biochim. Biophys. Acta - Biomembr.,* **2001**, *1514*, 261-279.
6. Stolnik, S.; Dunn, S.E.; Garnett, M.C.; Davies, M.C.; Coombes, A.G.A.; Taylor, D.C.; Irving, M.P.; Purkiss, S.C.; Tadros, T.F.; Davis, S.S. *et al.*, *Pharm. Res.,* **1994**, *11*, 1800-1808.
7. Chapter 4 of this thesis.
8. Maeda, H.; Wu, J.; Sawa, T.; Matsumura, Y. and Hori, K., *J. Control. Release,* **2000**, *65*, 271-284.
9. Brigger, I.; Dubernet, C. and Couvreur, P., *Adv. Drug Deliv. Rev.,* **2002**, *54*, 631-651.
10. Yasugi, K.; Nakamura, T.; Nagasaki, Y.; Kato, M. and Kataoka, K., *Macromolecules,* **1999**, *32*, 8024-8032.
11. Emoto, K.; Nagasaki, Y. and Kataoka, K., *Langmuir,* **1999**, *15*, 5212-5218.
12. Yamamoto, Y.; Nagasaki, Y.; Kato, M. and Kataoka, K., *Colloids Surf. B - Biointerfaces,* **1999**, *16*, 135-146.
13. Greene, T.W. and Wuts, P.G.M. *Protective groups in organic synthesis*; 3rd ed.; John Wiley & Sons, Inc.: New York, **1999**.
14. Boger, D.L.; Lerner, R.A. and Cravatt, B.F., *J. Org. Chem.,* **1994**, *59*, 5078-5079.
15. Rabiant, J., *S.T.P. Pharma,* **1991**, *1*, 278-283.
16. Kuijpers, A.J.; Engbers, G.H.M.; Krijgsveld, J.; Zaat, S.A.J.; Dankert, J. and Feijen, J., *J. Biomater. Sci. Polym. Ed.,* **2000**, *11*, 225-243.
17. Provencher, S.W.; Hendrix, J. and De Maeyer, L., *J. Chem. Phys.,* **1978**, *69*, 4273-4276.
18. Gilding, D.K. and Reed, A.M., *Polymer,* **1979**, *20*, 1459-1464.
19. Schwach, G.; Coudane, J.; Engel, R. and Vert, M., *Polym. Bull.,* **1996**, *37*, 771-776.
20. Tracy, M.A.; Ward, K.L.; Firouzabadian, L.; Wang, Y.; Dong, N.; Qian, R. and Zhang, Y., *Biomaterials,* **1999**, *20*, 1057-1062.
21. Wang, N.; Wu, X.S.; Chao, L. and Mei, F.F., *J. Biomater. Sci. Polym. Ed.,* **2000**, *11*, 301-318.
22. Kricheldorf, H.R.; Kreiser-Saunders, I. and Stricker, A., *Macromolecules,* **2000**, *33*, 702-709.

CHAPTER 7

Location of nanoparticles after in vitro intravascular administration

ABSTRACT

Polystyrene particles containing either carboxylic acid or amidine groups at the surface with sizes ranging from 120 to 1000 nm were locally administered to porcine carotid arteries in an in vitro model using a microporous balloon catheter. The effect of particle size and surface charge on the location of the nanoparticles within the arterial wall after administration was studied. It was shown that particles of 120 nm were present in all layers of the arterial wall, whereas the vascular wall was impermeable to particles of 230 and 1000 nm. Transport of particles via the vasa vasorum seems to play a minor role in the administration of particles to the arterial wall, as few particles were present in arteries with an inner diameter larger than the maximal outer diameter of the balloon catheter. For arteries with an inner diameter smaller than the outer diameter of the balloon catheter, the smaller the inner diameter of the artery, the more particles were introduced to the arterial wall. Fluorescent labeled biodegradable particles based on poly(ethylene oxide)-poly(DL-lactic-co-glycolic acid) block copolymers (PEO-PLGA) with a diameter of 120 nm were prepared by the salting-out method. These nanoparticles could be introduced to all layers of the arterial wall. Since PEO-PLGA particles are biodegradable and can be used for surface modification to enhance their targeting specificity, they are good candidates for the delivery of drugs for the reduction of the incidence of restenosis.

INTRODUCTION

Atherosclerosis is a disease that is characterized by a progressive narrowing and hardening of arteries. Besides aging [1,2] risk factors for this disease to develop are high cholesterol levels [2], high blood pressure [3], smoking [4] and diabetes [3]. In atherosclerotic lesions, lipid-rich macrophages and T lymphocytes have accumulated in the intima, smooth muscle cells have migrated from the media to the intima and proliferated and additional extracellular matrix has been deposited [5]. Frequently, regions of calcification are present [6]. Upon dilation of the atherosclerotic artery during percutaneous transluminal (coronary) angioplasty (PT(C)A), the intima and often the media are fractured [6]. This triggers a number of processes leading to restenosis in 30 to 50% of the PTCA-treated atherosclerotic lesions [7]. In the case of femoral superficial arteries restenosis occurs in 20 to 70% of the PTA-treated atherosclerotic lesions [8]. It is recognized that early elastic recoil, late artery remodeling and neointima formation play an important role in the development of restenosis [9].

Attempts have been made to decrease the incidence of restenosis. Potentially therapeutic agents have been injected into the arterial wall after PTA via a porous balloon catheter [10]. It was shown that because of the blood flow via the vasa vasorum, drugs injected as an aqueous solution had a short residence time in the arterial wall [11,12]. A successful approach was the introduction of a stent. Because of its rigid structure it provides mechanical strength, which minimizes the process of early elastic recoil and late artery remodeling [13]. Compared to PTCA, stenting leads to a decrease of 10-15% in the incidence of restenosis [14-16].

The use of polymer-coated, drug-eluting stents inhibited the incidence of (in-stent) restenosis. While drug-eluting stents are not biodegradable and are thus permanently present this could lead to long-term adverse tissue reactions. However, no long-term (>18 months) studies on adverse reactions of drug-eluting stents have been performed yet. Biodegradable drug-loaded nanoparticles may be a good alternative for, or complementary to, the use of drug-eluting stents.

For drug delivery to the arterial wall, the structure of the wall with its layers is important for the drug delivery characteristics. A healthy arterial wall consists of three identifiable layers, as schematically depicted in Figure 7.1. The inner layer, intima, consists mainly of endothelial cells, supported by a thin layer of fibrocollagenous tissue. The media, the middle layer, is predominantly composed of smooth muscle cells incorporated in a matrix of organized layers of elastic tissue. The outer layer, adventitia, is mainly composed of collagen and fibroblasts, but also smooth muscle cells can be present. Within the adventitia, a network of small blood vessels, the vasa vasorum, is present [17].

The role of the vasa vasorum is primarily nutritional, yet may also be homeostatic [18]. Most blood vessels within the vasa vasorum originate from branches of periadventitial arteries and only some appear to be derived from the luminal side of the artery [19]. The vasa vasorum might reach the media, but that is related to the thickness of the arterial wall. The thickness of the inner part of the arterial wall that is supplied with nutrients by diffusion from the arterial

lumen is approximately 0.5 mm [20]. Therefore, in arteries with a wall thickness of less than 0.5 mm, hardly any small vessels are observed in the media (e.g. in the rabbit carotid artery no medial vasa vasorum is observed [21]). The penetration of vasa vasorum into the media of thicker-walled arteries is correlated with the number of elastic laminar units found in the media [22]. A constant number of 29 laminar units are formed across a wide range of species (e.g. human, pig, sheep) in which there is a need for medial vasa vasorum [22]. In atherosclerotic lesions, the vasa vasorum is more extended than in healthy blood vessels [23,24].
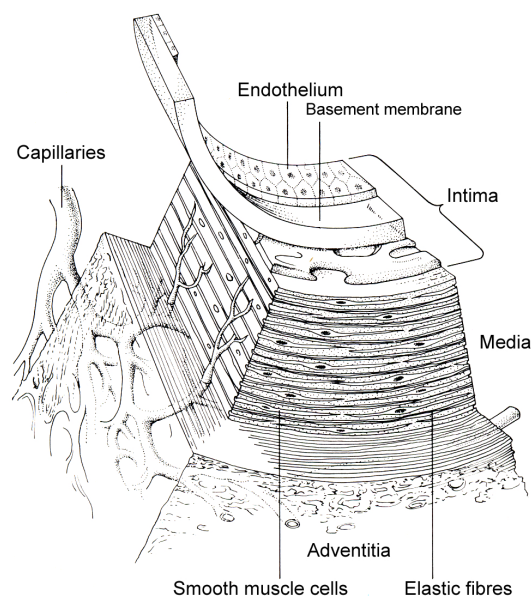
Figure 7.1 Schematic three-dimensional drawing of a cross-section of an artery in three identifiable layers: the inner layer (intima), the middle layer (media) and the outer layer (adventitia supplied by blood and nutrition through the vasa vasorum) (reprinted with permission from [25]).

Intravascular administration of particles (5 µm) has been performed first by Wilensky *et al.* in 1991 [24]. After PTA was performed on femoral arteries of rabbits that were on a high cholesterol diet, the particles were administered *in vivo* using a porous infusion catheter. The particles reached the vasa vasorum and adventitia through large tears and were retained there for as long as 2 weeks [24]. In a separate study, smaller microparticles (1 µm) were evaluated in the same *in vivo* animal model [26]. The smaller microparticles were mainly observed in the vasa vasorum and hardly in the neointima and media. The microparticle location was associated with tears in the neointima and media. The tears resulted from the PTA or the local particle administration procedure [26]. Rome *et al.* [27] administered nanoparticles (150-500 nm) to carotid and femoral arteries of healthy sheep *in vivo* using a double balloon catheter. The double balloon catheter consisted of two occluding balloons that were separated by a space that was filled with the nanoparticle dispersion. It was shown that nanoparticles were only present in the intima and adventitia. The particles reached the adventitia through the vasa vasorum [27]. These studies indicate that an intact vessel wall is an anatomic barrier to particles larger than 150 nm. Particles larger than 150 nm can therefore only be introduced to the wall of atherosclerotic arteries via tears or via transport through the vasa vasorum.

In an *ex vivo* model, drug-loaded biodegradable poly(lactic-co-glycolic acid) (PLGA) nanoparticles (100-270 nm) were infused in healthy dog carotid arteries that had been subjected to PTA and were allowed to penetrate the arterial wall for 30 s at 1 atm [28]. The nanoparticle retention was quantified and it was determined that particle introduction to the arteries was largest for the smallest nanoparticles (100 nm) [28]. PLGA nanoparticles may have penetrated the arterial wall or were present in the arterial wall via transport through the vasa vasorum. However, nanoparticle location was not studied.

The use of nanoparticles as drug carriers gives the possibility to provide particles with a targeting moiety that has a high affinity for specific cell types that are present in restenotic arterial segments, e.g. activated smooth muscle cells [29,30], macrophages [31], or dysfunctional endothelium [32-34]. Targeting moieties that bind to microvasculature (e.g. vasa vasorum and regions of neovascularization) can also be provided [35]. In this respect, it has been previously shown that biodegradable nanoparticles that are prepared from poly(ethylene oxide)-poly(DL-lactic-co-glycolic acid) block copolymers (PEO-PLGA) can be used for surface modification to enhance their targeting specificity [36]. Other surface characteristics, such as surface charge, might also be important for the introduction of nanoparticles to the arterial wall. In *ex vivo* and *in vivo* studies, for instance, it was shown that the concentration of positively charged particles in the arterial wall was higher than of negatively charged particles which may be caused by the electrostatic affinity of the positively charged particles for the negatively charged glycosaminoglycans of the arterial wall [37].

Although it has been shown that particle size and surface characteristics have a pronounced influence on the introduction of nanoparticles to the arterial wall, the location of nanoparticles as a function of the nanoparticle size and surface charge has not been studied systematically.

In this study, fluorescent labeled polystyrene (PS) particles were administered to porcine carotid arteries in an *in vitro* model. While several animals have been used in the administration of particles to the artery, including dog [28,37-39], pig [37,40,41], rat [42], sheep [27] and rabbit [12,24,39,43-47], porcine arties are preferred because the vascular system of pigs anatomically resembles the human vascular system most [48-50]. To study the effect of particle size and surface charge on the location and administration efficiency of nanoparticles to the arterial wall systematically, fluorescent labeled, negatively charged PS particles of different sizes (120, 230 and 1000 nm) and positively charged particles of 230 nm were administered. Furthermore, PEO-PLGA particles were labeled with a fluorescent dye and administered to porcine carotid arteries as well. Besides nanoparticle location, the nanoparticle retention and administration efficiency were determined by extraction of the fluorescent labeled particles from the artery.

MATERIALS AND METHODS

Materials

DL-lactide and glycolide were purchased from Purac Biochem b.v. (Gorinchem, The Netherlands). Stannous octoate was purchased from Sigma (St. Louis, USA) and monomethoxy poly(ethylene

glycol) (MPEG) ($\overline{M}_n$ = 3.0·10^3 g/mol) from Shearwater Polymers (Huntsville, USA). Microporous balloon catheters (multiple-layered porous balloon with an outer balloon diameter of 3.25 mm, an outer balloon length of 20 mm, an infusion segment length of 18 mm and a pore size of the outer balloon of 8 μm) (Figure 7.2) were supplied by Cordis (Warren, NJ, USA). PTA balloon catheters (a balloon diameter of 3.0 mm and a balloon length of 20 mm) (Boston Scientific, Maastricht, The Netherlands) were donated by the local hospital (Medisch Spectrum Twente, Enschede, The Netherlands). Polystyrene (PS) nanoparticles of different sizes (120, 220 and 1000 nm) with carboxylic acid (-Carb) or amidine (-Am) groups at the surface were purchased from Molecular Probes (Leiden, The Netherlands) and were dispersed in phosphate buffered saline (PBS; pH 7.4; NPBI, Emmer Compascuum, The Netherlands) at a concentration of 0.1 wt%. These particles contain a fluorescent dye that has a maximal emission at 605 nm when excited at 580 nm. Rhodamine B was obtained from Acros Organics (New Jersey, USA), oxalyl chloride (2 M solution in dichloromethane) from Aldrich (Milwaukee, USA) and formaldehyde solution (3.6% w/v) from Fresenius Kabi ('s-Hertogenbosch, the Netherlands). Dichloromethane (Biosolve, Valkenswaard, The Netherlands) was distilled from calcium hydride (Acros Organics) prior to use. All solvents were of analytical grade (Biosolve). All other reagents were obtained from Merck (Darmstadt, Germany).

Poly(ethylene oxide)-poly(DL-lactic-co-glycolic acid) diblock copolymer (PEO-PLGA) (molar ratio of lactyl:glycolyl = 52:48; $\overline{M}_{n,\text{PEO-block}}$ = 3.0·10^3 g/mol; $\overline{M}_{n,\text{PLGA-block}}$ = 8.2·10^3 g/mol and polydispersity index = 1.24) was synthesized by ring-opening polymerization of DL-lactide and glycolide using MPEG as initiator and stannous octoate as a catalyst at 130 °C for 24 h as described previously [51].
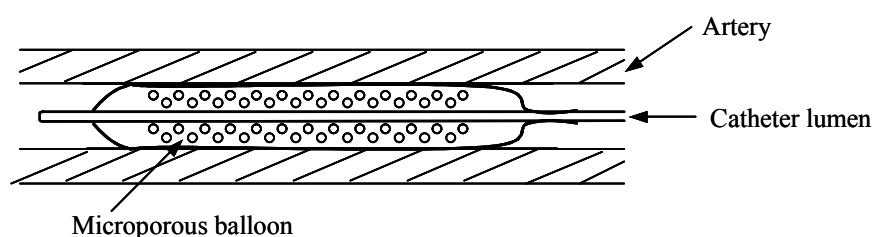
Figure 7.2 Schematic drawing of a microporous balloon catheter used for particle administration.

Labeling of PEO-PLGA with rhodamine B

A rhodamine B solution in dichloromethane (0.2 g; 4·10^{-4} mol in 5 ml) was added drop-wise to 0.3 ml of an oxalyl chloride solution in dichloromethane (6·10^{-4} mol) that was kept at 0 °C. After 10 min, the reaction mixture was warmed up to 25 °C to allow the reaction to go to completion. Subsequently, a PEO-PLGA (2 g; 2·10^{-4} mol) solution in dichloromethane (10 ml) containing triethylamine (56 μl; 4·10^{-4} mol) was added drop-wise to the reaction mixture. The reaction was allowed to proceed for 30 min at 25 °C under continuous stirring. The crude product was precipitated into a ten-fold volume of methanol, filtered, rinsed three times with methanol and dried in vacuo at 40 °C for three days.

Nanoparticle preparation

Nanoparticles were prepared using the salting-out method [51] in which acetone was chosen as the water-miscible organic solvent, because of its pharmaceutical acceptance with regard to toxicity [52]. The method consists of the addition of a highly concentrated salt solution in water (aqueous phase) to a polymer solution in acetone (organic phase). Although acetone is miscible with pure water in all

proportions, the high salt concentration of the aqueous phase prevents mixing of the phases. After emulsification, the addition of pure water in a sufficient quantity causes acetone to diffuse into the aqueous phase, resulting in the formation of nanoparticles.

Typically, an acetone solution (5.0 g) containing 2 wt% copolymer was emulsified under mechanical stirring (20,500 rpm; 40 s; T25 Ultraturrax equipped with a S25 dispersing tool, Ika-Labortechnik, Staufen, Germany) in an aqueous phase (7.5 g) containing 60 wt% $MgCl_2 \cdot 6H_2O$ as the salting-out agent (in a glass beaker; 3.5 cm diameter; 6.6 cm height). After the fast addition (5 s) of pure water (7.5 g) under mechanical stirring (20,500 rpm) causing acetone to diffuse into the water phase, nanoparticles were formed and stirring was continued (20,500 rpm; 20 s).

The nanoparticles were purified by rinsing with water. First, the nanoparticles were separated by ultracentrifugation (65,000×g for 30 min; Centrikon T-2180, Kontron Instruments, Watford, UK) and the supernatant was removed. The nanoparticles were redispersed in water, centrifuged and the supernatant was removed. This procedure was repeated three times. Subsequently, the purified nanoparticles were dispersed in PBS at a concentration of 0.1 wt%.

Particle size analysis

The nanoparticle size was determined by dynamic light scattering (DLS) (Zetasizer 4000, Malvern Instruments Ltd., Malvern, UK) at 25 °C at an angle of 90°, taking the average of three measurements. The particle dispersion was diluted with PBS to such a degree that the desired number of counts was obtained. The desired number of counts is the number of counts that is high enough to obtain a good signal to noise ratio, yet small enough to prevent multiple scattering to occur.

First, the polydispersity index (P.I.) is determined by the cumulants method. The P.I. is a dimensionless number indicating the width of the size distribution, and has a value between zero and one, being zero for monodisperse particles. If the P.I. is small enough (<0.08), the particle size can be determined by the cumulants method and the size distribution obtained is based on a log normal distribution characterized by a mean and width. For polydispersity indices higher than 0.08, the CONTIN-method is used to determine the particle size. The CONTIN-method, developed by Provencher *et al.* [53] describes bimodal and smooth distributions without the need for information such as an initial estimate for the particle size.

Zeta-potential measurements

Particles were dispersed in 1 mM phosphate buffer (pH 7.4) at the same concentration used for DLS (Zetasizer 2000, Malvern Instruments Ltd., Malvern, UK). The zeta-potential of the nanoparticles was determined by measuring the velocity of particles moving through phosphate buffer within stationary plane resulting from an applied electric field, taking the average of five measurements. Zero field correction was performed to ensure that the measured velocity was due to electrophoresis only. Measurements were carried out at a temperature of 25 °C with a cell drive voltage of 120 V and a modulator frequency of 250 Hz.

Determination of rhodamine B content of PEO-PLGA nanoparticles

After the last purification step, the nanoparticle sediment was lyophilized and dissolved in DMSO (0.16 mg/ml). The fluorescence intensity was determined at 605 nm while exciting the sample with light of a wavelength of 580 nm (LS-3 fluorescence spectrometer, Perkin-Elmer, Shelton, USA). The

rhodamine B content of PEO-PLGA nanoparticles was calculated from the fluorescence intensity and a calibration curve of rhodamine B in DMSO at various concentrations.
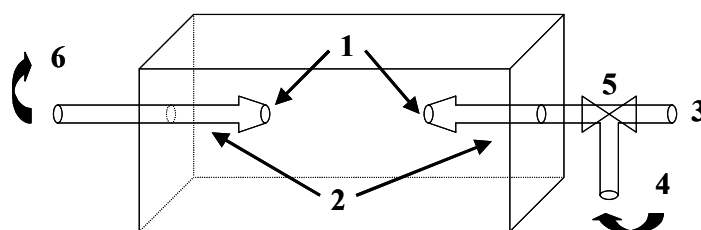
In vitro **intravascular nanoparticle administration**

Porcine carotid arteries (inner diameter varying from 2.5 to 3.6 mm) were isolated and stored on ice during transport (20 min). The arteries were cleaned from connective tissue, washed thoroughly with water and stored in Tyrode-like (Tyrode without glucose) solution ($[NaHCO_3] = 21.4$ mM; $[NaH_2PO_4] = 1.5$ mM; $[KCl] = 5.6$ mM; $[CaCl_2] = 1.1$ mM and $[NaCl] = 135.8$ mM [54]) at 4 °C.

Prior to the *in vitro* experiments, cross-sections with an approximate thickness of 1 mm were cut from both ends of the artery. The artery and both cross-sections were placed in a petri dish that was filled with Tyrode-like solution. The dimensions of the artery (inner and outer diameter and thickness of the arterial wall) were determined from digital pictures.

Prior to nanoparticle administration, the artery was mounted on stainless steel adapters (**1**) (Figure 7.3) in a thermostatic bath filled with Tyrode-like solution, kept at 37 °C. Through inlet **2** a PTA balloon catheter was inserted, with the balloon covering the section D to E (see Figure 7.4). In all experiments, the PTA balloon was inflated to 8 atm in 5 s and maintained at a balloon pressure of 8 ± 0.1 atm for 60 s. After deflation and retraction of the PTA balloon catheter, a microporous balloon catheter was inserted with the balloon in the same position as the balloon during PTA. A nanoparticle dispersion (0.1 wt% in PBS; 3 ml) was administered to the artery over a period of 60 s at a balloon pressure of 3 ± 0.3 atm. After retraction of the balloon catheter, inlet **3** was closed with stopcock **5** and the artery was flushed through inlet **4** for 30 min with a pulsatile flow of Tyrode-like solution with an average flow rate of 74 ml/min at 37 °C. This pulsatile flow at 120 pulse/min was generated by a peristaltic pump and circulated through inlet **6**, and mimics blood flow at a physiological flow rate through coronary arteries [55-59].

In the control experiment, PBS was used instead of a nanoparticle dispersion.

Figure 7.3 *Schematic drawing of the experimental setup for the in vitro intravascular particle administration. The inner diameter of the stainless steel adapters **1** was three mm. The inner diameter of the tubes (**2**) was one mm. Inlet **3** is used to insert the balloon catheters. To inlet **4** a peristaltic pump is connected to flush the artery through stopcock **5** and circulated through outlet **6**.*

The maximum delay between isolation of the artery and particle administration to the arteries was 4 days. Since it has been shown that mechanical characteristics of an artery do not deteriorate upon storage in Tyrode-like solution at 4 °C for 7 days [60], this experimental setting was chosen for practical reasons.

After flushing of the artery with Tyrode-like solution, the artery was rinsed with water and cut transversely at the center of the artery (position A) (Figure 7.4) and at both sides of the center

(positions D and E). One segment (A-D) was used for quantification of the amount of nanoparticles per artery, whereas the other segment (A-E) was used for evaluating the location of the nanoparticles in the arterial segment. It is noted that the length of the arterial segment used for quantification, A-D (10.4 ± 1.7 mm), is slightly longer than the infusion segment length, A-B (9 mm), which is caused by the fact that the total balloon is longer than the infusion segment. This is corrected for in the calculations of nanoparticle retention and administration efficiency.
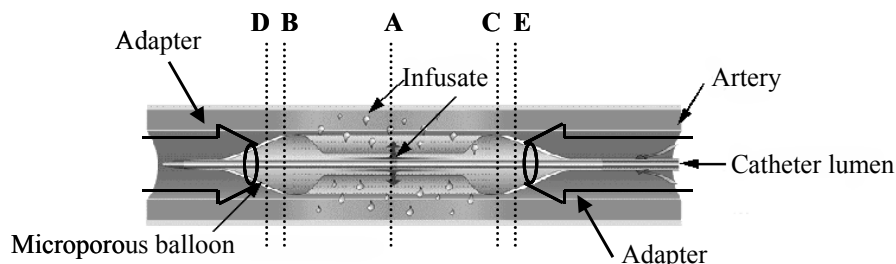
Figure 7.4 Schematic drawing of the position of the stainless steel adapters (see also Figure 7.3) and the microporous balloon catheter in the artery. A is the center of the balloon, the distance B to C is the infusion segment length, and the distance D to E the balloon length.

Quantification of the amount of nanoparticles administered to the artery

The arterial segment A-D was dried in a glass vial in vacuo for 24 h at room temperature. The dry segment was weighed and 1 ml of solvent was added to extract the particles and the glass vial was closed and sealed. In the case of PS particles, xylene was used as the solvent, whereas in the case of PEO-PLGA particles, DMSO was used. After 7 days of extraction, the amount of nanoparticles in the artery was quantified by measuring the fluorescence intensity of the solution. The fluorescence intensity was determined at an emission wavelength of 605 nm and an excitation wavelength of 580 nm (LS-3 fluorescence spectrometer, Perkin-Elmer, Shelton, USA). As a blank, arterial segments from the control experiment were used. The amount of nanoparticles in the artery (NP retention, which is expressed in weight (ng) of nanoparticles per dry weight (mg) of artery) is calculated from the fluorescence intensity of the solution and a calibration curve of the fluorescence intensity of solutions of PS particles in xylene or of labeled PEO-PLGA nanoparticles in DMSO. The efficiency of nanoparticle administration is calculated using Eq. (7.1).

$$\text{Efficiency (\%)} = \frac{\text{NP retention}}{[\text{NP}] \times V} \times 100\% \tag{7.1}$$

[NP] is the nanoparticle concentration in dispersion (1 mg/ml) and V is the infused volume (3 ± 0.3 ml).

Location of nanoparticles in the arterial wall

The arterial segment for determination of the position of the nanoparticles was fixed in a 3.6% (w/v) formaldehyde solution (pH 7) and embedded in JB4-plus (Gold standard series, Polysciences, Inc., Warrington, England; Lotnr. 516747). Cross-sections with a thickness of 2.5 μm were cut using a Reichert-Jung microtome (Leica, Rijswijk, The Netherlands) and placed on glass slides. Eight cross-sections were cut at both sides and in the middle of the arterial segment. Location of the nanoparticles in the cross-section was performed by fluorescence microscopy at an excitation wavelength of 543 nm

using a mercury lamp as the excitation source. A filter was used to block emitted light with a wavelength less than 560 nm.

To determine whether tears had been introduced by PTA or particle administration, arterial cross-sections were analyzed histologically after staining with haematoxylin-eosin (H&E) and van Gieson's elastin stain. The three layers in the arterial wall were distinguished based on their organization and staining intensity.

RESULTS AND DISCUSSION

Characterization of fluorescent labeled PEO-PLGA nanoparticles
During particle purification it was observed that the supernatant was slightly colored, indicating the presence of free rhodamine B in the polymer. The fluorescence intensity of PEO-PLGA nanoparticles in DMSO was measured and the rhodamine B content was calculated using a calibration curve of rhodamine B in DMSO. It was determined that the rhodamine B content of the PEO-PLGA nanoparticles was 2.8 wt%, which means that 70% of the PEO-PLGA chains were modified with rhodamine B.

Particle analyses
The characteristics of the nanoparticles used in this study are shown in Table 7.1. As their size distributions are very narrow (P.I. smaller than 0.08) and their zeta-potentials are similar, the negatively charged PS particles serve as a good model for evaluation of the size-dependency of the particle administration. The zeta-potential of particles containing carboxylic acid groups is negative, whereas the zeta-potential of particles of the same size that contain amidine groups is positive. This allows the evaluation of the effect of surface charge on the location of the nanoparticles in the arterial wall for nanoparticles with a size of approximately 225 nm. Furthermore, the particle size of PEO-PLGA particles is the same as of the smallest PS particles (approximately 120 nm), which affords a comparison of PEO-PLGA nanoparticles with PS particles of the same size.

Table 7.1 Particle size, polydispersity index (P.I.) and zeta-potential of the nanoparticles that were administered to the arterial wall (n=5).

Nanoparticle	Size (nm)	P.I. (-)	Zeta-potential (mV)
PS-Carb-1000	1001 ± 67	0.07 ± 0.03	-54 ± 2
PS-Carb-230	230 ± 3	0.03 ± 0.03	-51 ± 2
PS-Am-230	223 ± 1	0.03 ± 0.02	$+58 \pm 2$
PS-Carb-120	124 ± 1	0.02 ± 0.01	-56 ± 2
PEO-PLGA-120	114 ± 1	0.18 ± 0.05	-7 ± 2

Efficiency of nanoparticle administration

Xylene or DMSO was added to the arteries to extract the PS particles or the PEO-PLGA particles, respectively. After 7 days of extraction, the fluorescence intensity of the solution was measured and the amount of nanoparticles in the artery was calculated. From the amount of particles per artery, the efficiency of administration of particles to the artery was calculated using Eq. (7.1). The administration efficiency of the different particles is plotted as a function of the inner diameter of the artery (Figure 7.5).

It is seen in Figure 7.5 that the smaller the inner diameter of the artery, the higher is the efficiency of administration, ranging from 0.01 to 0.7%. Besides adsorption of particles via the intact intima layer of the artery, the particles can be introduced to the arterial wall by two ways, as described in the introduction of this Chapter: either via tears or via the vasa vasorum. If the inner diameter of the artery is larger than the outer diameter of the balloon catheters (3.25 mm), the pressure at the arterial wall is less than the balloon pressure (3 atm) and the artery is not overdilated. It is therefore not likely that tears in the arterial wall are formed. The fact that particles were introduced to arteries with an inner diameter larger than the outer diameter of the balloon catheters was either due to adsorption of particles onto the luminal surface of the artery or to introduction of particles to the arterial wall via transport through the vasa vasorum. As the administration efficiency was low for arteries with an inner diameter larger than the outer diameter of the balloon catheters, the vasa vasorum might not play a great role in particle administration. If transport via the vasa vasorum occurs, particles are expected to be also present in the adventitia. Therefore, experiments in which the inner diameter of the artery was larger than the outer diameter of the balloon catheters were also evaluated in order to determine the location of nanoparticles in the arterial wall.
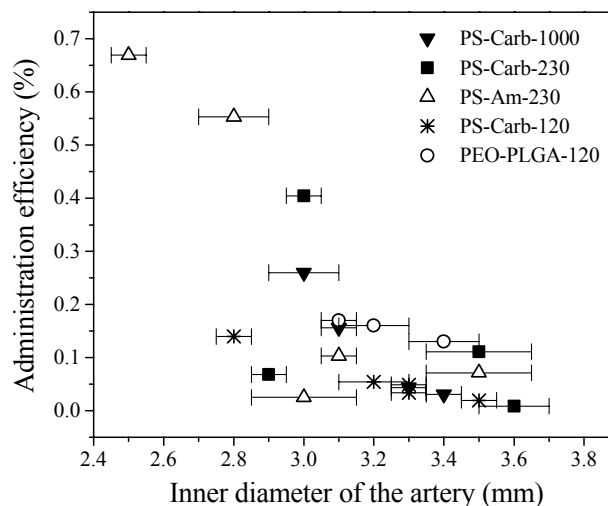
Figure 7.5 *The administration efficiency of PEO-PLGA particles and PS particles of different size and surface charge as a function of the inner diameter of the artery (each data point represents one artery; the bars show the variation in the inner diameter of each artery).*

For arteries with an inner diameter equal or smaller than the outer diameter of the balloon catheters, the trend is an increasing efficiency of particle administration with decreasing inner diameter of the artery. Overdilation of the artery has three effects on the arterial wall. Firstly, the pressure on the arterial wall is built up and the particles are forced into the arterial wall. Secondly, the arterial wall is stretched, probably resulting in the formation of small intima tears. Thirdly, the vasa vasorum is compressed, thus reducing transport capacity through the compressed vasa vasorum. The increase in pressure and the formation of intima tears leads to an increased penetration of particles into the arterial wall, whereas compression of the vasa vasorum decreases the introduction of particles to the arterial wall. Since the administration efficiency is higher when the artery is more overdilated, the higher pressure or the formation of tears is probably the predominant way of introducing particles to the arterial wall. Consequently, it is unlikely that the vasa vasorum plays a role in the introduction of particles to the arterial wall.

To be able to determine the effect of particle size and surface charge on the efficiency of administration, arteries of the same inner diameter were compared. Apart from the arteries with an inner diameter of 3.0 mm, no differences between the administration efficiency of PS-Carb-230, PS-Am-230 and PS-Carb-1000 particles were observed. Apparently, the surface charge does not have a large influence on the efficiency of administration. The efficiency of administration of PEO-PLGA-120 particles is generally higher than the efficiency of administration of PS-Carb-120 particles. In contrast to PS particles, PEO-PLGA particles have a high water-uptake and can be more easily deformed. Therefore, PEO-PLGA particles probably can be forced into the arterial wall more easily than PS particles of the same size.

Location of nanoparticles in the arterial wall
Cross-sections were cut-off from all arteries to which particles were administered. The cross-sections were analyzed by fluorescence microscopy. The position of nanoparticles of different size and surface charge within each layer of the arterial wall was determined by visual evaluation of the images. The relative number of cross-sections in which particles in a specific layer were detected and the relative amount of particles per arterial layer is shown in Table 7.2.

Except for PS-Carb-230 particles, particles were observed in the intima of all arteries. In 1 of the 4 arteries infused with PS-Carb-230 particles, no particles were observed in the intima. This artery had an inner diameter that was larger than the diameter of the balloon catheters, which might explain the absence of particles in the intima. In the case of particles of 1000 and 230 nm, the penetration of particles was mainly limited to the intima as indicated by the percentage of particles in the intima being (nearly) 100% (Table 7.2). The smallest particles penetrated the arterial wall deeper and were seen in the media and adventitia as well. The fact that for one artery no PS-Carb-120 particles were observed in the media and adventitia could again be ascribed to the inner diameter of the artery being larger than the outer diameter of the balloon catheters.

Table 7.2 The number of treated arteries, the relative number of cross-sections in which particles were observed per layer (between brackets is the number of arteries in which particles were observed) and the relative amount of particles per arterial layer.

Nanoparticle	Number of treated arteries	Relative number of cross-sections with particles (%)			Relative number of particles per layer (%)		
		Intima	Media	Adventitia	Intima	Media	Adventitia
PS-Carb-1000	4	100 (4)	3 (1)	0 (0)	100	0	0
PS-Carb-230	4	75 (3)	6 (1)	4 (1)	96	4	0
PS-Am-230	5	100 (5)	5 (1)	0 (0)	99	1	0
PS-Carb-120	5	100 (5)	70 (4)	70 (4)	54	27	19
PEO-PLGA-120	3	100 (3)	25 (1)	25 (1)	81	16	3

The location of PS-Carb particles of 1000 and 120 nm in the arterial wall is shown in Figure 7.6. The identification of intima, media and adventitia within the arterial wall was performed by light microscopy, after which images were made in fluorescence mode. PS-Carb-1000 particles were only observed in the intima (Figure 7.6). A very different picture is observed for PS-Carb-120 particles; these particles are seen in all layers of the arterial wall (Figure 7.6). From the quantification of the introduction of PS-Carb-230 and PS-Am-230 particles to the arterial wall, it was concluded that the surface charge did not affect the introduction of particles. This is confirmed by the microscopic observation that the distribution and relative amount of particles in the arterial wall is similar for PS-Carb-230 and PS-Am-230 particles when arteries of the same inner diameter are compared.
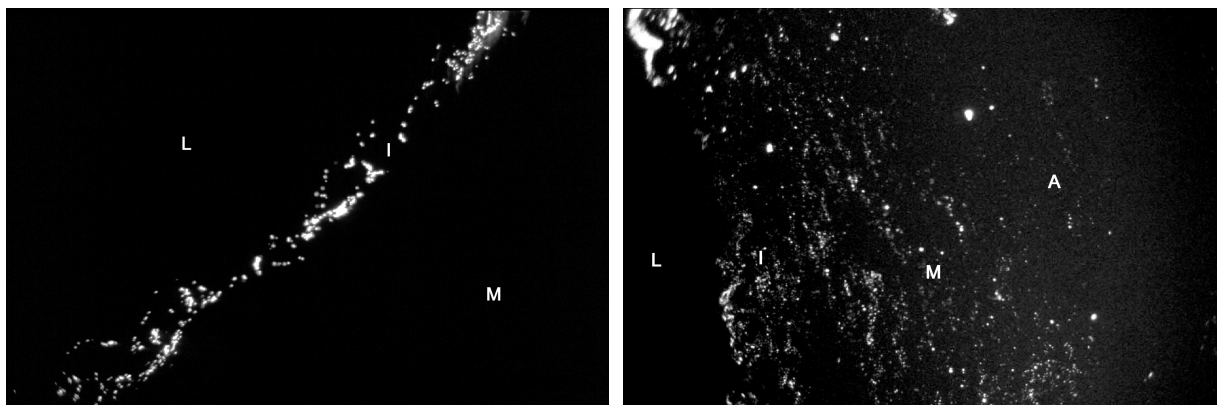
Figure 7.6 (Left) PS-Carb particles of 1000 nm and (right) PS-Carb of 120 nm administered to a porcine carotid arterial wall (L=Lumen; I=Intima; M=Media and A=Adventitia).

In *in vivo* experiments in rabbits and sheep, particles of 150 nm to several microns have been observed in the adventitia [24,26,27,43]. The presence of these particles in the adventitia was caused by tear formation in the artery during the PTA or the particle administration procedure [24,26] or by transport through the vasa vasorum [26,27,43]. Also in the experiments presented in this Chapter, the presence of particles in the arterial wall can be caused by transport through the vasa vasorum, by penetration through the arterial wall or by the formation of

tears. Particles of 120 nm were observed in all layers of the artery and were evenly distributed in the arterial wall. Yet, no intima tears in any of the arteries were observed with light microscopy. This indicates that these particles can penetrate the arterial wall or that tears smaller than one micrometer were formed. Since particles of 230 and 1000 nm were hardly present in the media and not present in the adventitia, it can be concluded that these particles cannot be transported through the vasa vasorum. Furthermore, this observation corresponds with the conclusion made before that it is unlikely that the vasa vasorum plays a role in the introduction of particles to the arterial wall.

The dependency of the depth of particle penetration into the arterial wall on the particle size enables the introduction of particles to the arterial layer of interest by selection of the proper particle size. This means that for instance particles of 120 nm can be used to deliver drugs to the media or adventitia, e.g. to inhibit smooth muscle cell proliferation, whereas particles of 1000 nm can be used to deliver drugs involved in blood coagulation or endothelial dysfunction, as these particles accumulate in the intima.

Besides PS particles, biodegradable, fluorescent labeled PEO-PLGA nanoparticles of 120 nm were administered to three arteries. Particles were observed in the intima of all three arteries and for one of these three arteries, particles were observed in all arterial layers (Table 7.2). In two arteries, particles were only seen in the intima, probably because the inner diameter of these arteries was slightly larger than the outer diameter of the balloon catheter. This confirms the results obtained with the model PS particles that PEO-PLGA particles of 120 nm can be introduced to all layers of the arterial wall in case balloon catheters with the appropriate dimensions are used, and that the vasa vasorum seems to play a minor role in the introduction of particles to the arterial wall.

In human atherosclerotic arteries, extracellular matrix is usually deposited [5] and frequently, regions of calcification are present [6]. This means that high pressures are required during the PTA and the particle administration procedure, resulting in strong compression of the vasa vasorum. Particle introduction via transport through the vasa vasorum might therefore not be very efficient. Similarly, large intima and probably also media tears are more likely to be formed in atherosclerotic arteries than in healthy arteries. Although the formation of large tears facilitates particle administration [26], the particles will only be present in close proximity of the tears in the arterial wall. In this respect it can be expected that smaller particles, such as PEO-PLGA particles with a diameter of 120 nm, are able to penetrate the arterial wall further away from the tears. However, this needs to be assessed in experiments using human atherosclerotic arteries.

The fact that PEO-PLGA particles are biodegradable and are able to penetrate the complete arterial wall makes these particles good candidates for the delivery of drugs for the reduction of the incidence of restenosis. As previously shown, these particles are also suitable for surface modification to enhance their targeting specificity [36]. Drug delivery from PEO-PLGA nanoparticles could be a good alternative or complementary to the use of drug-eluting

stents. Nanoparticles can be introduced to all layers of the arterial wall, whereas drug delivery from a drug-eluting stent is limited to the luminal surface of the artery. It is reported that administration of free drug from the luminal side of the artery leads to a short residence time of the drug in the artery, whereas injection of free drug into the adventitia leads to a much higher drug concentration in the artery and a residence time up to 21 days [61].

CONCLUSIONS

This study demonstrates that PS particles of 230 and 1000 nm were mainly introduced to the intima of the arterial wall, whereas PS particles of 120 nm could be introduced to all layers of the arterial wall. From the administration of particles to arteries that had a larger inner diameter than the outer diameter of the balloon catheters it is concluded that the vasa vasorum played a minor role in the introduction of the particles to the arterial wall. This is confirmed by the increase in the administration efficiency of particles to the arterial wall with decreasing inner diameter of the artery. Due to the relatively large variation in the artery diameter used in the administration experiments, it cannot be concluded whether the surface charge had an influence on the nanoparticle retention and the efficiency of particle administration.

This study has demonstrated that biodegradable PEO-PLGA particles of 120 nm can be introduced to all layers of the artery. Since PEO-PLGA particles are biodegradable and can be used for surface modification to enhance their targeting specificity, these particles are good candidates for the delivery of drugs for the reduction of the incidence of restenosis.

ACKNOWLEDGEMENTS

REFERENCES

1. Pathobiological Determinants of Atherosclerosis in Youth (PDAY) Research Group, *Arterioscler. Thromb.,* **1993**, *13*, 1291-1298.
2. McGill, H.C.; McMahan, C.A.; Malcom, G.T.; Oalmann, M.C. and Strong, J.P., *Arterioscler. Thromb. Vasc. Biol.,* **1997**, *17*, 95-106.
3. Schettler, F.G. and Boyd, G.S. *Atherosclerosis - Pathology, physiology, aetiology, diagnosis and clinical management*; Elsevier: Amsterdam, **1969**.

4. Botti, T.P.; Amin, H.; Hiltscher, L.; Wissler, R.W.; Robertson, A.L.; Strong, J.P.; Cornhill, J.F.; McGill, H.C.; McMahan, C.A.; Oalmann, M.C. *et al.*, *Atherosclerosis,* **1996**, *124*, 191-202.

5. Consigny, P.M., *Am. J. Röntgenol.,* **1995**, *164*, 553-558.

6. Geary, R.L.; Williams, J.K.; Golden, D.; Brown, D.G.; Benjamin, M.E. and Adams, M.R., *Arterioscler. Thromb. Vasc. Biol.,* **1996**, *16*, 34-43.

7. Lincoff, A.M.; Topol, E.J. and Ellis, S.G., *Circulation,* **1994**, *90*, 2070-2084.

8. Krüger, K.; Bendel, M.; Zähringer, M.; Weise, C. and Lackner, K., *Cardiovasc. Rad. Med.,* **2001**, *2*, 213-220.

9. Johnson, L.L.; Schofield, L.M.; Verdesca, S.A.; Sharaf, B.L.; Jones, R.M.; Virmani, R. and Khaw, B.A., *J. Nucl. Med.,* **2000**, *41*, 1535-1540.

10. Wolinsky, H. and Thung, S.N., *J. Am. Coll. Cardiol.,* **1990**, *15*, 475-481.

11. Mitchel, J.F.; Fram, D.B.; Palme, D.F.; Foster, R.; Hirst, J.A.; Azrin, M.A.; Bow, L.M.; Eldin, A.M.; Waters, D.D. and McKay, R.G., *Circulation,* **1995**, *91*, 785-793.

12. Dev, V.; Eigler, N.; Fishbein, M.C.; Tian, Y.; Hickey, A.; Rechavia, E.; Forrester, J.S. and Litvack, F., *Cathet. Cardiovasc. Diagn.,* **1997**, *41*, 324-332.

13. Chorny, M.; Fishbein, I. and Golomb, G., *Crit. Rev. Ther. Drug Carrier Syst.,* **2000**, *17*, 249-284.

14. Gershlick, A.H., *Atherosclerosis,* **2002**, *160*, 259-271.

15. Serruys, P.W.; De Jaegere, P.; Kiemeneij, F.; Macaya, C.; Rutsch, W.; Heyndrickx, G.; Emanuelsson, H.; Marco, J.; Legrand, V.; Materne, P. *et al.*, *N. Engl. J. Med.,* **1994**, *331*, 489-495.

16. Fischman, D.L.; Leon, M.B.; Baim, D.S.; Schatz, R.A.; Savage, M.P.; Penn, I.; Detre, K.; Veltri, L.; Ricci, D.; Nobuyoshi, M. *et al.*, *N. Eng. J. Med.,* **1994**, *331*, 496-501.

17. Stevens, A. and Lowe, J.S. *Human histology*; 2nd ed.; Mosby: London, **1997**.

18. Crotty, T.P., *Med. Hypotheses,* **1989**, *28*, 233-243.

19. Pels, K.; Labinaz, M. and O'Brien, E.R., *Jpn. Circ. J.,* **1997**, *61*, 893-904.

20. Geiringer, E., *J. Pathol. Bacteriol.,* **1951**, *6*, 201-211.

21. Barker, S.G.E.; Causton, B.E.; Baskerville, P.A.; Gent, S. and Martin, J.F., *J. Anatomy,* **1992**, *180,* 225-231.

22. Wolinsky, H. and Glagov, S., *Circ. Res.,* **1967**, *20*, 409-421.

23. Huehns, T.Y.; Gonschior, P. and Höfling, B., *Heart,* **1996**, *75*, 537-538.

24. Wilensky, R.L.; March, K.L. and Hathaway, D.R., *Am. Heart J.,* **1991**, *122*, 1136-1140.

25. Beurskens, H. *De bloedstolling: thrombose, atherosclerose en het hartinfarct*; Natuur en techniek: Diemen, **1979**.

26. Nasser, T.K.; Wilensky, R.L.; Mehdi, K. and March, K.L., *Am. Heart J.,* **1996**, *131*, 892-898.

27. Rome, J.J.; Shayani, V.; Flugelman, M.Y.; Newman, K.D.; Farb, A.; Virmani, R. and Dichek, D.A., *Arterioscler. Thromb.,* **1994**, *14*, 148-161.

28. Song, C.X.; Labhasetwar, V.; Murphy, H.; Qu, X.; Humphrey, W.R.; Shebuski, R.J. and Levy, R.J., *J. Control. Release,* **1997**, *43*, 197-212.

29. Pastore, C.J.; Isner, J.M.; Bachc, P.A.; Kearney, M. and Pickering, J.G., *Circ. Res.,* **1995**, *77*, 519-529.

30. Mattar, S.G.; Hanson, S.R.; Pierce, G.F.; Chen, C.; Hughes, J.D.; Cook, J.E.; Shen, C.; Noe, B.A.; Suwyn, C.R.; Scott, J.R. *et al.*, *J. Surg. Res.,* **1996**, *60*, 339-344.

31. Nagae, T.; Louie, A.Y.; Aizawa, K.; Ishimaru, S. and Wilson, S.E., *J. Cardiovasc. Surg.,* **1998**, *39*, 709-715.

32. Wickham, T.J.; Haskard, D.; Segal, D. and Kovesdi, I., *Cancer Immunol. Immunother.,* **1997**, *45*, 149-151.

33. Hillis, G.S. and Flapan, A.D., *Heart,* **1998**, *79*, 429-431.

34. Giuffre, L.; Cordey, A.-S.; Monai, N.; Tardy, Y.; Schapira, M. and Spertini, O., *J. Cell Biol.,* **1997**, *136*, 945-956.

35. Dashwood, M.R.; Barker, S.G.E.; Muddle, J.R.; Yacoub, M.H. and Martin, J.F., *J. Cardiovasc. Pharm.,* **1993**, *22*, S343-S347.

36. Chapter 6 of this thesis.

37. Labhasetwar, V.; Song, C.; Humphrey, W.; Shebuski, R. and Levy, R.J., *J. Pharm. Sci.,* **1998**, *87*, 1229-1234.

38. Song, C.; Labhasetwar, V.; Cui, X.; Underwood, T. and Levy, R.J., *J. Control. Release,* **1998**, *54*, 201-211.

39. Hong, M.K.; Wong, S.C.; Farb, A.; Mehlman, M.D.; Virmani, R.; Barry, J.J. and Leon, M.B., *Coron. Artery Dis.,* **1993**, *4*, 1023-1027.

40. Banai, S.; Wolf, Y.; Golomb, G.; Pearle, A.; Waltenberger, J.; Fishbein, I.; Schneider, A.; Gazit, A.; Perez, L.; Huber, R. *et al.*, *Circulation,* **1998**, *97*, 1960-1969.

41. Humphrey, W.R.; Erickson, A.; Simmons, C.A.; Northrup, L.; Wishka, D.G.; Morris, J.; Labhasetwar, V.; Song, C.; Levy, R.J. and Shebuski, R.J., *Adv. Drug Deliver. Rev.,* **1997**, *24*, 87-108.

42. Fishbein, I.; Chorny, M.; Rabinovich, L.; Banai, S.; Gati, I. and Golomb, G., *J. Control. Release,* **2000**, *65*, 221-229.

43. Gradus-Pizlo, I.; Wilensky, R.L.; March, K.L.; Fineberg, N.; Michaels, M.; Sandusky, G.E. and Hathaway, D.R., *J. Am. Coll. Cardiol.,* **1995**, *26*, 1549-1557.

44. Hong, M.K.; Wong, S.C.; Farb, A.; Mehlman, M.D.; Virmani, R.; Barry, J.J. and Leon, M.B., *Cathet. Cardiovasc. Diagn.,* **1995**, *34*, 263-270.

45. Klugherz, B.D.; Meneveau, N.; Chen, W.; Wade-Whittaker, F.; Papandreou, G.; Levy, R. and Wilensky, R.L., *J. Cardiovasc. Pharmacol. Therapeut.,* **1999**, *4*, 167-174.

46. Valero, F.; Hamon, M.; Fournier, C.; Meurice, T.; Flautre, B.; Van Belle, E.; Lablanche, J.-M.; Gosselin, B.; Bauters, C. and Bertrand, M., *J. Cardiovasc. Pharm.,* **1998**, *31*, 513-519.

47. Wilensky, R.L.; March, K.L.; Gradus-Pizlo, I.; Schauwecker, D.; Michaels, M.B.; Robinson, J.; Carlson, K. and Hathaway, D.R., *Am. Heart J.,* **1995**, *129*, 852-859.

48. Muller, D.W.M.; Ellis, S.G. and Topol, E.J., *J. Am. Coll. Cardiol.,* **1992**, *19*, 418-432.

49. Schwartz, R.S., *Lab. Invest.,* **1994**, *71*, 789-791.

50. Jackson, C.L., *Trends Cardiovasc. Med.,* **1994**, *4*, 122-130.

51. Chapter 4 of this thesis.

52. Rabiant, J., *S.T.P. Pharma,* **1991**, *1*, 278-283.

53. Provencher, S.W.; Hendrix, J. and De Maeyer, L., *J. Chem. Phys.,* **1978**, *69*, 4273-4276.

54. Vaartjes, S.R. and Boom, H.B.K., *Circ. Res.,* **1987**, *60*, 727-737.

55. Cooney, D.O. *Biomedical engineering principles - An introduction to fluid, heat, and mass transport processes*; Marcel Dekker, Inc.: New York, **1976**; Vol. 2.

56. Ferrari, M.; Andreas, S.; Werner, G.S.; Wicke, J.; Kreuzer, H. and Figulla, H.R., *Cathet. Cardiovasc. Diagn.,* **1997**, *42*, 84-89.

57. Sukavaneshvar, S.; Zheng, Y.; Rosa, G.M.; Mohammad, S.F. and Solen, K.A., *ASAIO J.,* **2000**, *46*, 301-304.

58. Nerem, R.M., Vascular endothelial responses to shear stress, In *Blood flow in large arteries: applications to atherogenesis and clinical medicine*; Liepsch, D.W., Ed.; Karger: Basel, **1990**; Vol. 15, p 117-124.

59. Back, L.H.; Kwack, E.Y. and Crawford, D.W., Flow measurements in a model of the mildly curved femoral artery of man, In *Blood flow in large arteries: applications to atherogenesis and clinical medicine*; Liepsch, D.W., Ed.; Karger: Basel, **1990**; Vol. 15, p 96-108.

60. Steenhuijsen, J., Stress and strain in atherosclerotic arteries during angioplasty, University of Twente, Enschede, The Netherlands **1997**, Ph.D. thesis.

61. Gonschior, P.; Wilensky, R.; March, K. and Höfling, B., *Zeitschrift für Kardiologie,* **1996**, *85*, 155-165.

CHAPTER 8

Release of anti-restenosis drugs from poly(ethylene oxide)-poly(DL-lactic-co-glycolic acid) nanoparticles

ABSTRACT

Dexamethasone- or rapamycin-loaded nanoparticles based on poly(ethylene oxide) and poly(DL-lactic-co-glycolic acid) block copolymers (PEO-PLGA) were prepared without additional stabilizer using the salting-out method. A fast release of drug in PBS (pH 7.4) at 37 °C resulting in 100% release within 5 hours was observed for both drugs. The rate of drug release was substantially reduced by treating the particles with gelatin or albumin after drug loading, resulting in a linear drug release in time. It was shown that the rate of drug release is related to the amount of protein associated with the nanoparticles. After gelatin treatment of drug-loaded nanoparticles, sustained release of dexamethasone for 17 days and of rapamycin for 50 days could be achieved.

INTRODUCTION

After percutaneous transluminal coronary angioplasty (PTCA), restenosis of 30 to 50% of the treated coronary arteries occurs [1]. Attempts have been made to decrease the incidence of restenosis. A successful approach was the introduction of a stent. Because of the rigid structure they provide mechanical strength, which minimizes the process of early elastic recoil and late artery remodeling [2]. Although tissue growth in and around the stent is equal or higher than tissue growth after PTCA, the final arterial diameter is larger [3]. Compared to PTCA, stenting leads to a decrease of 10-15% in the incidence of restenosis [3-5]. Nevertheless, stented small arteries tend to reocclude more easily than stented large arteries and conditions where excessive smooth muscle cell response occurs (e.g. in diabetics) lead to relatively high in-stent restenosis [3]. Due to the decrease in the incidence of restenosis, stents are nowadays also used in more complex lesions, resulting in an overall in-stent restenosis of 10 to 50% of the stented lesions [6].

The use of polymer-coated, drug-eluting stents reduced the incidence of (in-stent) restenosis. Besides as a drug depot, the polymer coating can be used to regulate the drug release rate [7]. It has been shown in clinical trials that the use of rapamycin-eluting stents, stents coated with a drug-containing non-erodable polymer layer, which released the drug for more than 28 days, leads to complete inhibition of restenosis [7,8]. This is due to the inhibition of vascular smooth muscle cell proliferation [9]. Also after 18 months, no delayed restenosis was observed [10].

The Food and Drug Administration (FDA) approved rapamycin in 1999 for the use in kidney transplantations [11]. Rapamycin suppresses the immune response, thus leading to a better acceptance of the donor kidney by the patient. Furthermore, rapamycin inhibits proliferation of smooth muscle cells, which are suspected to play a role in chronic rejection in transplanted patients [12].

Although drug-eluting stents inhibit restenosis completely, they are not biodegradable and are thus permanently present, which could lead to long-term adverse tissue reactions. However, no long-term (>18 months) studies on adverse reactions of drug-eluting stents have been performed yet. Biodegradable drug-loaded nanoparticles may be a good alternative for, or complementary to, the use of drug-eluting stents. It has been shown, that drug-loaded nanoparticles can be locally delivered to the site of the atherosclerotic lesion [13] and that the size of the nanoparticles mainly determines the particle localization in the arterial wall [14]. By using nanoparticles of different sizes, drug delivery to specific layers in the arterial wall can be achieved simultaneously. Furthermore, it was previously shown that nanoparticles prepared from poly(ethylene oxide)-poly(DL-lactic-co-glycolic acid) diblock copolymer (PEO-PLGA) can be prepared without additional stabilizer [15] and that they are suitable for surface modification to enhance their targeting specificity [16].

To our knowledge, the preparation of rapamycin-loaded nanoparticles and the rapamycin release from nanoparticles has not been studied before. Besides rapamycin (see Figure 8.1A), dexamethasone (see Figure 8.1B) has also proven to reduce the incidence of restenosis [17].

Both drugs are well soluble in various organic solvents [18,19], but differ in terms of molecular weight and hydrophobicity. Rapamycin has a higher molecular weight (914,2 g/mol) than dexamethasone (392,5 g/mol) and a lower water solubility (2.6 µg/ml for rapamycin [20] compared to 100 µg/ml for dexamethasone [18]). This difference may influence drug loading and drug release characteristics.

In this study, the preparation of PEO-PLGA nanoparticles loaded with dexamethasone and rapamycin and the release of these active agents in PBS (pH 7.4) at 37 °C are described.
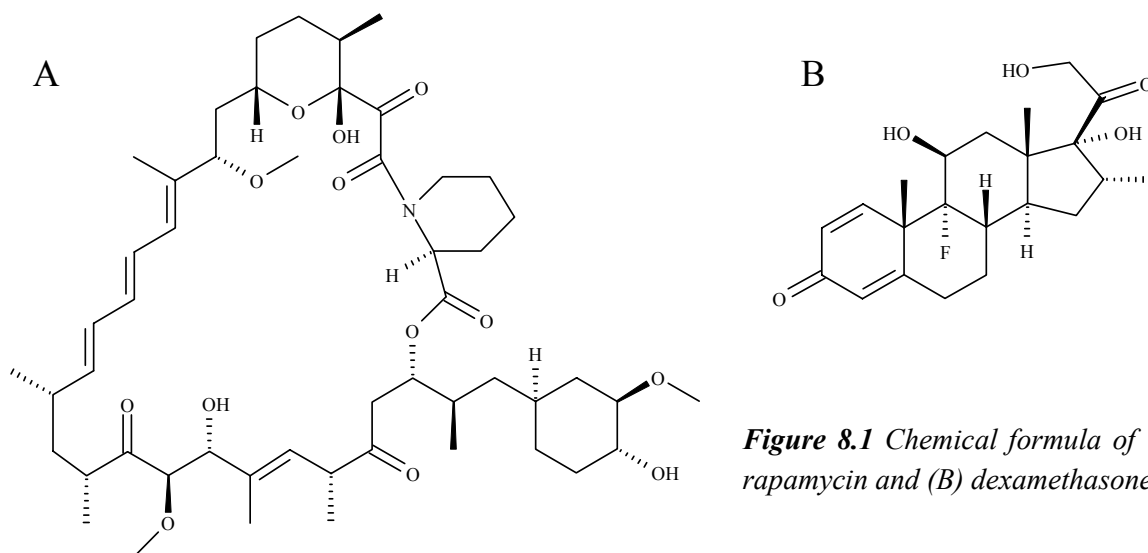
Figure 8.1 Chemical formula of (A) rapamycin and (B) dexamethasone.

MATERIALS AND METHODS

Materials

DL-lactide and glycolide were purchased from Purac Biochem b.v. (Gorinchem, The Netherlands). Stannous octoate, gelatin B (bovine skin, 75 bloom, approximate $\overline{M}_w = 22 \cdot 10^3$ g/mol), bovine serum albumin (BSA) (approximate $\overline{M}_w = 66 \cdot 10^3$ g/mol; minimum 98% pure), dexamethasone and rapamycin were purchased from Sigma (St. Louis, USA) and used as received. Monomethoxy poly(ethylene glycol) (MPEG) ($\overline{M}_n = 3.0 \cdot 10^3$ g/mol) was obtained from Shearwater Polymers (Huntsville, USA) and sodium dodecyl sulfate (SDS) and deuterated dimethylsulfoxide were purchased from Aldrich (Milwaukee, USA). Phosphate buffered saline (PBS; pH 7.4) was purchased from NPBI (Emmer Compascuum, The Netherlands). All solvents used were of analytical grade (Biosolve, Valkenswaard, The Netherlands). All other reagents were obtained from Merck (Darmstadt, Germany).

Poly(ethylene oxide)-poly(DL-lactic-co-glycolic acid) block copolymer (PEO-PLGA) (molar ratio of lactyl:glycolyl = 52:48; $\overline{M}_{n,\text{PEO-block}} = 3.0 \cdot 10^3$ g/mol; $\overline{M}_{n,\text{PLGA-block}} = 8.2 \cdot 10^3$ g/mol and polydispersity index = 1.24) was synthesized by ring-opening polymerization of DL-lactide and glycolide using MPEG as initiator and stannous octoate as a catalyst at 130 °C for 24 h as described previously [15].

Nanoparticle preparation

Nanoparticles were prepared using the salting-out method [15] in which acetone was chosen as the water-miscible organic solvent, because of its pharmaceutical acceptance with regard to toxicity [21].

The method consists of the addition of a highly concentrated salt solution in water (aqueous phase) to a polymer solution in acetone (organic phase). Although acetone is miscible with pure water in all ratios, the high salt concentration of the aqueous phase prevents mixing of both phases. After emulsification, the addition of pure water in a sufficient quantity causes acetone to diffuse into the aqueous phase, resulting in the formation of nanoparticles.

Typically, an acetone solution (3.5 g) containing 3 wt% PEO-PLGA and various amounts (0-1.2 wt%) of drug was emulsified under mechanical stirring (20,500 rpm; 40 s; T25 Ultraturrax equipped with a S25 dispersing tool, Ika-Labortechnik, Staufen, Germany) in an aqueous phase (8.75 g) containing 60 wt% $MgCl_2 \cdot 6H_2O$ as the salting-out agent (in a glass beaker; 3.5 cm diameter; 6.6 cm height). After the fast addition (5 s) of pure water (7.5 g) under mechanical stirring (20,500 rpm) causing acetone to diffuse into the water phase, nanoparticles were formed and stirring was continued (20,500 rpm; 20 s). The nanoparticles were purified by rinsing with water. First, the nanoparticles were separated by ultracentrifugation (65,000×g for 30 min; Centrikon T-2180, Kontron Instruments, Watford, UK) and the supernatant was removed. The nanoparticles were redispersed in water, centrifuged and the supernatant was removed. This procedure was repeated three times.

All nanoparticle preparations were performed in duplo, unless stated otherwise.

Nanoparticle treatment with protein

After the first purification step by ultracentrifugation (see nanoparticle preparation), the nanoparticles were redispersed in 5 ml of a protein solution (0.02, 0.1 or 0.5 mg/ml) in millipore water (MilliQ, Molsheim, France) for 1 h and centrifuged (65,000×g for 30 min). After removal of the supernatant, the protein-treated particles were rinsed with water twice by redispersion in millipore water, centrifugation and subsequent removal of the supernatant. The proteins used were gelatin and BSA.

Particle size analysis

The nanoparticle size was determined by dynamic light scattering (DLS) (Zetasizer 4000, Malvern Instruments Ltd., Malvern, UK) at 25 °C at an angle of 90°, taking the average of three measurements. The particle dispersion was diluted with water to such degree that the desired number of counts was obtained. The desired number of counts is the number of counts that is high enough to get the highest possible signal to noise ratio, yet small enough to prevent multiple scattering to occur.

First, the polydispersity index (P.I.) is determined by the cumulants method. The P.I. is a dimensionless number indicating the width of the size distribution, and has a value between zero and one, being zero for monodisperse particles. If the P.I. is small enough (<0.08), the particle size can be determined by the cumulants method and the size distribution obtained is based on a log normal distribution characterized by a mean and width. For polydispersity indices higher than 0.08, the CONTIN-method is used to determine the particle size. The CONTIN-method, developed by Provencher *et al.* [22] describes bimodal and smooth distributions without the need for information such as an initial estimate for the particle size.

To examine the size and morphology of the nanoparticles in the dry state, samples were analyzed by scanning electron microscopy (SEM) using a LEO 1500 (LEO Electron Microscopy Ltd., Cambridge, UK). Silicon substrates (∅ 15 mm) were cleaned ultrasonically, successively in isopropanol (10 min, two times), in methanol (10 min, two times) and in acetone (10 min, two times). The nanoparticle samples were prepared by dropping an aqueous particle dispersion on a freshly cleaned silicon

substrate and by drying for 2 h at ambient temperature. SEM-analysis was performed at 1 kV at magnifications ranging from 2000× to 15000×. The particle size in the dry state was determined by averaging the size of 35 particles.

Determination of protein content of the nanoparticles

The surface of protein-treated and untreated drug-loaded particles was analyzed by X-ray photoelectron spectroscopy (XPS). Nanoparticle samples were prepared on silicon substrates as described above for SEM analysis. Spectra of the nanoparticle samples were obtained using a Quantum 2000 Scanning ESCA Microprobe (Physical Electronics, Eden Prairie, MN, USA) using monochromatized Al Kα (25 W) X-rays and an electron take off angle of 45°. The X-ray spot size was 100 µm. A single survey spectrum (0-1100 eV) was recorded on each sample on three different spots using a pass energy of 187.85 eV and an acquisition time of 5 min. Charge neutralization was performed using a 1 eV electron source and a 5 eV ion source. The measured peak areas were converted into atomic percentages by using sensitivity factors known from literature [23].

The nitrogen content of lyophilized, protein-treated and untreated dexamethasone-loaded nanoparticles, gelatin and albumin was determined by elemental analysis using an EA 1108 (Fisons Instruments, Interscience b.v., Breda, The Netherlands). From the percentage of nitrogen in the nanoparticle samples and in the gelatin and albumin samples, the amount of gelatin and albumin associated with the nanoparticles was calculated. The analysis of all samples was performed in duplo.

Determination of the rapamycin content of nanoparticles

The rapamycin content of the nanoparticles was analyzed by high-performance liquid chromatography (HPLC). Lyophilized nanoparticles were dissolved in acetonitrile (0.75 mg/ml) and 20 µl of this solution was injected (Injector 20 µl loop Valco) on a Polaris C18-A column (150×4.6 mm; 5 µm; Ansys Technologies, Torrance, USA). Acetonitrile/water (80/20 v%) was used as an eluent at a flow rate of 2 ml/min (Varian HPLC pump 2510). A Varian variable λ detector 2550 was used to detect rapamycin at 278 nm. The amount of rapamycin in the sample was calculated using a calibration curve of rapamycin in acetonitrile at various concentrations.

Determination of the dexamethasone content of nanoparticles

The dexamethasone content of the nanoparticles was determined by proton nuclear magnetic resonance (^{1}H-NMR). A known amount of drug-loaded nanoparticles (approximately 5 mg) was dissolved in 1 ml of deuterated DMSO. Spectra were obtained using a Varian Inova (Varian, Palo Alto, USA) operating at 300 MHz. The dexamethasone content of the nanoparticles was calculated from the integral of a dexamethasone peak (d, 2H, δ=7.2 ppm) and the integral of a glycolyl peak (m, 2H, δ=4.6-4.9 ppm), using the integrals of the peaks of dexamethasone and of the glycolyl units of polymer solutions in deuterated DMSO containing known amounts of dexamethasone and polymer.

Drug release study

Dexamethasone release from the nanoparticles was studied by dispersing nanoparticles in PBS containing 0.02% (w/v) of sodium azide (NaN$_3$) at 37 °C. For rapamycin-loaded nanoparticles, PBS containing 0.02% (w/v) of NaN$_3$ and 1 mM SDS was used as the release medium. SDS was used to increase the solubility of rapamycin in PBS to levels well detectable by HPLC. Drug-loaded nanoparticles were redispersed in 2 ml of release medium at a known concentration (approximately 10

mg/ml) and transferred to a dialysis tube (1 cm width, 20 cm length; Spectra/Por® 6 Membrane; MWCO: 25,000; Medicell International Ltd., London, UK). One end of the dialysis tube was tied up. After transfer of the nanoparticle dispersion, the other end of the dialysis tube was clamped. The tube was incubated in Erlenmeyer flasks in 500 ml or 67 ml release medium at 37 °C for dexamethasone- and rapamycin-loaded particles, respectively. These volumes were chosen to ensure that the maximum concentration of the drug in the release medium would always be less than 10% of the maximum solubility, i.e. sink conditions [24]. The Erlenmeyer flasks were continuously shaken. At different time points, 1.5 ml of the eluate was removed for analysis and replaced by fresh release medium.

Drug concentration in release medium

The concentration of drug in the release medium was determined by HPLC. In the case of dexamethasone, 20 µl of eluate was injected (Injector 20 µl loop Valco) on an RP-18e column (100×4.6 mm; 5 µm; Merck, Darmstadt, Germany). Water/tetrahydrofuran/acetonitrile (80/12/8 v%) was used as an eluent at a flow rate of 2 ml/min (Varian HPLC pump 2510). Dexamethasone was detected at 240 nm using a Varian variable λ detector 2550. In the case of rapamycin, 20 µl of eluate was injected on a Polaris C18-A column (150×4.6 mm; 5 µm; Ansys Technologies, Torrance, USA). Acetonitrile/water (80/20 v%) was used as an eluent at a flow rate of 2 ml/min. Rapamycin was detected at 278 nm. The drug concentration in the release medium was calculated using a calibration curve of the drug in the corresponding release medium at various concentrations.

***In vitro* degradation of dexamethasone-loaded nanoparticles**

The *in vitro* degradation of dexamethasone-loaded PEO-PLGA nanoparticles was studied by dispersing nanoparticles in PBS containing 0.02% (w/v) NaN_3. The nanoparticle dispersions in closed ultracentrifugation tubes were kept at 37 °C. At different time points (0-24 days), the particle size was determined and subsequently the nanoparticles were separated from the medium by ultracentrifugation (65,000×g for 40 min). The sediment was lyophilized and analyzed with respect to the molecular weight of the polymer. The molecular weight was determined by gel permeation chromatography (GPC) using chloroform at 25 °C and a flow rate of 1.5 ml/min. The GPC setup consisted of a Waters Model 510 pump, a HP Ti-Series 1050 autosampler, a Waters Model 410 Differential Refractometer, and a Viscotek H502 Viscometer Detector with HR0.5, HR2 and HR4 Waters Ultra-Styragel columns (Waters, Milford, USA) placed in series. Polystyrene standards with narrow molecular weight distributions (PSS, Mainz, Germany) were used for calibration.

RESULTS AND DISCUSSION

Particle analysis

Dexamethasone- and rapamycin-loaded PEO-PLGA nanoparticles were prepared and some of these nanoparticle formulations were treated with an aqueous protein solution. The drug concentration of the organic phase during particle preparation was varied and its influence on drug loading and particle size was determined. The drug content and the particle characteristics in the wet state of untreated and protein-treated nanoparticles and the particle characteristics in the dry state of untreated nanoparticles are shown in Table 8.1.

Table 8.1 The drug content, swelling and polydispersity index (P.I.) of untreated and protein-treated PEO-PLGA nanoparticles in water and the size of protein-treated and untreated PEO-PLGA nanoparticles in the wet and in the dry state.

Nanoparticle type[a]	Drug during NP-preparation (wt%)[b]	Drug loading (wt%)[c]	Size (nm)[d]	P.I. (-)[d]	Size (nm)[e]	Swelling (%)[f]
NP-0	0	0	230 ± 10	0.16 ± 0.05	190 ± 70	77 ± 28
NP-dex-0	17	2 ± 0	210 ± 2	0.33 ± 0.04	-	-
NP-dex-0	29	29 ± 2	197 ± 3	0.31 ± 0.08	170 ± 50	56 ± 16
NP-dex-gel-0.5	29	29 ± 2	193 ± 3	0.45 ± 0.06	-	-
NP-dex-gel-14	29	29 ± 2	194 ± 3	0.42 ± 0.05	-	-
NP-dex-alb-0.5	29	29 ± 2	199 ± 5	0.44 ± 0.03	-	-
NP-rap-0	0.3	0.1 ± 0	163 ± 6	0.49 ± 0.04	-	-
NP-rap-0	1.0	0.4 ± 0	192 ± 3	0.46 ± 0.03	-	-
NP-rap-gel-0.5	1.0	0.4 ± 0	193 ± 3	0.52 ± 0.05	-	-
NP-rap-gel-3	1.0	0.4 ± 0	192 ± 5	0.38 ± 0.02	-	-

[a]nanoparticles (NP) loaded with dexamethasone (dex) or rapamycin (rap); the numbers denote the weight percentage of gelatin (gel) or albumin (alb) relative to the polymer weight in the particle preparation procedure. The data of NP-dex are of two nanoparticle preparations, the data of NP-rap are of one nanoparticle preparation.
[b]the wt% of drug relative to the total drug and polymer weight during particle preparation.
[c]the wt% of drug in the nanoparticle preparation after purification as determined by HPLC.
[d]determined by DLS; the standard deviations denote the variation in size within three size measurements.
[e]determined by SEM by averaging the diameter of 35 particles of a representative part of the sample.
[f]calculated by dividing the hydrodynamic volume (from DLS) by the volume in dry state (from SEM).

The dexamethasone content of the nanoparticles strongly depends on the relative amount of dexamethasone being present during particle preparation. For a low amount of dexamethasone during particle preparation, the drug content of the nanoparticles is rather low, which is in agreement with the results of Hickey *et al*. [25] who prepared nanoparticles from a blend of PLGA and PEO (9:1), loaded with dexamethasone, by an oil-in-water emulsification-evaporation method. They determined a dexamethasone content of 3 wt% using 16 wt% of drug relative to the weight of drug and polymer during particle preparation. The relatively high solubility of dexamethasone in water (100 μg/ml [18]) causes dexamethasone to diffuse into the aqueous phase during particle formation, and could explain the low content of dexamethasone for low amounts of drug relative to the total drug and polymer weight during particle preparation.

For nanoparticle preparations in which 29 wt% of dexamethasone was used, the dexamethasone content was 29 wt%. To make sure that this high dexamethasone content was not due to the formation of dexamethasone particles, the nanoparticle preparation procedure was performed in the absence of PEO-PLGA polymer. In this experiment, no particles were obtained. The high efficiency of drug incorporation might be explained by crystallization of dexamethasone in the particles. In lidocaine-loaded poly(lactic acid) nanoparticles, lidocaine crystals were only observed at high lidocaine contents (approximately 30 wt%) and not at low

contents (approximately 10 wt%) [26]. A possible method to study the state of dexamethasone in the nanoparticle could be differential scanning calorimetry (DSC). However, because the decomposition temperature of PEO-PLGA is lower than the melting temperature of dexamethasone, DSC-analysis of the PEO-PLGA nanoparticles was not possible. An alternative technique to study the state of dexamethasone in the nanoparticles, which is not explored thus far, could be X-ray diffraction analysis.

For both weight fractions drug/(drug and polymer) that were applied during nanoparticle preparation, the rapamycin content of the nanoparticle is approximately 40% of this weight fraction (Table 8.1). For a relatively low amount of drug during particle preparation, the rapamycin content is relatively high compared to dexamethasone, which might be due to the low solubility of rapamycin in water (2.6 μg/ml [20]) and in the mixture of acetone and aqueous salt solution.

The hydrodynamic diameter of drug-loaded nanoparticles is slightly smaller than of unloaded nanoparticles (Table 8.1). A possible reason for this might be that the hydrophobic drug decreases the interfacial tension between the organic and aqueous phase, which results in an increase of the area to volume ratio and thus in smaller particles.

Furthermore, unloaded and loaded PEO-PLGA nanoparticles appear to have a spherical shape in the dry state as was determined by SEM (Figure 8.2).
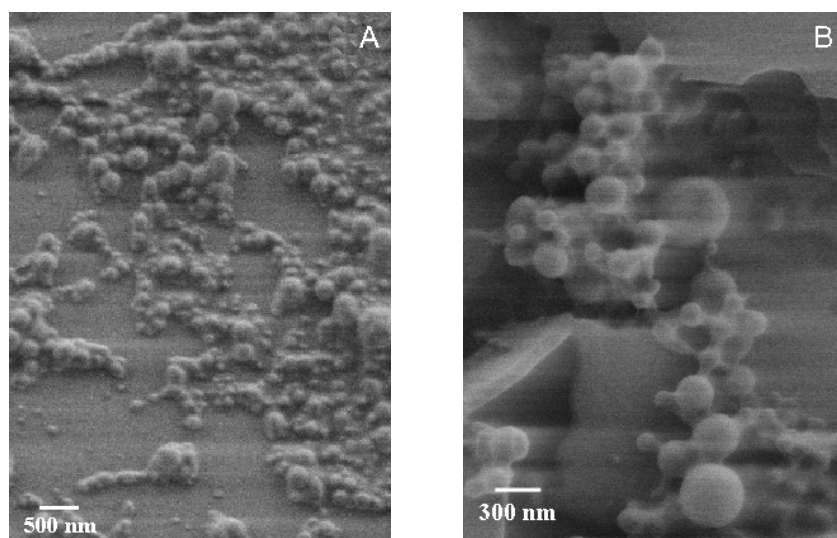
Figure 8.2 Scanning electron microscopy image of (A) unloaded and (B) dexamethasone-loaded PEO-PLGA nanoparticles on a silicon substrate.

Drug release from nanoparticles

For the drug release from degrading PLGA or PEO-PLGA particles, a triphasic profile has been described in literature [27-29]. The first phase is a burst effect, caused by the release of drug that is adsorbed onto the outer particle surface. The second phase is characterized by a relatively slow release due to diffusion of drug out of the matrix. The third phase is a phase of increased drug release, caused by (extensive) polymer degradation, resulting in an increased permeability of the drug in the polymer matrix.

The release of dexamethasone and rapamycin from untreated and protein-treated PEO-PLGA nanoparticles in PBS is depicted in Figure 8.3A and B, respectively.
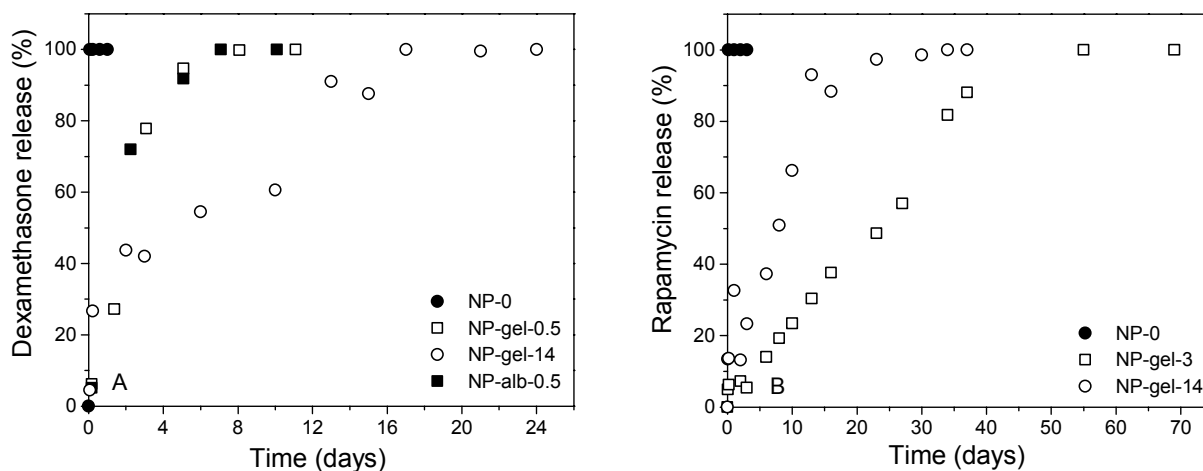
Figure 8.3 *Drug release in PBS (pH 7.4) at 37 °C from PEO-PLGA nanoparticles loaded with (A) 29 wt% dexamethasone and (B) 1 wt% of rapamycin as a function of time and amount of protein (gelatin (gel) or albumin (alb)). The numbers in the nanoparticle code represent the wt% of protein relative to the initial polymer weight (n=1).*

A rapid drug release was observed for untreated drug-loaded nanoparticles, being complete within 5 h (second data point, Figure 8.3). The rapid release of all drug could indicate that all drug is present at the surface. To verify this, the surface of drug-loaded nanoparticles was analyzed by XPS. As the ratio of carbon and oxygen atoms (C/O-ratio) of dexamethasone (4.40) and of rapamycin (3.92) is much higher than of PEO-PLGA (1.50) or unloaded PEO-PLGA nanoparticles (1.50) [15], the C/O-ratio can be used to determine whether all drug is present at the surface. Assuming that all dexamethasone is present at the surface of dexamethasone-loaded nanoparticles (29 wt%; 197 nm (Table 8.1)), the thickness of the dexamethasone layer would be approximately 11 nm, which equals the depth of analysis. The C/O-ratio of nanoparticles loaded with 29 wt% of dexamethasone was determined to be 1.57 ± 0.06. Although some reorganization due to the drying process might occur [15], it is highly unlikely that all dexamethasone is present at the surface. In the case of rapamycin-loaded particles (0.4 wt%; 192 nm (Table 8.1)) the thickness of the rapamycin layer would be approximately 0.1 nm, which is much lower than the depth of analysis. Since the C/O-ratio of nanoparticles loaded with 0.4 wt% of rapamycin was determined to be 1.57 ± 0.08 it cannot be concluded whether rapamycin was preferentially present at the surface.

The rapid drug release is in accordance with the rapid release of savoxepine and estradiole from poly(DL-lactic acid) (PDLLA) nanoparticles prepared by the salting-out method [30,31] and the rapid release of propranolol hydrochloride and lidocaine from PEO-PLLA microparticles prepared by an emulsification-evaporation method [32]. The rapid release was explained by the presence of pores in the nanoparticles [31,32]. The presence of pores increases the total surface area available for diffusion of drug out of the matrix, resulting in a

relatively rapid drug release. Similarly, the rapid release of drug in this study could indicate that the PEO-PLGA particles contain pores. The presence of pores and the high water-uptake of PEO-PLGA nanoparticles (Table 8.1) [33] could explain the high permeability of the drug in the polymer matrix [34]. During nanoparticle preparation, liquid-liquid demixing resulting in a polymer poor and a polymer rich phase may occur, which will lead to pore formation. In principle, two kinds of particles can be formed, namely particles with a phase-separated polymer phase or with a mixed polymer phase. However, whether phase separation occurs cannot be concluded from the data presented in this study. A reason that no pores were observed by SEM-analysis might be that these have collapsed during drying of the particles.

The time to release all drug was extended by redispersion of drug-loaded nanoparticles in an aqueous gelatin or albumin solution (Figure 8.3). First, a small burst effect was observed, possibly resulting from desorption of drug from the nanoparticle surface. This was followed by a linear release of dexamethasone over a period of 8 (for 0.5 wt% protein) to 17 (for 14 wt% protein) days and of rapamycin over a period of 25 (for 14 wt% gelatin) to 50 (for 3 wt% gelatin) days. No difference in the release profile or release time was observed between gelatin- and albumin-treated dexamethasone-loaded particles (for 0.5 wt% protein).

The *in vitro* degradation study of dexamethasone-loaded PEO-PLGA nanoparticles showed that during the first 3 weeks of drug release the particle size and PEO-PLGA molecular weight as a function of drug release time were similar to the particle size and PEO-PLGA molecular weight of unloaded PEO-PLGA nanoparticles [35]. This means that the $\overline{M}_n$ of PEO-PLGA decreases during the first 2 weeks, is stable during the following few weeks and decreases again to reach a value of $2 \cdot 10^3$ g/mol after 8 weeks. The initial decrease of $\overline{M}_n$ was due to the preferential cleavage of the ester linkage between PLGA and PEO. The particles retained their size in the first 2 weeks but then (partially) aggregated as a result of the release of PEO.

Classical equations describing diffusion of drug out of a spherical matrix, such as the Baker-Lonsdale equation [36,37] cannot be applied to describe drug release from these particles for several reasons. First of all, mass loss occurs due to the preferential cleavage of the ester linkage between PLGA and PEO [35]. This results in an increase of hydrophobicity of the polymer matrix in time. As the particle size remains constant in time, this means that the porosity increased in time, resulting in an increased diffusion of drug out of the matrix. Secondly, the molecular weight of the block copolymer decreases in time, which leads to an increase in the diffusion coefficient of the drug [38]. Thirdly, the particle size distribution plays a role in the drug release. Smaller particles release drug at a higher rate than larger particles [30,34,39], probably caused by the higher surface to volume ratio.

Several effects of the protein treatment on the drug release characteristics might play a role. Protein can be adsorbed onto the surface, thereby forming a coating that decreases diffusion of the drug out of the polymer matrix. The protein can also be incorporated in the

nanoparticles and can interact with drug and/or polymer, decrease the degree of swelling or reduce the porosity, which all result in a lower diffusion coefficient of the drug.

Since the amount of protein that is associated with the nanoparticle is very small and the hydrodynamic diameter of protein-treated and untreated drug-loaded particles is equal (Table 8.1), the effect of the protein treatment on drug release is not caused by a difference in swelling of the particles.

The amount of protein associated with the nanoparticle was calculated by determining the nitrogen content using elemental analysis. The results are shown in Table 8.2. It can be seen that the higher the protein concentration during treatment of the nanoparticles, the more protein is associated with the unloaded and dexamethasone-loaded nanoparticles. No protein was present in the unloaded nanoparticles after treatment with an aqueous solution containing 0.5 wt% of protein. If it is assumed that all protein is present at the outer particle surface, the surface concentration of protein is maximally 0.09 $\mu g/cm^2$, which is less than the surface concentration of a monolayer of albumin [40].

Table 8.2 *The protein content (wt%) of dexamethasone-loaded (29 wt%) (dex) and unloaded PEO-PLGA nanoparticles after treatment with an aqueous solution of gelatin (gel) or albumin (alb).*

Nanoparticle formulation[a]	Protein content of particles (wt%)
NP-dex-0	< 0.07[b]
NP-dex-alb-0.5	0.76 ± 0.35
NP-dex-gel-0.5	0.63 ± 0.19
NP-dex-gel-14	2.46 ± 0.69
NP-0	< 0.07[b]
NP-alb-0.5	< 0.07[b]
NP-gel-0.5	< 0.07[b]
NP-gel-14	1.70 ± 0.44

[a]the numbers denote the amount of protein relative to the initial polymer weight.
[b]below detection limit (=0.01 % N, which corresponds to 0.07 wt% protein).

The protein content of the dexamethasone-loaded particles was higher than of the unloaded particles that were treated with the same amount of protein, irrespective of the amount of protein in the aqueous protein solution with which the particles were treated. This indicates that dexamethasone influenced the uptake of protein in the nanoparticles. The protein might coat or bind to the dexamethasone present in the nanoparticles or a combination of both. The effect of the protein incorporated in the nanoparticles on the release of drug from the nanoparticles will probably depend on the state of the drug in the nanoparticles. If dexamethasone is homogeneously dispersed in the nanoparticle, the protein is likely to interact with dexamethasone, either through hydrophobic interaction or through hydrogen bonding [32]. In the case that dexamethasone is present in the nanoparticle as dexamethasone crystals, the protein may also be present as a coating on the dexamethasone crystals. This

probably reduces the dissolution rate of the crystals, leading to a lower drug release rate. The more protein is associated with the nanoparticles, the higher is the probability that the protein coats the dexamethasone or interacts with dexamethasone and the slower is the dexamethasone release, as seen in Figure 8.2A. However, it has to be noted that the amount of protein present in the nanoparticles in relation to the amount of drug present is rather small. Therefore, a more likely explanation for the effect of protein treatment on the drug release is that the protein molecules penetrate and/or block the pores of the particles, thereby decreasing diffusion of drug through the pores, as also was suggested by Huang *et al*. [32]. Due to the presence of protein, the viscosity of the aqueous phase in the pores will increase resulting in a decrease of diffusion of the drug through the pores [24]. Consequently, the drug release rate is decreased.

For rapamycin, the same trend is observed for the effect of protein treatment on drug release. However, the total drug release time of particles treated with an aqueous gelatin solution containing low amounts of gelatin was longer than that of particles treated with an aqueous gelatin solution containing higher amounts of gelatin. As the amount of gelatin in rapamycin-loaded nanoparticles is not known, it is difficult to give an explanation for this observation. Besides, the presence of SDS in the release medium might play a role in the release of rapamycin as it can complex with the protein or desorb protein.

The degree of interaction between the protein and the drug is dependent on drug characteristics, such as hydrophobicity, molecular weight and ability to form hydrogen bonds. In this respect, the interaction between rapamycin and protein is expected to be stronger than between dexamethasone and protein and the diffusion of rapamycin through the pores is expected to be slower than of dexamethasone. This explains the longer drug release times of protein-treated rapamycin-loaded particles compared to dexamethasone-loaded particles.

In this study, a sustained rapamycin release from biodegradable PEO-PLGA nanoparticles containing 0.4 wt% of rapamycin for 50 days was observed. This means that the release time is long enough to inhibit smooth muscle cell proliferation, and thus restenosis. From a comparison with rapamycin-eluting stents [7,8] it can be concluded that the rapamycin content probably has to be increased to be efficient in this respect. This might be achieved by using relatively high rapamycin amounts during nanoparticle preparation.

CONCLUSIONS

Dexamethasone- and rapamycin-loaded PEO-PLGA nanoparticles were prepared without stabilizer using the salting-out method. High dexamethasone loadings (29 wt%) were obtained by using 29 wt% of dexamethasone during nanoparticle preparation. The rapamycin content of the PEO-PLGA nanoparticles (0.1-0.4 wt%) was 40% of the amount of rapamycin during

nanoparticle preparation, irrespective of the absolute amount of rapamycin. The release of dexamethasone and rapamycin from the nanoparticles dispersed in PBS at 37 °C reached 100% within 5 hours. This rapid drug release was largely reduced by redispersion of the particles in an aqueous gelatin or albumin solution. This approach resulted in a linear dexamethasone release for 17 days and in a linear rapamycin release for 50 days.

It is concluded that biodegradable PEO-PLGA nanoparticles, prepared without additional stabilizer, have the potential to be used for the intravascular delivery of anti-restenosis drugs.

ACKNOWLEDGEMENTS

REFERENCES

1. Lincoff, A.M.; Topol, E.J. and Ellis, S.G., *Circulation,* **1994**, *90*, 2070-2084.
2. Chorny, M.; Fishbein, I. and Golomb, G., *Crit. Rev. Ther. Drug Carrier Syst.,* **2000**, *17*, 249-284.
3. Gershlick, A.H., *Atherosclerosis,* **2002**, *160*, 259-271.
4. Serruys, P.W.; De Jaegere, P.; Kiemeneij, F.; Macaya, C.; Rutsch, W.; Heyndrickx, G.; Emanuelsson, H.; Marco, J.; Legrand, V.; Materne, P. *et al.*, *N. Engl. J. Med.,* **1994**, *331*, 489-495.
5. Fischman, D.L.; Leon, M.B.; Baim, D.S.; Schatz, R.A.; Savage, M.P.; Penn, I.; Detre, K.; Veltri, L.; Ricci, D.; Nobuyoshi, M. *et al.*, *N. Eng. J. Med.,* **1994**, *331*, 496-501.
6. Lowe, H.C.; Oesterle, S.N. and Khachigian, L.M., *J. Am. Coll. Cardiol.,* **2002**, *39*, 183-193.
7. Rensing, B.J.; Vos, J.; Smits, P.C.; Foley, D.P.; van den Brand, M.; van der Giessen, W.J.; de Feijter, P.J. and Serruys, P.W., *Eur. Heart J.,* **2001**, *22*, 2125-2130.
8. Sousa, J.E.; Costa, M.A.; Abizaid, A.C.; Rensing, B.J.; Abizaid, A.S.; Tanajura, L.F.; Kozuma, K.; Van Langenhove, G.; Sousa, A.; Falotico, R. *et al.*, *Circulation,* **2001**, *104*, 2007-2011.
9. Klugherz, B.D.; Llanos, G.; Lieuallen, W.; Kopia, G.A.; Papandreou, G.; Narayan, P.; Sasseen, B.; Adelman, S.J.; Falotico, R. and Wilensky, R.L., *Coronary Artery Dis.,* **2002**, *13*, 183-188.
10. Tanabe, K.; Degertekin, M.; Regar, E.; Ligthart, J.M.R.; Van der Giessen, W.J. and Serruys, P.W., *Cathet. Cardiovasc. Intervent.,* **2002**, *57*, 65-68.
11. Huang, S. and Houghton, P.J., *Cancer Metastasis Rev.,* **2001**, *20*, 69-78.
12. Shaw, L.M.; Kaplan, B. and Brayman, K.L., *Clin. Ther.,* **2000**, *22*, B1-B13.
13. Song, C.X.; Labhasetwar, V.; Murphy, H.; Qu, X.; Humphrey, W.R.; Shebuski, R.J. and Levy, R.J., *J. Control. Release,* **1997**, *43*, 197-212.
14. Chapter 7 of this thesis.
15. Chapter 4 of this thesis.
16. Chapter 6 of this thesis.
17. Guzman, L.A.; Labhasetwar, V.; Song, C.; Jang, Y.; Lincoff, M.; Levy, R. and Topol, E.J., *Circulation,* **1996**, *94*, 1441-1448.
18. Budavari, S. *The Merck index: an encyclopedia of chemicals, drugs, and biologicals*; Merck: Whitehouse Station, NJ, **1996**; Vol. 12.

19. Sehgal, S.N.; Baker, H. and Vézina, C., *J. Antibiot.,* **1975**, *28*, 727-732.
20. Simamora, P.; Alvarez, J.M. and Yalkowsky, S.H., *Int. J. Pharm.,* **2001**, *213*, 25-29.
21. Rabiant, J., *S.T.P. Pharma,* **1991**, *1*, 278-283.
22. Provencher, S.W.; Hendrix, J. and De Maeyer, L., *J. Chem. Phys.,* **1978**, *69*, 4273-4276.
23. Briggs, D. and Seah, M.P. *Practical surface analysis by auger and X-ray photoelectron spectroscopy*; John Wiley & Sons, Inc.: Chichester, **1983**.
24. Bisrat, M.; Anderberg, E.K.; Barnett, M.I. and Nystrom, C., *Int. J. Pharm.,* **1992**, *80*, 191-201.
25. Hickey, T.; Kreutzer, D.; Burgess, D.J. and Moussy, F., *Biomaterials,* **2002**, *23*, 1649-1656.
26. Gref, R.; Minamitake, Y.; Peracchia, M.T.; Trubetskoy, V.; Torchilin, V. and Langer, R., *Science,* **1994**, *263*, 1600-1603.
27. Siepmann, J. and Göpferich, A., *Adv. Drug Deliv. Rev.,* **2001**, *48*, 229-247.
28. Yang, Z.H.; Birkenhauer, P.; Julmy, F.; Chickering, D.; Ranieri, J.P.; Merkle, H.P.; Luscher, T.F. and Gander, B., *J. Control. Release,* **1999**, *60*, 269-277.
29. Li, X.H.; Deng, X.M. and Huang, Z.T., *Pharm. Res.,* **2001**, *18*, 117-124.
30. Leroux, J.-C.; Allémann, E.; De Jaeghere, F.; Dölker, E. and Gurny, R., *J. Control. Release,* **1996**, *39*, 339-350.
31. Rafler, G. and Jobmann, M., *Pharm. Ind.,* **1997**, *59*, 620-624.
32. Huang, Y.Y.; Chung, T.W. and Tzeng, T.W., *Int. J. Pharm.,* **1999**, *182*, 93-100.
33. Gref, R.; Quellec, P.; Sanchez, A.; Calvo, P.; Dellacherie, E. and Alonso, M.J., *Eur. J. Pharm. Biopharm.,* **2001**, *51*, 111-118.
34. Bezemer, J.M.; Radersma, R.; Grijpma, D.W.; Dijkstra, P.J.; van Blitterswijk, C.A. and Feijen, J., *J. Control. Release,* **2000**, *67*, 249-260.
35. Chapter 5 of this thesis.
36. Baker, R. *Controlled release of biologically active agents*; John Wiley & Sons: New York, **1987**.
37. Costa, P.; Manuel, J. and Lobo, S., *Eur. J. Pharm. Sci.,* **2001**, *13*, 123-133.
38. Zuleger, S. and Lippold, B.C., *Int. J. Pharm.,* **2001**, *217*, 139-152.
39. Polakovic, M.; Görner, T.; Gref, R. and Dellacherie, E., *J. Control. Release,* **1999**, *60*, 169-177.
40. Bos, G.W.; Scharenborg, N.M.; Poot, A.A.; Engbers, G.H.M.; Terlingen, J.G.A.; Beugeling, T.; Van Aken, W.G. and Feijen, J., *Tissue Eng.,* **1998**, *4*, 267-279.

Atherosclerosis is a disease that is characterized by accumulation of lipids, cells and minerals at damaged sites of the arterial wall. It results in the development of a plaque, hardening of the artery and eventually the formation of thrombi. This leads to a decreased blood flow at the site of the plaque. Heart attacks and strokes that result from the decreased blood flow or the release of thrombi are the main cause of mortality in the western world.

Many techniques are available to restore the blood flow at the site of the atherosclerotic lesion. Percutaneous transluminal angioplasty (PTA) is used most frequently. It involves the introduction of a balloon catheter at the site of the plaque. The balloon is inflated and deflated. The inflation and deflation procedure is repeated until the plaque is deformed to such an extent that the diameter equals the original diameter of the artery.

Although the blood flow is initially restored, restenosis takes place in 30 to 50% of the patients within three to six months after the treatment. An important step in the process that leads to restenosis is the migration and proliferation of smooth muscle cells. Therefore, medication that prevents migration and proliferation of smooth muscle cells could lead to a reduction in the incidence of restenosis. As smooth muscle cell migration and proliferation take place in the first 4 weeks after treatment, sustained drug delivery for at least 1 month is desirable.

Whereas systemic administration of drugs appeared to be inefficient and is hampered by adverse side effects, local delivery of drugs seems to be a promising approach. However, drugs locally delivered as an aqueous solution had a short residence time in the arterial wall. Therefore, drug carriers were used to extend the residence time of the drug in the arterial wall. Due to their small size, nanoparticles seem to be suited as a drug carrier, and the use of biodegradable polymers for the preparation of the nanoparticles minimizes the long-term risk of adverse tissue reactions. Furthermore, the use of particles allows modification of the surface, thus enhancing the targeting of particles in the arterial wall. It was the aim of this study to prepare, characterize and surface-modify biodegradable nanoparticles that can be used for the delivery of anti-proliferative drugs to atherosclerotic vascular walls. Furthermore, the degradation behavior of nanoparticles, the release of two anti-proliferative drugs from the nanoparticles and the delivery of nanoparticles to arterial porcine carotid arteries were studied *in vitro*.

In **Chapter 1** a general introduction on the subject of this thesis is given. Atherosclerosis, the current treatments and the development of restenosis are reviewed in **Chapter 2**. In addition, approaches that have the potential to reduce the incidence of restenosis are described, with a highlight on the local delivery of drugs by use of biodegradable nanoparticles.

Poly(DL-lactic acid) (PDLLA) and poly(DL-lactic-co-glycolic acid) (PLGA) are biodegradable and biocompatible materials, which were used as material for the preparation of nanoparticles. The salting-out method was selected to prepare PDLLA and PLGA nanoparticles (**Chapter 3**). The main advantages of the salting-out method are the use of non-toxic solvents, the high nanoparticle yields and the fact that no elevated temperatures are necessary. Using this method, spherical particles with a narrow size distribution were obtained. Since the particle size is an important parameter in the effectiveness of the delivery of particles to the arterial wall, the influence of process variables on the final nanoparticle size was determined. Particles with a specific size and narrow distribution could be prepared in the range of 100-400 nm by varying the process conditions. Of all variables, the polymer concentration had the most pronounced effect.

Surface properties of the nanoparticles, such as surface charge and the presence of targeting units play a role in the effectiveness of the delivery of particles to the arterial wall, and also in the biological interactions of the nanoparticles with blood components. This means that control over the surface properties is desirable. In the preparation of PLGA nanoparticles a stabilizer is needed. The stabilizer is present at the surface and thus determines the surface chemistry. This has the disadvantage that the stabilizer might affect biological interactions and targeting of the nanoparticles. Therefore, nanoparticles of poly(ethylene oxide)-PLGA diblock copolymers (PEO-PLGA) were prepared without additional stabilizer (**Chapter 4**). For a nanoparticle system prepared from mixtures of PEO-PLGA block copolymer with molecular weights of 3 and 8 kD for the PEO and PLGA block respectively, and PLGA copolymer with a molecular weight of 11 kD a minimal PEO content of 13 wt% was required to obtain stable particle dispersions. For particles with a higher PEO content in the wet state, analysis revealed surface enrichment with PEO. For particles in the dry state, no surface enrichment with PEO was observed which was possibly due to rearrangement of the nanoparticle surface upon drying of the nanoparticles. For particles with a PEO content lower than 13 wt%, particle aggregation was observed.

The *in vitro* degradation of PDLLA, PLGA and PEO-PLGA nanoparticles in PBS (pH 7.4) at 37 °C is the subject of **Chapter 5**. The particle size, the molecular weight of the polymers and the amount of lactic and glycolic acid formed were followed in time. The polymer molecular weight of PDLLA nanoparticles gradually decreased over a period of 2 years, while the nanoparticles retained their size during that period. PLGA nanoparticles degraded faster and the degradation was nearly complete after 10 weeks. PLGA nanoparticles retained their size during that time. For PEO-PLGA nanoparticles, the ester bond connecting the PEO and the PLGA segments was preferentially cleaved, which led to a relatively fast decrease in molecular weight and to (partial) aggregation of the nanoparticles. PEO-PLGA nanoparticles were almost completely degraded within 8 weeks.

As mentioned before, targeting of the nanoparticles might enhance the effectiveness of the drug delivery in the arterial wall. In **Chapter 4** it was shown that PEO-PLGA nanoparticles could be prepared without stabilizer and that PEO was present at the surface. In **Chapter 6** the introduction of functional groups at the surface of PEO-PLGA nanoparticles is described. These functional groups can be used to couple targeting units (e.g. antibody or peptide) to the surface. As a model compound, diamine 1,8-diamino-3,6-dioxaoctane was used. First, PEO-PLGA nanoparticles containing carboxylic acid groups at the PEO chain end were prepared without stabilizer. Then the diamine was coupled to carboxylic acid groups at the nanoparticle surface under mild conditions in aqueous media. Coupling of the diamine resulted in free amine groups at the surface that were readily quantified. It is concluded that 80% of the carboxylic acid end groups present at the surface could be reacted with the diamine.

The location of nanoparticles in the arterial wall after intravascular administration using an *in vitro* model is described in **Chapter 7**. Polystyrene (PS) nanoparticles of different surface charge and particle size served as model particles to study the influence of these two properties on the delivery efficiency. PS particles were administered to porcine carotid arteries using a microporous balloon catheter. PS particles of 120 nm were present in all layers of the arterial wall, whereas the vascular wall was impermeable to PS particles of 230 and 1000 nm. The amount of particles that was detected in the arterial wall strongly depended on the outer diameter of the microporous balloon at full inflation, relative to the inner diameter of the artery at the site of nanoparticle delivery. When the inner diameter was larger than the maximal balloon diameter only a few particles were detected in the artery. This led to the conclusion that delivery of nanoparticles to the arterial wall via the vasa vasorum plays a minor role in the administration of particles to the arterial wall. For arteries with an inner diameter smaller than the maximal outer diameter of the balloon catheter, it was observed that the smaller the inner diameter of the artery, the more particles were introduced into the arterial wall. Fluorescent labeled biodegradable PEO-PLGA particles with a diameter of 120 nm were prepared and could be delivered to all layers of the arterial wall.

Finally, dexamethasone- or rapamycin-loaded PEO-PLGA nanoparticles were prepared (**Chapter 8**). In PBS (pH 7.4) at 37 °C both drugs were completely released within 5 hours indicating that pores are present in the nanoparticles. Treatment of the particles with gelatin or albumin after drug loading substantially reduced the rate of drug release and resulted in a linear drug release in time. Possibly, the protein molecules penetrate and/or block the pores, thereby decreasing diffusion of drug through the pores. It was shown that the rate of drug release was related to the amount of protein associated with the nanoparticles. After gelatin treatment of drug-loaded nanoparticles, a sustained release of dexamethasone or rapamycin for 17 and 50 days, respectively, was achieved.

Since PEO-PLGA particles are biodegradable (**Chapter 5**), can be used for surface modification to enhance their targeting specificity (**Chapter 6**), can be delivered to all layers of the arterial wall (**Chapter 7**) and after modification with proteins release anti-proliferative drugs over a period of more than 1 month (**Chapter 8**), PEO-PLGA nanoparticles have the potential to be successfully applied for the intravascular delivery of anti-proliferative drugs to reduce the incidence of restenosis.

Atherosclerose oftewel aderverkalking is een ziekte die wordt gekenmerkt door ophoping van vetten, cellen en mineralen op plaatsen waar de vaatwand is beschadigd. Dit leidt tot de vorming van een plak (of stenose genaamd), een verlaagde bloedstroom en uiteindelijk van bloedproppen. Hartaanvallen en infarcten ten gevolge van de verlaagde bloedstroom en het vrijkomen van bloedproppen zijn doodsoorzaak nummer één in de westerse wereld (van alle doden in Nederland in 2001 was 36% als gevolg van hartkwalen vergeleken met 27% als gevolg van kanker). Er zijn veel technieken ontwikkeld om de bloedstroom op de plek van een stenose te herstellen. Dotteren is heden ten dage de meest gebruikte techniek. Bij deze techniek wordt een balloncatheter naar de plek van de stenose geleid. De ballon wordt meerdere malen opgeblazen en leeggezogen tot de vatdiameter overeenkomt met de oorspronkelijke vatdiameter.

Hoewel de bloedstroom in eerste instantie is hersteld, treedt restenose bij 30 tot 50% van de patiënten binnen 3 tot 6 maanden na dotteren op. Een belangrijke stap in het proces dat uiteindelijk leidt tot restenose, is de migratie en snelle vermenigvuldiging van gladde spiercellen. Dienovereenkomstig zou de afgifte van medicijnen, die deze processen kunnen voorkomen, kunnen leiden tot een vermindering van het optreden van restenose. Aangezien de migratie en snelle vermenigvuldiging van gladde spiercellen binnen 4 weken plaatsvindt, is een afgifte van anti-restenose medicijnen van tenminste 1 maand wenselijk.

Medicijnen, die systemisch werden toegediend, verminderden echter het optreden van restenose niet, waarschijnlijk door een te lage lokale medicijnconcentratie. Verhoging van de dosis leidde echter tot nadelige neveneffecten. Gezien de lokale aard van de ziekte is een benadering gebaseerd op lokale medicijnafgifte efficiënter, hetgeen de kans op nadelige neveneffecten verlaagt. Lokale toediening via een catheter van medicijnen in oplossing resulteerde echter in een korte verblijftijd van het medicijn in de vaatwand. Om de verblijftijd te verhogen zijn dragers gebruikt die veel langzamer uit de vaatwand worden verwijderd. Geschikte dragers zijn nanodeeltjes, omdat ze klein genoeg zijn om overal in de vaatwand gebracht te worden. Het is bovendien mogelijk afbreekbare polymeren als basis voor de bereiding van de deeltjes te gebruiken. De afbreekbaarheid minimaliseert nadelige neveneffecten op de lange termijn. Tevens is het mogelijk het oppervlak van de deeltjes te modificeren, zodat locatie en verblijftijd van de deeltjes kan worden geoptimaliseerd. Het doel van dit onderzoek was de bereiding, karakterisering en oppervlaktemodificatie van afbreekbare nanodeeltjes, die gebruikt kunnen worden als dragers voor een effectieve afgifte van anti-restenose medicijnen in atherosclerotische vaatwanden. Tevens werd het degradatiegedrag van de nanodeeltjes, de afgifte van twee anti-restenose medicijnen uit de nanodeeltjes en de toediening van deeltjes in de wand van halsslagaders van varkens *in vitro* bestudeerd.

In **hoofdstuk 1** is een algemene inleiding voor het onderwerp van dit proefschrift gegeven. Aderverkalking, de huidige behandelingen en het ontstaan van restenose zijn beschreven in **hoofdstuk 2**. Hierin worden tevens de benaderingen beschreven, die mogelijkerwijs het optreden van restenose voorkomen, waarbij de nadruk ligt op de lokale afgifte van medicijnen door het gebruik van biologisch afbreekbare deeltjes.

Vanwege de afbreekbaarheid en biocompatibiliteit zijn poly(DL-melkzuur) (PDLLA) en poly(DL-melkzuur-co-glycolzuur) (PLGA) gebruikt als materialen voor de deeltjes. De uitzoutingsmethode is gekozen om PDLLA en PLGA nanodeeltjes te maken (**hoofdstuk 3**), omdat bij deze techniek geen toxische oplosmiddelen worden gebruikt, hoge opbrengsten kunnen worden bereikt en geen hoge temperaturen nodig zijn. Met behulp van deze methode zijn ronde deeltjes met een smalle deeltjesgrootteverdeling gemaakt. Aangezien de deeltjesgrootte een belangrijke parameter is voor de effectiviteit van toediening van deeltjes aan de vaatwand, is de invloed van de procesparameters op de uiteindelijke deeltjesgrootte bestudeerd. Er is aangetoond dat de deeltjesgrootte controleerbaar tussen 100 en 400 nm kan worden gevarieerd door de procesparameters te variëren. Van alle parameters heeft de polymeerconcentratie het grootste effect op de deeltjesgrootte.

Eigenschappen, zoals oppervlaktelading en de aanwezigheid van specifieke moleculen aan het oppervlak, spelen een rol bij de toediening van nanodeeltjes in de vaatwand, maar ook in de biologische interactie tussen nanodeeltjes en bloedcomponenten. Controle over het uiteindelijke oppervlak van de deeltjes is dus gewenst. Bij de bereiding van PLGA deeltjes is een stabilisator nodig. Aangezien de stabilisator aan het oppervlak aanwezig is, bepaalt de stabilisator de oppervlaktechemie. Daardoor kan de stabilisator de biologische interactie en de specificiteit van het oppervlak beïnvloeden. Om dit te vermijden zijn nanodeeltjes van poly(ethyleenoxide)-PLGA diblokcopolymeren (PEO-PLGA) zonder stabilisator gemaakt (**hoofdstuk 4**). Voor deeltjes in een waterig milieu werd verwacht, dat PEO zich aan het oppervlak zou bevinden, waarmee de deeltjes zouden worden gestabiliseerd. Door deeltjes te maken van mengsels van PEO-PLGA blokcopolymeren met een moleculair gewicht van 3 en 8 kD voor het PEO- en PLGA-blok respectievelijk en PLGA copolymeren met een moleculair gewicht van 11 kD, is bepaald dat minimaal 13 gew% PEO nodig is om stabiele dispersies te maken. Voor deeltjes met een hoger PEO-gehalte in de natte toestand is vastgesteld dat er relatief meer PEO aanwezig is aan het oppervlak dan in de bulk. Deeltjes met een lager PEO-gehalte vertonen aggregatie. Voor deeltjes in de droge toestand is geen verschil tussen de PEO-concentratie aan het oppervlak en in de bulk waargenomen. Dit is mogelijk veroorzaakt door reorganisatie van het deeltjesoppervlak tijdens het drogen van de deeltjes.

De *in vitro* degradatie van PDLLA, PLGA en PEO-PLGA nanodeeltjes in PBS (pH 7.4) bij 37 °C staat beschreven in **hoofdstuk 5**. De deeltjesgrootte, het moleculair gewicht van de polymeren en de hoeveelheden melkzuur en glycolzuur zijn bepaald in de tijd. Het moleculair gewicht van PDLLA wordt gaandeweg binnen 2 jaar minder, maar de PDLLA deeltjes

behouden hun grootte in de tijd. PLGA nanodeeltjes breken sneller af en de degradatie is vrijwel volledig na 10 weken. Ook deze deeltjes behouden hun grootte in de tijd. In PEO-PLGA nanodeeltjes wordt de esterbinding tussen PEO en PLGA bij voorkeur verbroken. Dit resulteert in een relatief snelle moleculaire gewichtsafname en (gedeeltelijke) aggregatie van de deeltjes. PEO-PLGA deeltjes zijn vrijwel volledig afgebroken na 8 weken.

Zoals hierboven vermeld kan de aanwezigheid van specifieke moleculen aan het oppervlak zorgen voor een efficiëntere toediening van de deeltjes in de vaatwand. In **hoofdstuk 4** is gebleken dat PEO-PLGA nanodeeltjes kunnen worden gemaakt zonder stabilisator, waarbij PEO aan het oppervlak aanwezig is. In **hoofdstuk 6** wordt de introductie van functionele groepen aan het oppervlak beschreven. Deze functionele groepen kunnen worden gebruikt om specifieke moleculen (bijv. antilichamen of peptiden) aan het oppervlak te koppelen. Als modelstof is 1,8-diamino-3,6-dioxaoctaan gebruikt. Allereerst zijn PEO-PLGA deeltjes met carboxylzuurgroepen aan het PEO-uiteinde gemaakt. Vervolgens is de diamine gekoppeld aan deze zuurgroepen onder milde condities in waterig milieu. De koppeling van de diamine resulteert in vrije aminegroepen aan het oppervlak, die eenvoudig gekwantificeerd kunnen worden. Er is aangetoond dat 80% van de zuurgroepen kunnen worden gemodificeerd met de diamine.

De locatie van nanodeeltjes in de vaatwand na intravasculaire toediening waarbij gebruik gemaakt wordt van een *in vitro* model is in **hoofdstuk 7** bestudeerd. Polystyreen (PS) deeltjes van verschillende grootte en oppervlaktelading dienen als modeldeeltjes om de invloed van grootte en lading op de efficiëntie van toediening en locatie in de vaatwand te bepalen. PS deeltjes zijn met behulp van een microporeuze ballondcatheter in de wand van halsslagaders van varkens gebracht. PS deeltjes van 120 nm zijn waargenomen in alle lagen van de vaatwand, terwijl de vaatwand niet toegankelijk is voor deeltjes van 230 en 1000 nm. Het aantal deeltjes dat in de vaatwand is waargenomen, is sterk afhankelijk van de buitendiameter van de ballondcatheter in vergelijking met de binnendiameter van het vat op de plaats waar de deeltjes zijn toegediend. Wanneer de binnendiameter groter is dan de maximale buitendiameter van de ballondcatheter zijn slechts enkele deeltjes aangetroffen in de vaten. Hieruit is geconcludeerd dat de toediening van deeltjes aan de vaatwand via het vasa vasorum geen grote rol speelt. Voor vaten met een binnendiameter kleiner dan de maximale buitendiameter van de ballondcatheter geldt, dat hoe kleiner de binnendiameter van het vat, des te meer deeltjes in de vaatwand terechtkomen. Fluorescent gelabelde PEO-PLGA deeltjes van 120 nm werden na toediening in alle lagen van de vaatwand waargenomen.

Tenslotte zijn dexamethasone- en rapamycinebeladen PEO-PLGA nanodeeltjes gemaakt (**hoofdstuk 8**). In PBS (pH 7.4) bij 37 °C worden beide medicijnen binnen 5 uur afgegeven. Dit wijst erop dat er waarschijnlijk poriën in de deeltjes aanwezig zijn. Behandeling van de medicijnbeladen deeltjes met het eiwit gelatine of albumine verlaagde de afgiftesnelheid

beduidend en resulteerde in een constante medicijnafgifte in de tijd. Mogelijkerwijs dringen de eiwitmoleculen de poriën binnen en/of blokkeren de poriën, wat tot gevolg heeft dat de afgiftesnelheid van het medicijn wordt verlaagd. Er is aangetoond dat de afgiftesnelheid is gerelateerd aan de hoeveelheid eiwit, dat met de nanodeeltjes is geassocieerd. Door de behandeling van medicijnbeladen deeltjes met gelatine is een afgifte van dexamethasone en van rapamycine over een periode van 17 respectievelijk 50 dagen bewerkstelligd.

Daar PEO-PLGA nanodeeltjes afbreekbaar zijn (**hoofdstuk 5**), kunnen worden gebruikt voor oppervlaktemodificatie om de effectiviteit van medicijnafgifte te verhogen (**hoofdstuk 6**), kunnen worden toegediend aan alle lagen van de vaatwand (**hoofdstuk 7**) en na modificatie met eiwitten langer dan 1 maand anti-restenose medicijnen kunnen afgeven (**hoofdstuk 8**), hebben PEO-PLGA nanodeeltjes de potentie om succesvol te worden gebruikt voor de intravasculaire toediening van medicijnen, die de snelle vermenigvuldiging van gladde spiercellen tegengaan en daarmee het optreden van restenose te verminderen.

Miechel Lambertus Theodorus Zweers is geboren op 25 februari 1974 te Zevenaar. Hij volgt het VWO aan het Liemers College te Zevenaar en behaalt zijn diploma in 1992. In datzelfde jaar begint hij aan de studie "Chemische Technologie" aan de Universiteit Twente te Enschede.

Na een leuke studieperiode en een leerzame stage bij Bayer in Leverkusen, Duitsland, studeert hij in maart 1998 af binnen de vakgroep "Polymeerchemie en Biomaterialen" op het onderwerp "Temperatuurgevoelige micellen van afbreekbare blok-copolymeren".

Van april 1998 tot augustus 2002 werkt hij als assistent in opleiding binnen dezelfde vakgroep. Het in dit proefschrift beschreven onderzoek voert hij uit onder leiding van dr. ir. G.H.M. Engbers, dr. D.W. Grijpma en prof. dr. J. Feijen.